Title

Budding yeast gametogenesis: A natural paradigm of cellular quality control

Author

Goodman, Jay

Publication Date

2021

Peer reviewed|Thesis/dissertation

Budding yeast gametogenesis: A natural paradigm of cellular quality control

By

Jay S. Goodman

A dissertation submitted in partial satisfaction of the requirements

for the degree of Doctor of Philosophy

in

Molecular and Cell Biology

in the

Graduate Division

of the

University of California, Berkeley

Committee in charge:

Professor Elçin Ünal, Chair
Professor Andrew Dillin
Professor Roberto Zoncu
Professor James Olzmann

Summer 2021

Abstract

Budding yeast gametogenesis: A natural paradigm of cellular quality control

by

Jay S. Goodman

Doctor of Philosophy in Molecular and Cell Biology

University of California, Berkeley

Professor Elçin Ünal, Chair

Protein aggregation, DNA damage and organelle dysfunction are hallmarks of aging and age-related diseases in metazoans. However, given the multicellular complexity of metazoans, it remains challenging to distinguish which factors cause cellular aging, versus those that arise because of aging. Budding yeast, although unicellular, exhibit similar age-associated abnormalities as metazoans. During mitosis, budding yeast mother cells accumulate cellular damage, in the form of protein aggregates, ribosomal DNA (rDNA) circles and organelle abnormalities as they continue to produce daughter cells. While age-induced damage persists in mother cells throughout mitosis, these age-associated traits are eliminated during meiotic differentiation, the developmental program that generates gametes in sexually reproducing organisms. Furthermore, gametes derived from aged diploids reset their aging clock, suggesting that the elimination of age-induced damage leads to cellular rejuvenation. Our study reveals that protein aggregate and nucleolar abnormalities that accumulate in aged cells are excluded from the gametes and illustrate that their exclusion is coupled to nuclear pore complex (NPC) disposal and nuclear remodeling that occurs naturally as part of gametogenesis. We additionally found that the gamete-excluded cellular material is subsequently degraded by a programmed cell death pathway that depends on the expression of a gamete plasma membrane proton pump and vacuolar lysis of the mother cell. We conclude that nuclear remodeling and vacuolar lysis promote the elimination of age-induced damage during budding yeast gametogenesis. Our work demonstrates natural paradigms of quality control in a developmental program and may reveal therapeutic strategies to combat cellular aging in metazoans.

For Bubby

February 14th, 1925 - October 31st, 2018

Acknowledgments

There are so many people that I owe for my success. I first and foremost would like to express my appreciation to my advisor, Elçin Ünal for being the best PhD mentor in the world! My research and growth as a scientist would not have been possible without her ongoing support, encouragement, compassion, and devotion to train students to critically think independently. There have also been so many other faculty members at UC Berkeley that have been very helpful, including Gloria Brar, Andy Dillin, Roberto Zoncu, James Olzmann and James Hurley. Additionally, I would like to acknowledge my previous mentors over the years: Martin Gruebele, Shohei Koide, Maxim Prigozhin and Taras Pogorelov, for putting me on an exceptional career path.

I was very fortunate to be surrounded by so many talented undergraduates, PhD students and post-docs throughout my PhD. I especially like to thank: 1) Grant King for being a fantastic collaborator in the Ünal Lab. 2) Eric Sawyer for helping me learn techniques that were critical to my research, 3) Jennifer Schick for being an exceptional undergraduate who assisted me throughout my PhD, and 4) Christiane Brune for being the best lab manger possible. I would also like to thank other members of the Brar-Ünal Lab, including Jing Chen, Leon Chan, Keerthana Chetlapalli, Ina Hollerer, Christopher Mugler George Otto, Cyrus Ruediger, and Tina Sing for providing minor technical assistance and stimulating intellectual discussions. I am additionally grateful for other UC Berkeley PhD students and post-docs outside the Brar-Ünal Lab who have made a positive impact on my research over the years, including Ashley Frakes, Thomas Laughlin, Ross Pedersen, Arturo Ortega, Daniel Serwas and Kersh Theva.

None of this would have been possible without the ongoing support from my loved ones. Special thanks belongs to my significant other, Yating, for completely going out of her way to keep me at ease everyday of my life, especially towards the end of my PhD. Thank you to my mom, my dad, Valentino, my twin brother Alex and sisters Juliana and Tessa. Finally, thank you to my grandparents, Gita Miriam Goodman, and Gerald Major Goodman, for being tremendous role models in science and continuing to inspire me to achieve greater aspirations.

Table of Contents

Chapter 1

*The following chapter contains material discussed from reviews which I am first author (Goodman and Ünal, 2020; Goodman et al., 2020).

Introduction

1.1 Segregation of age-induced damage in budding yeast

A hallmark of aging is the progressive accumulation of cellular damage. Age-induced damage arises as a result of organelle dysfunction and a decline in quality control (Sinclair et al., 1997; Sinclair and Guarente, 1997; Aguilaniu et al., 2003; Erjavec et al., 2007; Hughes and Gottschling, 2012; Morlot et al., 2019; Rempel et al., 2019). Over the last few decades, budding yeast have become a tractable model organism to study cellular aging, given their very short lifespan and that many of their age-associated abnormalities are conserved in metazoans. Akin to stem-cell renewal, budding yeast divides asymmetrically to generate rejuvenated daughter cells, while mother cells inherit age-induced damage before reaching senescence with 25-30 generations (**Figure 1.1**; Mortimer and Johnston, 1959; Longo et al., 2012). Many different factors that accumulate with age are preferentially retained in mother cells during mitosis, culminating in daughter cells that are devoid of cellular damage.

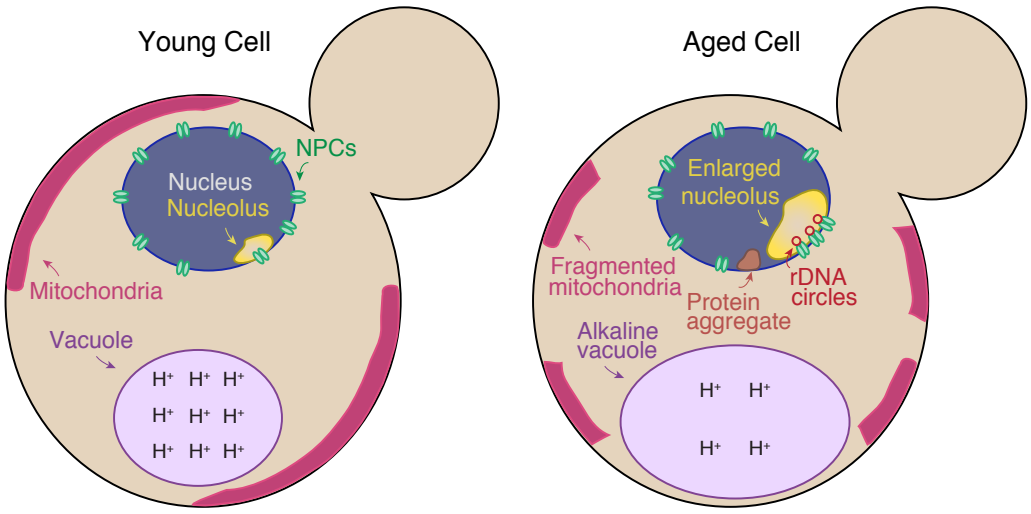

Figure 1.1. Age-associated abnormalities in budding yeast. With replicative age, mother cells retain protein and DNA damage, including protein aggregates and rDNA circles respectively. Mother cells additionally accumulate organelle

damage, such as fragmented mitochondria with lower membrane potential, vacuoles with a declined acidity, and nuclei containing misassembled NPCs (Sinclair et al., 1997; Sinclair and Guarente, 1997; Aguilaniu et al., 2003; Erjavec et al., 2007; Hughes and Gottschling, 2012; Morlot et al., 2019; Rempel et al., 2019). Note endoplasmic reticulum, golgi and peroxisomes are not shown for simplicity.

1.1.1 Segregation of protein damage

Several types of age-induced damage in budding yeast are conserved in other eukaryotic organisms. The most prevalent example is protein aggregation, which is also a conserved feature present in many age-related and neurodegenerative diseases in humans. Initial studies confirmed that oxidatively damaged proteins carrying carbonyl groups preferentially segregate to mother cells (Aguilaniu et al., 2003). Deletion of *SIR2*, which encodes a nicotinamide adenine dinucleotide (NAD) dependent deacetylase, shortens lifespan and leads to elevated levels of oxidatively damaged molecular chaperones (Erjavec et al., 2007). Interestingly, overexpressing the heat shock protein disaggregase Hsp104, which associates with carbonylated proteins in aged mother cells, suppresses the inability of the *sir2Δ* cells to retain oxidatively damaged proteins (Erjavec et al., 2007). Additionally, *hsp104Δ* cells have a decreased ability to asymmetrically segregate misfolded proteins, suggesting that it serves a function in spatial quality control in mother cells. A subsequent study revealed that *SIR2* genetically interacts with various components of the actin cytoskeletal network. Notably, *SIR2* induces the expression of a subunit of the CCT chaperonin, to facilitate the folding of actin (Liu et al., 2010). This is consistent with the observation that depolymerizing actin with Latrunculin-A significantly perturbs asymmetric retention of protein aggregates in a *SIR2* dependent fashion (Erjavec et al., 2007). Other factors such as the formin *BNI1* and the tropomyosin motor *MYO2* facilitate the retention Hsp104-assoicated aggregates in mother cells (Liu et al., 2010).

Additional models have been proposed to address how protein aggregates are asymmetrically retained in aged mother cells. Recently, Hsp104-associated aggregates have been reported to associate with various organelles, particularly the nuclear envelope (NE) and endoplasmic reticulum (ER) upon replicative aging (**Figure 1.1**; Cabrera et al 2017; Saarikangas et al., 2017). It was later determined that age-induced protein aggregates can associate with the ER by Ydj1 (Saarikangas et al., 2017). This small heat shock protein is post-translationally modified by farnesylation, which allows it to associate with the ER membrane. It was later indicated that Ydj1's ability to deposit protein aggregates in mother cells was due to the NE and ER diffusion barriers, which normally form at the bud neck. These diffusion barriers are dependent on septins, along with other cell polarity machinery, to target sphingolipids to the

bud neck in order to prevent NE and ER proteins from entering the daughter cells (Clay et al., 2014). *BUD6*, a gene implicated in generating NE and ER diffusion barriers, establishes protein aggregate retention in mother cells (Saarikangas et al., 2017). However, it remains unclear which misfolded proteins comprise protein aggregates that interact with the NE and ER. Furthermore, it remains unclear whether the nature of these protein aggregates is truly acting as causative factors to replicative aging.

1.1.2 Segregation of extrachromosomal DNA elements

In addition to protein aggregation, budding yeast accumulate abnormal DNA structures during replicative aging (**Figure 1.1**; Sinclair and Guarente, 1997). 150-200 tandem copies of rDNA repeats reside in the yeast nucleolus. These repetitive regions can undergo unequal sister chromatid exchange to generate extrachromosomal rDNA circles (Sinclair and Gaurente, 1997). These circular pieces of DNA can self-propagate through their autonomously replicating sequence (origin of replication) and are asymmetrically retained in mother cells. While the molecular trigger that induces rDNA circles remains unknown, several rDNA binding proteins have been characterized to stimulate or suppress their induction. Intriguingly, cells lacking *SIR2* generate rDNA circles at a much younger age than wild-type cells and have a shorter replicative lifespan (Kaeberlein et al, 1999). Other rDNA binding proteins, such as Fob1, increase the propensity of rDNA circles by replication fork blocking, which induces double stranded breaks. Aged *fob1Δ* cells have a reduced frequency of rDNA circles and exhibit a longer replicative lifespan (Defossez et al, 1999). Interestingly, this lifespan defect is suppressed in *sir2Δ fob1Δ* cells (Kaeberlein et al., 1999), highlighting that both genes operate in the same pathway in controlling cellular fitness.

Similar to protein aggregates, a lateral diffusion barrier also facilitates the asymmetric retention of circular DNA (Denoth-Lippuner et al., 2014). Recent work has shown that nonchromosomal DNA circles, which model rDNA circle behavior, exhibit a decreased retention frequency when the nuclear envelope diffusion barrier is perturbed in *bud6Δ* cells. It was later discovered that artificially generated DNA circles tether to nuclear pore complexes (NPCs) via the SAGA complex, which subjects them to the nuclear envelope diffusion barrier established at the bud neck (Denoth-Lippuner et al., 2014). Indeed, deletion of the SAGA subunit *SGF73* leads to a decrease in DNA circle retention in the mother cells resulting in extended replicative lifespan. Artificially tethering DNA circles to nucleoporins (Nups) in SAGA mutants restores the retention of circles in mother cells, suggesting that SAGA interaction with the Nups is directly driving their asymmetric segregation.

1.1.3 Segregation of organelle damage

Budding yeast contain most of the same organelles as metazoans. Like protein and DNA damage, organelles are asymmetrically retained throughout mitosis in replicatively aged yeast cells. Like protein aggregates and extrachromosomal DNA circles, dysfunctional organelles are also retained in the mother cells. The function of several organelles in budding yeast, including the nucleus, mitochondria, and vacuole, decline as a function of replicative age (discussed below). Though it is unclear to what degree each organelle contributes to the replicative aging process, the types of damage that are generated by them are also found in aging metazoans (David et al., 2010; Colacurcio and Nixon, 2016; Sun et al., 2016; Tiku et al., 2017).

1.1.3.1 Segregation of nuclear damage

The nucleus is an integral organelle that allows eukaryotes to store and protect their genetic content. The genome, along with other nucleoplasmic contents is compartmentalized by the NE, which is mainly comprised of a double lipid bilayer. Because budding yeast undergo a closed cell division, NE proteins are more susceptible to damage during replicative aging. Protein aggregates and rDNA circles associate with the nuclear periphery (Denoth-Lippuner et al., 2014; Cabrera et al., 2017; King and Goodman et al., 2019), suggesting that the NE can recognize age-induced damage to be segregated away from the daughter cells. As previously mentioned, rDNA circles tether to the NE via the SAGA complex (Denoth-Lippuner et al., 2014), though the nature by which protein aggregates associate with NE during replicative aging remains to be explored.

Recent work has demonstrated that nuclear envelope permeability increases with age. Nuclear permeability is controlled by the nuclear pore complexes (NPCs), comprised of multiple Nups, which together span the outer and inner nuclear membrane to regulate shuttling between the nucleus and cytoplasm. With age, a fraction of Nups that are enriched with phenylalanine glycine repeats (Nup2, Nup100, Nup116 and Nsp1) decrease in abundance in mother cells (Rempel et al., 2019). Additionally, herniations of the nuclear envelope has been reported to increase with age, which is associated with decreased levels of inner nuclear membrane (INM) quality control proteins Apq12, Brl1, Heh2, and Vps4. A similar type of herniation exists in *apq12Δ*, and *vps4Δ pom152Δ* cells and exhibits an asymmetric pattern of segregation (Scarcelli et al., 2007; Webster et al., 2014). Overall, little is known about what promotes the asymmetric segregation of misassembled NPCs, and it would be intriguing to investigate whether perturbing the nuclear envelope diffusion barrier can cause nuclear envelope herniations to be inherited by daughter cells. On the other hand, a subset of Nups can bypass the diffusion barrier in an actin-dependent process. Specifically, the type V myosin motor Myo2 can transmit a cytoplasmic pool of Nsp1 to the bud neck (Colombi et al., 2013; Makio et al., 2013). A more

thorough understanding of NPC inheritance is required to assess how NE permeability declines and the contribution it has on cellular aging.

1.1.3.2 Segregation of mitochondrial damage

Mitochondria are dynamic organelles that are responsible for consuming oxygen to generate energy for the cell. In budding yeast, mitochondria form an interconnected network along the cell cortex, but become increasingly fragmented and oxidized with age. As cells become older, mitochondria have a lower membrane potential in comparison to younger cells (**Figure 1.1**; Higuchi et al., 2013; Hughes and Gottschling 2012). Additionally, daughter cells maintain their youth by expressing cytosolic catalases to combat elevated ROS levels originating from damaged mitochondria (Erjavec and Nyström, 2007).

Similar to other age-associated factors, the actin cytoskeleton has been shown to facilitate the retention of damaged mitochondria in mother cells. Cells that lack the type II myosin *MYO1* exhibit a decreased velocity in retrograde actin cable flow, which negatively affects asymmetric retention of oxidized mitochondria (Higuchi et al., 2013). Conversely, deleting *TPM2*, a tropomyosin which negatively regulates the rate of retrograde actin cable flow via its binding to Myo1, increases the degree of mitochondrial asymmetry generated in mother cells. Deleting *SIR2* also lowers the rate of retrograde actin cable flow of oxidized mitochondria to mother cells. Whether or not Sir2's function in altering retrograde actin cable flow is linked to retaining other senescent factors requires further investigation.

1.1.3.2 Segregation of vacuolar damage

The budding yeast vacuole is functionally analogous to lysosomes in metazoans: its primary roles include metabolite storage and degrading long-lived proteins and damaged organelles via autophagy (Settembre et al., 2013). With age, lysosomal function declines due to a decline in autophagy, though whether other aspects of lysosomal function are affected remains to be determined (Cuervo, 2008; Colacurcio and Nixon, 2016). Vacuolar function is regulated by maintaining an acidic pH inside the lumen. Similar to lysosomes, vacuolar function declines during budding yeast replicative aging. This is mainly attributed the to an increase in the mother cell's vacuolar pH, while daughter cells are born with more acidified vacuoles (**Figure 1.1;** Hughes and Gottschling 2012). Surprisingly, the decline in vacuolar acidity does not appear to affect autophagy mediated protein degradation, but rather the ability to transport and store amino acids (Hughes and Gottschling 2012; Hughes et al., 2020;). Interestingly, vacuoles in replicatively aged cells exhibit defects in importing cysteine, which directly leads to impairment in mitochondrial respiration (Hughes et al., 2020). More work is required to better understand if this is conserved in lysosomes in aging metazoans and if there are additional

ways a decline in vacuolar acidity negatively impacts budding yeast during replicative aging.

Enhancing the activity of the vacuolar-type H^+-ATPase (V-ATPase), which lowers vacuolar pH, increases replicative lifespan, suggesting vacuolar acidity directly promotes aging independent of autophagy. Very little is known, however, with regards to what causes vacuolar pH differences between mother and daughter cells. The plasma membrane proton pump *PMA1*, one of the most asymmetrically retained proteins in budding yeast, accumulates in mother cells and exports protons outside of the cell (Henderson et al., 2014). Retention of Pma1 in mother cells consequently limits the pool of available protons in the cytoplasm for the V-ATPase proton pump to import into the vacuole, which could therefore cause vacuoles to lose their acidity over time. Whether or not there are other factors antagonizing vacuolar pH in mother cells, however, remains to be determined.

While daughter cells are devoid of age-induced damage, mother cells continue to accumulate protein, DNA, and organelle abnormalities. As observed in metazoan somatic tissues, age-induced damage persists in mother cells prior to senescence due to a decline in protein and organelle quality control. Although somatic tissues deteriorate with age, the germline maintains cellular homeostasis to ensure the production of healthy progeny (Labbadia and Morimoto, 2015; Taylor and Dillin, 2013; Vilchez et al., 2012; Ben-Zvi et al., 2009; Hsu et al, 2003; Verbeke, 2001). While germline quality control has been primarily studied in multicellular organisms, recent evidence suggests the existence of gametogenesis-specific quality control mechanisms in budding yeast, highlighting the evolutionary conservation of meiotic events beyond chromosome morphogenesis (Ünal et al., 2011; King and Goodman et al., 2019; Sawyer et al., 2019; Otto et al., 2021).

1.2 Quality control in budding yeast gametogenesis

Germ cells undergo gametogenesis to give rise to egg and sperm. Gametogenesis depends on meiosis, which is achieved with one round of DNA replication followed by two successive rounds of chromosome segregation. Gametes are integral to give rise to new offspring, which in turn make them essential for species to pass down genetic content to the next generation. Budding yeast diploids undergo gametogenesis (also known as sporulation) to generate four haploid gametes. Remarkably, meiotic yeast cells exhibit unique modes of organelle and protein quality control, resulting in cellular rejuvenation of the nascent haploid gametes.

1.2.1 Gametogenesis overview

Prior to the first meiotic division (meiosis I or MI), homologous chromosomes recombine to generate genetic products with half of their parental DNA. Cellular differentiation events take place in parallel to meiosis to generate gametes with

content distinct from the parents, which can give progeny an evolutionary advantage. While these aspects of gametogenesis are conserved, there are certain features that vary across organisms. In metazoans, female germ cells are only capable of generating one egg during oogenesis, whereas male germ cells can generate four sperm during spermatogenesis. Like sperm, budding yeast and other types of fungi generate four gametes (also defined as spores). However, unlike sperm, budding yeast gametes can resume mitotic proliferation. In addition, gametogenesis in metazoans is initiated from environmental cues that are different from budding yeast: while metazoans rely on unique cellular signalling events, yeast cells initiate gametogenesis through nutrient starvation (**Figure 1.2;** Fuller and Spradling, 2007; van Werven and Amon, 2011).

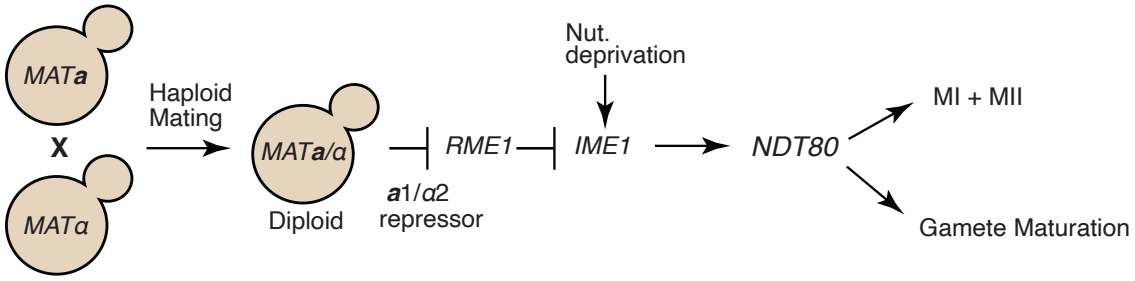

Figure 1.2. Budding yeast gametogenesis overview. Haploid *MAT**a*** cells mate with *MATα* to generate *MAT**a**/α* diploids. Meiotic entry is achieved when diploids are nutrient deprived and express the ***a***1/*α2* transcriptional repressor, leading to *IME1* activation (Mitchell and Herskowitz, 1986; Kassir et al., 1988; Covitz et al., 1991; van Werven and Amon, 2011). *IME1* activates the transcription factor *NDT80*, which is responsible for facilitating the meiotic divisions and other processes leading to gamete maturation (Chu and Herskowitz, 1998).

Analogous to egg fertilization, budding yeast generate zygotes with haploids of differing mating types. Haploid yeast can either exist as *MAT**a*** or *MATα* mating types. *MAT**a*** haploids can mate with *MATα* haploids to produce *MAT**a**/α* diploids that are able to undergo gametogenesis (**Figure 1.2**). Entry into gametogenesis is transcriptionally regulated by two genes: 1) *IME1,* a transcriptional activator that promotes meiotic entry and 2) *RME1*, which inhibits the transcription of *IME1* mRNA (**Figure 1.2;** Mitchell and Herskowitz, 1986; Kassir et al., 1988; Covitz et al., 1991). The activity of both genes is dependent on the ploidy number and the nutrient environment (**Figure 1.2**; Mitchell and Herskowitz, 1986; Covitz et al., 1991; van Werven and Amon, 2011). Rme1-mediated repression of *IME1* is alleviated by the ***a***1/*α2* transcriptional repressor, which is only generated in *MAT**a**/α* diploids (**Figure**

1.2; van Werven and Amon, 2011). *RME1* repression by the ***a***l/*α2* heterodimer, while necessary, is not sufficient to initiate meiotic entry. Though poorly understood, activation of *IME1* additionally requires nutritional cues that are not present during mitotic proliferation: under rich nutrient conditions (i.e., a high availability of nitrogen and fermentable carbon sources), diploid cells maintain mitotic proliferation, but can quickly initiate meiosis when subjected to nutrients only containing a non-fermentable carbon source (**Figure 1.2;** van Werven and Amon, 2011).

During meiotic entry, Ime1 up-regulates many different genes required to complete gametogenesis. One of these genes includes *NDT80*, which encodes a transcriptional activator responsible for turning on middle and late meiotic genes (Chu and Herskowitz, 1998). Yeast cells that lack *NDT80* are arrested in prophase I (during pachytene) and are therefore unable to progress through the meiotic divisions. It is thought that Ndt80 activates 100-400 transcripts including the M-phase cyclins (*CLB1*, *CLB3*, *CLB4)* to initiate the meiotic divisions (Benjamin et al., 2003; Berchowitz et al., 2013; Carlile and Amon, 2008; Chu et al., 1998; Chu and Herskowitz, 1998). *CLB1* and *CLB4* act primarily in meiosis I whereas *CLB3*, along with other *NDT80* targets act primarily in meiosis II. The latter transcripts are translationally repressed by the RNA-binding protein Rim4. Following the meiosis I-II transition, Rim4 is degraded, allowing *CLB3* and other *NDT80* targets to be expressed to initiate meiosis II and the later stages of gametogenesis (Berchowitz et al., 2013; Berchowitz et al., 2015; Carpenter et al., 2018).

Following the second meiotic division, four haploid nuclei are generated and eventually cellularize into gametes. Each nucleus is encapsulated by plasma membranes made *de novo* (**Figure 1.3**; Moens and Rapport, 1971). Gamete plasma membrane (also known as prospore membrane) nucleation occurs in conjunction with meiosis II at the spindle pole bodies (SPBs), which serve an analogous function to centrosomes in metazoans. Embedded in the NE, SPBs recruit post-Golgi secretory vesicles to initiate gamete plasma membrane formation (Moens and Rapport, 1971; Knop and Strasser, 2000). This process additionally requires the formation of the meiotic outer plaque (MOP), which is recruited to the cytoplasmic side of the SPBs (Moens and Rapport, 1971; Knop and Strasser, 2000). Therefore, cells lacking components comprising the MOP, including *SPO21* (another *NDT80* target), are unable to generate gamete plasma membranes after the meiotic divisions and fail to make mature gametes (Knop and Strasser, 2000). Once post-Golgi secretory vesicles are docked on to the MOP, gamete plasma membranes expand beyond the SPB through additional vesicle fusion events (Moens and Rapport, 1971; Knop and Strasser, 2000). The growing ends of the gamete plasma membranes associate with many different protein complexes including: 1) septins, which form rod-shaped heteroctamers which comprise of Spr3, Spr28, Cdc3 Cdc10, Cdc11, Cdc12 and Shs1 (Fares et al., 1996; McMurray and Thorner, 2008; Pablo-Hernando et al., 2008), as well as 2) the leading edge complex, a ring-like structure generated

by Ssp1, Don1, Irc10 and Ady3 (Lam et al., 2014; Moreno-Borchart et al., 2001). The precise roles of meiotic septins and leading edge components in gamete plasma membrane formation and downstream gamete maturation, however, remain poorly understand.

Once the plasma membranes become enclosed, multiple cell wall layers are assembled to complete gametogenesis (Lynn and Magee, 1970; Coluccio et al., 2004). Unlike in metazoans, yeast cells normally contain two cell wall layers during mitotic proliferation: an inner layer containing glucan and an outer layer containing mannan (Smits et al., 2001). In contrast, meiotic gametes evolved with four cell wall layers (also referred to as spore wall), most of which are made of polysaccharides, to survive environmentally harsh conditions. The two inner layers are the same as those present in mitotic cells, but assembled in reverse order (Lynn and Magee, 1970; Coluccio et al., 2004). The third layer is mainly composed of chitosan, while the fourth layer is composed of dityrosine (Briza et al., 1988; Briza et al., 1990). The formation of each layer is dependent on a unique set of biosynthetic enzymes, but the signaling cascade leading to their recruitment to the gamete plasma membranes has not yet been well characterized. Following cell wall formation, the mother cell collapses onto the gametes to form the ascus, allowing each gamete to physically associate with one another to form a tetrad. Under very low carbon conditions, some nuclei are not packaged and only generate one, two or three mature gametes, which are also defined as monads, dyads and triads respectively (Davidow et al., 1980; Okamoto and Iino, 1981; Taxis et al., 2005). Together, gametogenesis is a highly regulated program that requires chromosome segregation, gamete plasma membrane biogenesis and gamete cell wall formation to take place in a timely stepwise fashion. Interestingly, novel gene regulation and organelle remodeling are implicated in gametogenesis, but their contribution to producing healthy progeny has remained largely unexplored.

1.2.2 Gene regulation as a driver of quality control in gametogenesis

Throughout the process of gametogenesis, intricate tuning of gene expression occurs to ensure that the proper steps leading to gamete maturation take place. Approximately 66% of genes expressed throughout gametogenesis exhibit greater than a 10-fold change in protein synthesis (Brar et al., 2012), highlighting that a dynamic degree of gene regulation occurs. A subset of these genes includes transcription factors inducing the expression of quality control genes in response to environmental stress (Brar et al., 2012).

The ER unfolded protein response (UPR) is a conserved stress response pathway that operates in budding yeast gametogenesis. In metazoan model systems, the UPR has three distinct branches operating in the ER: the PERK pathway, the ATF6 pathway, and the IRE1/XBP1 pathway (Hetz, 2012). The IRE1/XBP1 pathway, which is also conserved in budding yeast, relies on the

alternative splicing of *XBP1*[1] to transcriptionally activate UPR genes that alleviate the burden of misfolded proteins (Cox and Walter, 1996; Mori et al., 1996). The ortholog of *XBP1* in budding yeast, *HAC1*, exhibits two periods of activity in meiosis, with one occurring during the meiotic divisions (Brar et al., 2012).

It is well appreciated that temporal gene activation controls many developmental processes, but recent work in budding yeast has shown that there are unique ways to modulate gene expression to promote subsequent gamete health. Throughout specific stages of gametogenesis, roughly 400 transcripts encoding a canonical open reading frame (ORF) also express a long undecoded transcript isoform (LUTI) (Chen and Tresenrider et al., 2017; Tresenrider, 2018; Cheng and Otto et al., 2018; Cheng and Brar, 2019; Tresenrider et al., 2021). Each LUTI contains an extended 5' transcript generated from a distal promoter that encodes for upstream open reading frames (uORFS), which prevent the translation of their canonical ORFs. Intriguingly, 61 of the 74 defined LUTIs generated in prophase I contain a sequence-binding motif that is recognized by the Ime1-Ume6 transcription factor complex. For example, *NDC80*, an essential gene that encodes a conserved kinetochore subunit, contains a LUTI that is regulated by the Ime1-Ume6 complex (Chen and Tresenrider et al., 2017; Tresenrider, 2018; Tresenrider et al., 2021). Upon meiotic entry, the LUTI of *NDC80* is transcribed to reduce expression of the canonical ORF in order to regulate timely kinetochore function during meiotic prophase (Chen and Tresenrider et al., 2017; Tresenrider, 2018; Tresenrider et al., 2021).

LUTIs have also been observed in vegetative cells and can be induced by the UPR. Recent studies have shown that treating mitotic yeast cells with the ER-stress inducing drugs DTT or tunicamycin causes *HAC1* to produce LUTIs that inhibit the transcription and translation of their canonical protein-coding mRNA isoforms (Van Dalfsen et al., 2018). This process may act to mimic the PERK branch of the UPR found in metazoans, which attenuates protein synthesis (Hetz et al., 2012). Therefore, it is possible that *HAC1*, along with other stress response transcription factors may stimulate LUTI induction as a quality control measure during gametogenesis to limit protein synthesis and minimize proteotoxic stress.

Other types of protein quality control pathways are upregulated during gametogenesis. For example, certain elements of the Heat Shock Response (HSR), one of the most well characterized quality control pathways, are expressed early in gametogenesis (Brar et al., 2012). The HSR relies on the conserved transcription factor *HSF1* to promote the expression of heat shock proteins (Hsps). Hsps, which include chaperones, predominantly act to reduce the level of proteotoxicity either by refolding or degrading proteins. In budding yeast, some Hsps are upregulated in gametogenesis, though their functional

[1] For consistency, all metazoan gene nomenclature is referred as "*Xbp1*" while metazoan protein nomenclature is referred as "XBP1."

roles in meiosis remain to be determined (Brar et al., 2012). In parallel, oxidative stress response genes *SKN7* and *YAP1* are expressed (Raitt et al, 2000; Okazaki et al, 2007; Brar et al., 2012). Additionally, analysis of data from Brar et al., 2012 revealed that several targets of these oxidative stress response transcription factors are upregulated following the meiotic divisions of gametogenesis, yet their biological impact on gamete differentiation requires further investigation.

1.2.3 Organelle remodelling as a driver of quality control in gametogenesis

The various modes of gene regulation taking place in gametogenesis lead to essential cellular remodeling for progeny to be born. While the mechanisms behind chromosome segregation and *de novo* plasma membrane formation have been thoroughly studied, the factors that control organelle inheritance during gametogenesis remain largely elusive. In mitosis, most daughter cells rely on lateral diffusion barriers and the actin cytoskeletal network to partition organelles from mother cells (Clay et al., 2014; Higuchi et al., 2013). The primary role of the actin cytoskeletal network during gametogenesis remains poorly characterized. Though recent work has highlighted that actin bundles are present in the nucleus during prophase I (Takagi et al., 2021), it is not known if lateral diffusion barriers or the actin cytoskeletal network are required for gamete organelle inheritance. Intriguingly, many organelles exhibit unique remodeling events that coincide with meiosis II and gamete plasma membrane biogenesis.

Although each gamete receives an equal amount of genetic material, other components of the nucleus do not divide symmetrically. Interestingly, a fifth nuclear body is generated during meiosis II (**Figure 1.3;** Fuchs and Loidl, 2004; King and Goodman et al., 2019). Also known as the Gametogenesis Uninherited Nuclear Compartment (GUNC), this compartment is mainly comprised of NPCs and other nucleolar proteins that eventually are left behind the nascent gametes (Fuchs and Loidl, 2004; King and Goodman et al., 2019). To account for the loss of this compartment, each nuclei generates NPCs and nucleolar proteins *de novo* following gamete plasma membrane biogenesis (King and Goodman et al., 2019).

Mitochondrial inheritance during meiosis is also regulated by a dynamic remodeling event. As yeast cells progress through the meiotic divisions, mitochondria detach from the plasma membrane and collapse prior to their inheritance (**Figure 1.3**; Sawyer et al. 2019). Mitochondrial detachment is dependent on a meiosis-specific kinase, Ime2, which is analogous to cyclin-dependent kinases (Benjamin et al., 2003). Induced by Ndt80, Ime2 phosphorylates mitochondrial-plasma membrane tethers Num1 and Mdm36, resulting in their degradation (Sawyer et al., 2019). Following mitochondrial detachment, a subset of mitochondria is inherited by the nascent gametes,

while the remaining pool is left behind the nascent gametes with the GUNC (**Figure 1.3;** Gorsich and Shaw, 2004; Neiman, 2011).

The ER behaves in a similar fashion as the mitochondria during meiosis: the cortical ER detaches from the mother cell plasma membrane during the second meiotic division, although it occurs somewhat independently of mitochondrial collapse (E. Sawyer, personal communication). Instead, ER detachment is dependent on the reticulon genes, which promote membrane curvature of the ER (De Craene et al., 2006; Voeltz et al., 2006; Hu et al., 2008). Yeast cells devoid of reticulon genes *RTN1*, *RTN2*, and *YOP1* are unable to detach their ER from the plasma membrane (Otto et al., 2021). How reticulons positively influence ER collapse during meiosis II remains to be determined. Like mitochondria, a subset of ER is not inherited by the nascent gametes, though little is known if inherited ER exhibits features that are distinct from the ER that is left behind (Neiman, 2011). Notably, ER autophagy is upregulated in an *NDT80* dependent matter and leads to the degradation of reticulon proteins (Otto et al., 2021). Perhaps damaged ER proteins are also subjected to autophagic machinery to ensure healthy ER inheritance into gametes.

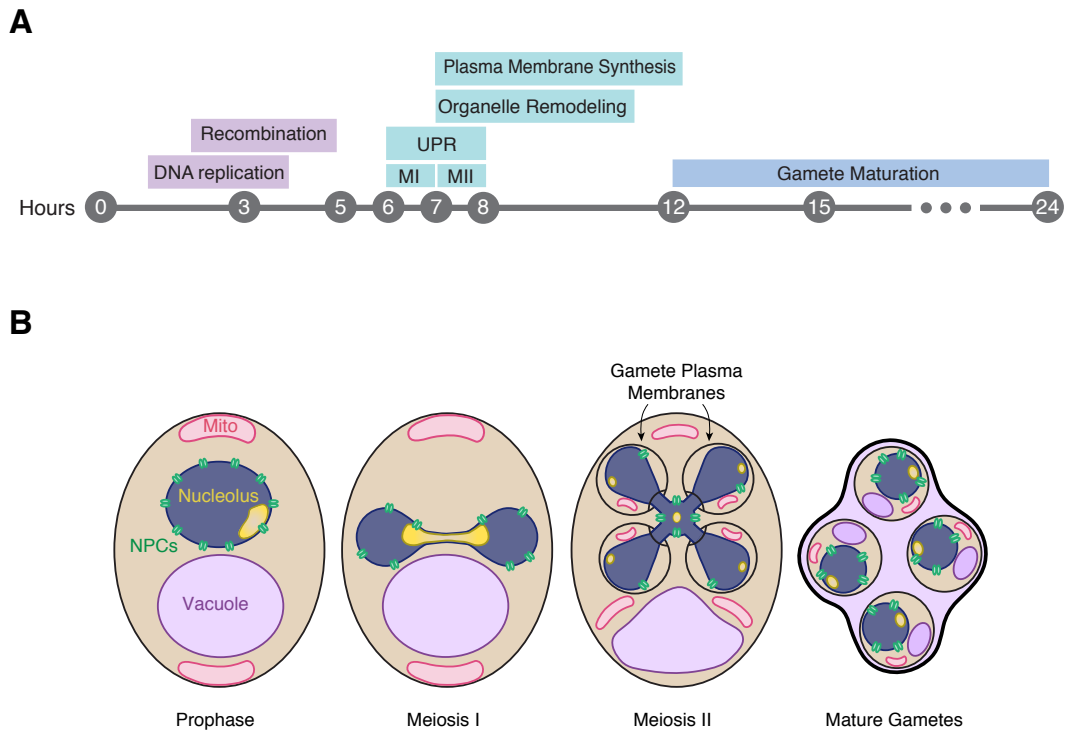

Figure 1.3. Organelle remodeling and protein quality control in budding yeast gametogenesis. A. Summary of organelle remodeling and protein

quality control events that take place hours post yeast gametogenesis induction. Timing of UPR induction was estimated by assessing ribosome footprint levels of *HAC1* (Brar et al., 2012). **B.** A subpopulation of NPCs, nucleolar proteins mitochondria is not inherited by the nascent gametes during anaphase II (King and Goodman et al., 2019; Sawyer et al., 2019; Fuchs and Loidl, 2004). Vacuoles are generated in the gametes *de novo*, while mother cell vacuole undergoes lysis during gamete maturation (Roeder and Shaw, 1996; Eastwood et al., 2012; Eastwood and Meneghini, 2015). The ER is not shown for simplicity. Prospore membrane is referred to as gamete plasma membrane or plasma membrane for simplicity.

What happens to organelle content left outside the developing gametes? Intriguingly, vacuoles of the diploid mother cell are not inherited by the nascent gamete and are generated *de novo* (Roeder and Shaw, 1996). The nature in which vacuoles are newly synthesized into the gametes is unknown. Late in gametogenesis, the vacuole of the mother cell undergoes a lysis event (termed Megautophagy) that allows its proteases to eliminate cellular material that is left outside of the gametes a few hours after plasma membrane biogenesis (**Figure1.3;** Eastwood et al., 2012; Eastwood and Meneghini, 2015;). The steps involved in achieving vacuolar lysis are poorly understood, but it does not depend on vacuole fission or macroautophagy (Eastwood and Meneghini, 2015; Eastwood et al., 2012). However, deleting the gametogenesis genes *SMK1*, a kinase that acts upstream of cell wall biosynthesis, and *CHS3*, and enzyme implicated in generating the chitosan cell wall layer, affects timely vacuolar lysis (Eastwood and Meneghini, 2015). It remains to be determined if vacuolar lysis is truly tied to cell wall deposition, or if *SMK1* and *CHS3* deficient cells negatively affect vacuolar lysis in an indirect manner by perturbing other critical steps of gametogenesis.

In concert with vacuolar lysis, certain types of viruses are also eliminated during budding yeast gametogenesis in an apoptosis-like fashion. During gamete maturation, mitochondrial endonuclease *NUC1,* an ortholog to apoptosis gene Endonuclease G, localizes to the cytoplasm. Mitochondrial release of *NUC1* depends on the mitochondrial outer membrane protein Por1, which allows the endonuclease to fragment genetic content derived from unpackaged nuclei. Interestingly, *NUC1* also protects gametes from accumulating the L-A and killer viruses (Gao et al., 2019). In the absence of *NUC1*, spores accumulate more killer virus, which can be lethal if additional antiviral genes are no longer present. Together, these diverse quality control mechanisms may pose a common requirement to ensure the next generation of progeny to be devoid of cellular material that would comprise their ensuing health.

1.2.4 Cellular rejuvenation during budding yeast gametogenesis

In conjunction with organelle remodeling and protein quality control, gametes can astonishingly destroy cellular damage derived from old diploid cells.

Particularly, nuclear protein aggregates, rDNA circles and abnormal nucleoli are eliminated from the developing gametes. Additionally, gametes that are derived from old mother cells are born young, with the same replicative potential as those generated from young mother cells (**Figure 1.4**; Unal et al., 2011; King and Goodman et al., 2019). The mechanism behind asymmetrically segregating age-induced damage away from gametes, however, remains poorly understood.

Interestingly, inducing meiosis-specific genes in mitotic cells is sufficient to extend the replicative capacity of aged mother cells. Upon the transient expression of *NDT80*, the replicative lifespan of aged mitotic cells increases approximately four-fold (Unal et al., 2011). Strikingly, only a subset of age-induced damage is eliminated in mitotic cells that express *NDT80*: while certain nucleolar features are no longer abnormal in aged mother cells, protein aggregates and rDNA circles persist (Unal et al., 2011). This leads to the interesting possibility that elimination of age-induced damage itself is not driving meiotic rejuvenation, but rather the sequestration of damaged material away from the developing gametes.

The work described in this thesis, identifies a sequestration event that facilitates the elimination of age-induced cellular damage during gametogenesis. Using time-lapse fluorescence microscopy, we found that protein aggregates, rDNA circles, and a subset of nucleolar proteins are sequestered away from chromosomes during meiosis. Additionally, we found that the generation of plasma membranes is required for the sequestration of nuclear age-associated abnormalities away from the developing gametes. Finally, we observed that the destruction of nuclear age-induced damage is coincident with vacuolar lysis during gamete maturation, which depends on the timely expression of a gamete specific plasma membrane proton pump. Together, these studies uncover novel mechanisms of quality control and provide insight to meiotic cellular rejuvenation.

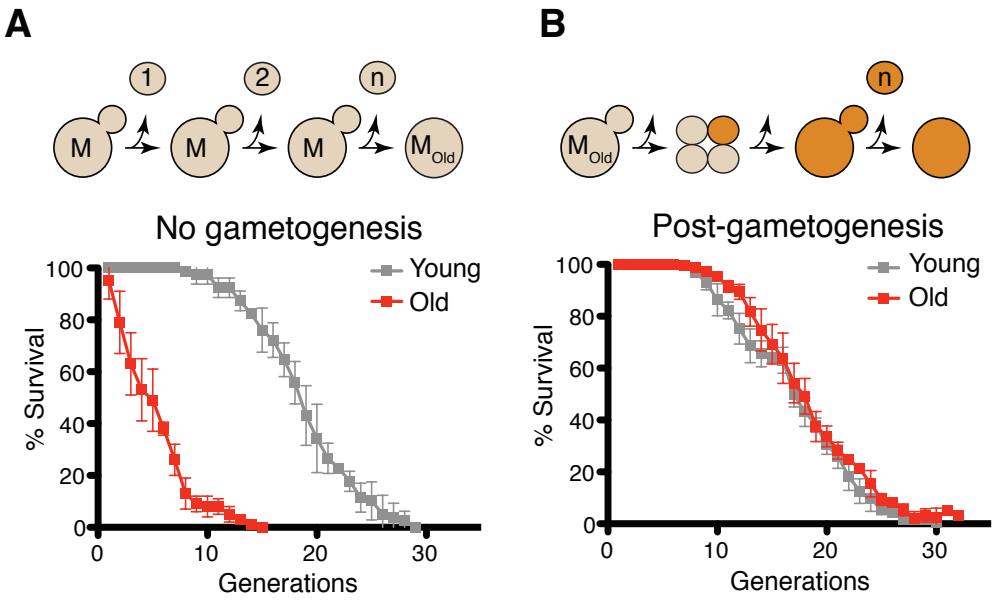

Figure 1.4. Budding yeast gametogenesis resets the aging clock. A. Young diploid cells (mean = 1 generation) exhibit a high mean replicative lifespan (grey graph, mean = 18 generations), while old diploid cells (mean = 13 generations) exhibit a low mean replicative life span (red graph, mean= 5 generations) during mitosis. **B.** Gametes derived from old diploid cells (mean = 13 generations) and young diploid cells (mean = 1 generation) exhibit similar mean replicative lifespans (red and grey graphs, mean = 18 generations for both conditions). Adapted from Unal et al., 2011.

Chapter 2

Nuclear remodeling drives the removal of age-induced damage during meiotic differentiation.

*The following chapter contains material derived from a publication on which I am a co-first author (King and Goodman et al., 2019).

2.1 Introduction

Aging occurs as an organism loses its ability to maintain homeostasis over time. The cellular changes that accompany aging have been most extensively characterized in the budding yeast, *Saccharomyces cerevisiae* (Denoth Lippuner et al., 2014; Kaeberlein, 2010; Longo et al., 2012). Disrupted protein homeostasis results in the accumulation of protein aggregates that contain oxidatively damaged proteins (Aguilaniu et al., 2003; Erjavec et al., 2007). Many organelles exhibit signs of dysfunction: mitochondria fragment and aggregate, mitochondrial membrane potential decreases, and the vacuole becomes less acidic (Henderson et al., 2014; Hughes and Gottschling, 2012; Veatch et al., 2009). Notably, the nucleus also undergoes a number of changes including enlargement of the nucleolus (Lewinska et al., 2014; Morlot et al., 2019; Sinclair et al., 1997), misorganization of nuclear pore complexes (Lord et al., 2015; Rempel et al., 2019), and accumulation of extrachromosomal ribosomal DNA (rDNA) circles (Denoth-Lippuner et al., 2014; Sinclair and Guarente, 1997). Many of the cellular changes that accrue with age are conserved across eukaryotes (Colacurcio and Nixon, 2016; David et al., 2010; Sun et al., 2016; Tiku et al., 2017).

In budding yeast mitosis, age-induced damage is asymmetrically retained by the mother cell resulting in the formation of an aged mother cell and a young daughter cell (Mortimer and Johnston, 1959). In contrast, meiotic cells reset aging symmetrically such that all of the meiotic products are born young, independent of their progenitor's age (Unal et al., 2011). Importantly, senescence factors originally present in the aged precursor cells, including protein aggregates, nucleolar damage, and rDNA circles, are no longer present in the newly formed gametes (Ünal and Amon, 2011; Unal et al., 2011). How gametes avoid inheriting age-associated damage and how this event is coupled to the meiotic differentiation program remains unknown.

Meiotic differentiation, also known as gametogenesis, is a tightly regulated developmental program whereby a progenitor cell undergoes two consecutive nuclear divisions, meiosis I and meiosis II, to form haploid gametes. Meiotic differentiation requires extensive cellular remodeling to ensure that gametes inherit the necessary nuclear and cytoplasmic contents. In yeast gametogenesis, the nucleus undergoes a closed division, with the nuclear

envelope remaining continuous until karyokinesis forms four new nuclei (Moens, 1971; Moens and Rapport, 1971; Neiman, 2011). Mitochondria and cortical endoplasmic reticulum also undergo regulated morphological changes, separating from the cellular cortex and localizing near the nuclear envelope at the transition between meiosis I and II (Gorsich and Shaw, 2004; Miyakawa et al., 1984; Sawyer et al., 2019; Stevens, 1981; Suda et al., 2007). Around the same time, new plasma membranes, also known as prospore membranes, grow from the centrosome-like spindle pole bodies embedded in the nuclear envelope. This directed growth of plasma membrane ensures that nascent nuclei and a fraction of the cytoplasmic contents are encapsulated to form gametes (Brewer et al., 1980; Byers, 1981; Knop and Strasser, 2000; Moens, 1971; Neiman, 1998). Subsequently, the uninherited cellular contents are destroyed by proteases released upon permeabilization of the progenitor cell's vacuole, the yeast equivalent of the mammalian lysosome (Eastwood et al., 2012; Eastwood and Meneghini, 2015). Whether these cellular remodeling events are integral to the removal of age-induced damage has not been characterized.

In this study, we aimed to determine the mechanism by which nuclear senescence factors are eliminated during budding yeast meiosis. Using time-lapse fluorescence microscopy, we found that protein aggregates, rDNA circles, and a subset of nucleolar proteins are sequestered away from chromosomes during meiosis II. Importantly, we show that the core subunits of the nuclear pore complex (NPC) also undergo a similar sequestration process in both young and aged cells. The damaged material localizes to a nuclear envelope-bound compartment containing the excluded NPCs that is eliminated upon vacuolar lysis. Finally, we found that the proper development of plasma membranes is required for the sequestration of core NPCs and senescence factors away from the newly forming gametes. Our study defines a key nuclear remodeling event and demonstrates its involvement in the elimination of age-induced cellular damage during meiotic differentiation.

2.2 Results

2.2.1 Senescence factors are sequestered away from chromosomes with core nucleoporins in meiosis II and subsequently eliminated

To gain a deeper understanding of gametogenesis-induced rejuvenation, we first sought to characterize the meiotic dynamics of age-induced protein aggregates, rDNA circles, and nucleolar damage using time-lapse fluorescence microscopy. To isolate aged cells, we employed a previously established protocol that uses pulse-labeling of cells with biotin followed by harvesting with anti-biotin magnetic beads (Boselli et al., 2009; Smeal et al., 1996). All three types of damage have been reported to localize to the nuclear periphery in aged mitotic cells (Cabrera et al., 2017; Denoth-Lippuner et al., 2014; Saarikangas et al., 2017; Sinclair et al., 1997). Therefore, we monitored

their meiotic localization relative to chromosomes, marked with a fluorescently tagged chromatin protein: either histone H2A (Hta1) or histone H2B (Htb1).

Similar to mitosis, we observed that protein aggregates, visualized by the fluorescently tagged chaperone Hsp104-eGFP (Glover and Lindquist, 1998; Saarikangas et al., 2017), localized to a perinuclear region inside the nucleus prior to the meiotic divisions and in meiosis I **(Figure 2.1B, right panel; Figure A1.1.1)**. In contrast, during meiosis II, the protein aggregates localized away from chromosomes, a phenomenon we termed sequestration (**Figure 2.1A and 2.1C)**. The sequestration was highly penetrant (>99%) and occurred with consistent timing shortly after the onset of anaphase II **(Figure 2.1C).** Subsequently, the aggregates disappeared late in gametogenesis **(Figure 2.1A, right panel)**. By comparison, young cells did not contain any Hsp104-associated aggregates but instead displayed diffuse Hsp104 signal throughout meiosis **(Figure 2.1A, left panel)**. We conclude that age-associated protein aggregates undergo stereotypical sequestration and elimination during meiotic differentiation, suggesting developmentally controlled induction of these events.

We next tested whether the extrachromosomal rDNA circles that accumulate in aged cells displayed a similar behavior. To visualize ribosomal DNA in single cells, we used a strain carrying five tandem copies of the tetracycline operator sequence integrated within each rDNA repeat in one of the two chromosome XII homologs (tetO-rDNA). The strain additionally contained a tetracycline repressor protein fused to GFP (TetR-GFP) under the control of a meiotic promoter (Li et al., 2011). These two modifications, namely the meiosis-restricted expression of TetR-GFP and the heterozygosity of the tetO-rDNA array, did not affect growth rate in vegetative cells. Using this method, we observed that, in aged cells, a substantial fraction of the tetO-rDNA/TetR-GFP signal and a small fraction of the Hta1-mApple signal were sequestered away from the dividing chromosomes after the onset of anaphase II and disappeared during late stages of gamete maturation (**Figure 2.1B- right panel; Figure 2.1D)**. By comparison, in young cells, the gamete nuclei retained the entire tetO-rDNA array and histone-bound chromatin after completion of anaphase II **(Figure 2.1B- left panel)** consistent with previous work (Fuchs and Loidl, 2004; Li et al., 2011). In aged cells carrying TetR-GFP without the tetO-rDNA array, the GFP signal remained diffuse throughout meiosis **(Figure A1.1.2),** confirming that the extrachromosomal GFP puncta were due to sequestered rDNA circles as opposed to TetR-GFP aggregation. These findings demonstrate that, similar to age-associated protein aggregates, extrachromosomal rDNA circles also undergo programmed sequestration and destruction during meiotic differentiation.

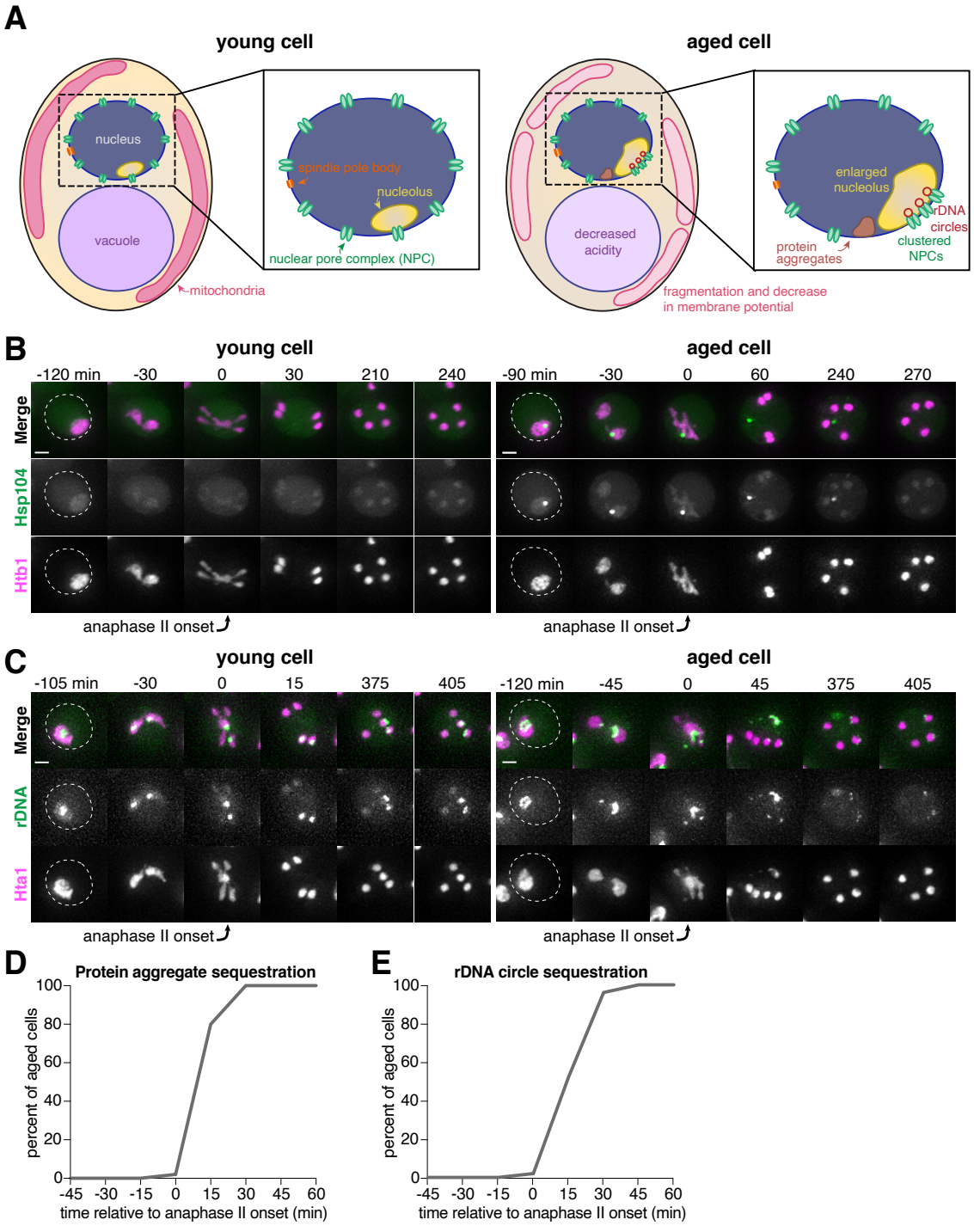
A
young cell
aged cell
nucleus
vacuole
spindle pole body
nucleolus
nuclear pore complex (NPC)
mitochondria
decreased acidity
enlarged nucleolus
rDNA circles
clustered NPCs
protein aggregates
fragmentation and decrease in membrane potential
B
young cell
aged cell
-120 min -30 0 30 210 240
-90 min -30 0 60 240 270
Merge
Hsp104
Htb1
anaphase II onset
anaphase II onset
C
young cell
aged cell
-105 min -30 0 15 375 405
-120 min -45 0 45 375 405
Merge
rDNA
Hta1
anaphase II onset
anaphase II onset
D
Protein aggregate sequestration
percent of aged cells
100 80 60 40 20 0
-45 -30 -15 0 15 30 45 60
time relative to anaphase II onset (min)
E
rDNA circle sequestration
percent of aged cells
100 80 60 40 20 0
-45 -30 -15 0 15 30 45 60
time relative to anaphase II onset (min)

Figure 2.1. Senescence factors are sequestered away from chromosomes in meiosis II and are subsequently eliminated. A. Schematic depiction of a young and aged budding yeast cell. **B.** (left panel) Montage of a young cell (1 generation old) with diffuse Hsp104-eGFP progressing through meiosis (UB9724). (right panel) Montage of an aged cell (7 generations old) containing protein aggregates labeled with Hsp104-eGFP progressing through meiosis (UB9724). Chromosomes were visualized with histone marker Htb1-mCherry. **C.** (left panel) Montage of a young cell (0 generations old) with rDNA repeats, visualized with TetR-GFP binding to tetO arrays in the rDNA repeats, progressing through meiosis (UB17338). (right panel) Montage of an aged cell (9 generations old) containing rDNA circles, visualized with TetR-GFP binding to tetO arrays in the rDNA repeats, progressing through meiosis. (UB17338). Chromosomes were visualized with histone marker Hta1-mApple. For B-C, the time point depicting anaphase II onset was defined as 0 minutes as indicated by the arrows. **D.** Quantification depicting the timing of protein aggregate sequestration relative to the timing of anaphase II onset (median replicative age = 7, mean replicative age = 6.3 ± 1.5, n = 50 cells). **E.** Quantification depicting the timing of rDNA circle sequestration relative to the timing of anaphase II onset (median replicative age = 8, mean replicative age = 8.2 ± 2.4, n = 50 cells). Scale bars, 2 μm.

In addition to rDNA circles, other nucleolar aberrations also accumulate during cellular aging. As a mother cell continues to divide mitotically, factors involved in ribosomal biogenesis are upregulated, leading to the formation of enlarged and fragmented nucleoli (Janssens et al., 2015; Morlot et al., 2019; Sinclair et al., 1997). To visualize nucleoli in more detail, we fluorescently tagged the rRNA processing factor Nsr1 at its endogenous locus (Lee et al., 1992). A previous study found that two other rRNA processing factors, the fibrillarin homolog Nop1 and the high mobility group protein Nhp2, are partially sequestered away from chromosomes during gametogenesis (Fuchs and Loidl, 2004). Nsr1 similarly demonstrated partial sequestration after the onset of anaphase II in young cells **(Figure 2.2A)**. In aged cells, Nsr1 foci appeared enlarged and fragmented prior to the meiotic divisions, consistent with previously reported changes in nucleolar morphology (**Figure 2.2B;** Janssens et al., 2015; Morlot et al., 2019; Sinclair et al., 1997). As in young cells, Nsr1 was sequestered away from chromosomes following the onset of anaphase II and subsequently eliminated **(Figure 2.2B-C**). Interestingly, a significantly higher fraction of the total Nsr1 was sequestered in older cells **(mean = 23% for 0–3 generation-old cells, 36% for 5–8 generation-old cells and 42% for nine or more generation-old cells; Figure 2.2D).** A portion of the histone H2B (Htb1-mCherry) was also sequestered away from the gamete nuclei, reminiscent of the behavior of histone H2A in the GFP-marked rDNA strain. This chromatin demarcation occurred predominantly in aged cells and always co-localized with the sequestered nucleoli. Since the extrachromosomal histone

mass is present in aged cells independent of the GFP-marked rDNA array, the discarded rDNA circles are likely assembled into chromatin, and the extrachromosomal histone signal can be used as a proxy for rDNA circles.

Finally, we analyzed the behavior of protein aggregates with respect to nucleoli and found that both the timing and location of the sequestration event were coincident (**Figure 2.2E-F).** Taken together, these data reveal that distinct types of age-induced damage all undergo a spatiotemporally linked sequestration and elimination process, suggesting a common mode of meiotic regulation.

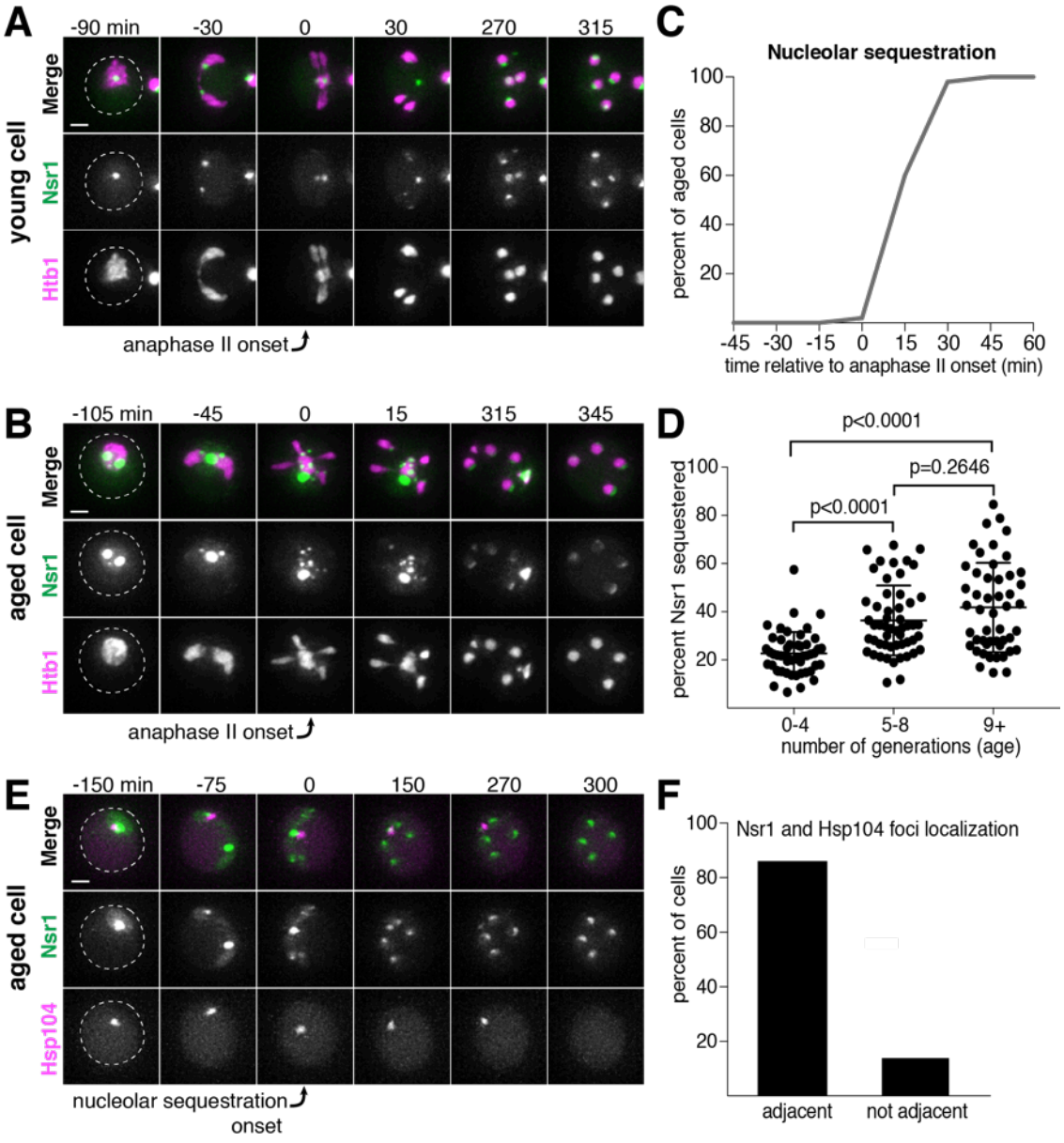

Figure 2.2. Nucleolar material is sequestered away from chromosomes during meiosis II in young and aged cells. A. Montage of a young cell (1 generation old) with the nucleolar tag Nsr1-GFP progressing through meiosis (UB16712). **B.** Montage of an aged cell (9 generations old) containing abnormal nucleolar material, labeled with Nsr1-GFP, progressing through meiosis (UB16712). For A-B, chromosomes were visualized with the histone marker Htb1-mCherry and the time point depicting anaphase II onset was defined as 0 minutes as indicated by the arrows. **C.** Quantification depicting timing of Nsr1 sequestration relative to timing of anaphase II onset (median replicative age = 8, mean replicative age = 7.2 ± 2.4, n = 50 cells). **D.** Quantification depicting the degree of Nsr1 sequestration in cells of different ages (n = 50 for cells with 0-4 doublings, n = 53 for cells with 5-8 doublings, and n = 49 for cells with 9 or more doublings). The Mann-Whitney nonparametric test was used to test statistical significance, and data were generated from two biological replicates. **E.** Montage of an aged cell (9 generations old) with the nucleolus marked by Nsr1-GFP and protein aggregates marked by Hsp104-mCherry progressing through meiosis (UB13299). For E, the time point depicting Nsr1-GFP sequestration was defined as 0 minutes as indicated by the arrow. **F.** Quantification depicting the frequency of sequestered Hsp104-mCherry aggregates localizing adjacent to sequestered Nsr1-GFP (UB13299) immediately after nucleolar segregation (median replicative age = 7, mean replicative age = 6.7 ± 1.5, n = 100 cells). Adjacency was defined as sequestered Nsr1-GFP signal either neighboring or exhibiting partial overlap with sequestered Hsp104-mCherry signal in individual z-sections. Scale bars, 2 μm.

2.2.2 Core nucleoporins exhibit a meiotic behavior similar to senescence factors in young cells

Since nucleolar constituents localize away from dividing chromosomes even in young cells, we reasoned that the sequestration of age-induced nuclear damage might involve a nuclear remodeling event that takes place naturally as part of meiotic differentiation. As a means of assessing nuclear behavior, we sought to characterize the dynamics of nuclear pore complexes (NPCs) during meiosis in young cells.

Nuclear pore complexes are large protein structures that span the nuclear envelope and primarily function in selective nucleocytoplasmic transport. NPCs contain multiple copies of at least 30 distinct types of proteins termed nucleoporins. Nucleoporins are organized into different subcomplexes with distinct structural roles (Beck and Hurt, 2017; Kim et al., 2018). Intriguingly, one nucleoporin, Nsp1, has been previously shown to localize away from chromosomes in meiosis II (Fuchs and Loidl, 2004). Using time-lapse microscopy, we surveyed the meiotic dynamics and localization of 17 different

endogenously GFP-tagged nucleoporins representing different subcomplexes **(Figure 2.3A).** We found that majority of nucleoporins, including those most integral to the NPC structure, exhibited sequestration and elimination similar to age-induced damage. The nucleoporins localized to the nuclear periphery before the meiotic divisions and during meiosis I, but largely localized away from chromosomes after the onset of anaphase II (**Figure 2.3B-F, Figure A1.2.1-5**). Although a large fraction of the nucleoporins persisted away from the chromosomes, some nucleoporins re-appeared around the gamete nuclei, either by de novo synthesis or return of the pre-existing pool. Several hours after the meiotic divisions, any remaining nucleoporin signal outside of the gamete nuclei abruptly disappeared (**Figure 2.3B-F, Figure A1.2.1-5**)

Interestingly, the nucleoporins from one subcomplex, the nuclear basket, exhibited a markedly different behavior: although briefly localizing outside of the developing nuclei during anaphase II along with the nucleoporins from other subcomplexes, they largely returned to the nascent nuclei within 30 min **(Figure 2.3G-H, Figure A1.2.6).** The simplest interpretation of these findings was that the nuclear basket detached from the rest of the NPC during meiosis II. Given that all other NPC subcomplexes tested persist outside of developing nuclei, we propose that intact NPCs without nuclear baskets are left outside of gamete nuclei.

Since senescence factors and NPCs were sequestered with similar timing, we next asked whether they were sequestered to a similar location. We monitored the localization of protein aggregates, rDNA circles, and sequestered nucleolar material relative to NPCs and found that they co-localize with the sequestered NPCs after the onset of anaphase II **(Figure 2.4A-C; Figure A1.3.1-2).** These results suggest that a common nuclear remodeling event is responsible for the spatial separation of various nuclear components from the dividing chromosomes.

2.2.3 Sequestered nuclear material localizes to a nuclear envelope-bound compartment

The nuclear envelope remains continuous during budding yeast meiosis, dynamically changing shape to accommodate the chromosomal divisions (Moens, 1971; Moens and Rapport, 1971). After the second meiotic division, karyokinesis occurs to form the nascent nuclei of the four gametes. Given the abrupt change in NPC distribution during anaphase II, we sought to determine how other nuclear membrane proteins behave during this time. We found that the integral LEM-domain protein Heh1 (Gene ID: 854974) and a generic inner nuclear membrane (INM) marker, eGFP-h2NLS-L-TM, localized to both nascent gamete nuclei and the sequestered NPCs during anaphase II (**Figure 2.5A—B, Figure A1.4.1;** King et al., 2006; Meinema et al., 2011), suggesting the existence of a separate membranous compartment.

We next performed serial section transmission electron microscopy (TEM) to observe this compartment directly. Reconstructions of individual cells, either during anaphase II or during gamete development, confirmed the existence of nuclear envelope-bound space outside of the four nuclei **(Figure 2.5C-D).** The compartment seemed deformed in comparison to the nascent gamete nuclei in that the nuclear envelope membrane structure appeared abnormal and the compartment was often fragmented into multiple nuclear envelope-bound regions (**Figure 2.5C-F)**. These regions were located outside of the gamete plasma membranes, also known as prospore membranes **(Figure 2.5C-D).** Importantly, individual sections showed that the compartment contained nucleolar material and NPCs (**Figure 2.5E-F, Figure A1.4.2)**. We conclude that, during meiosis II, the nuclear envelope undergoes a five-way division to form the four nuclei and a separate compartment containing discarded nuclear proteins.

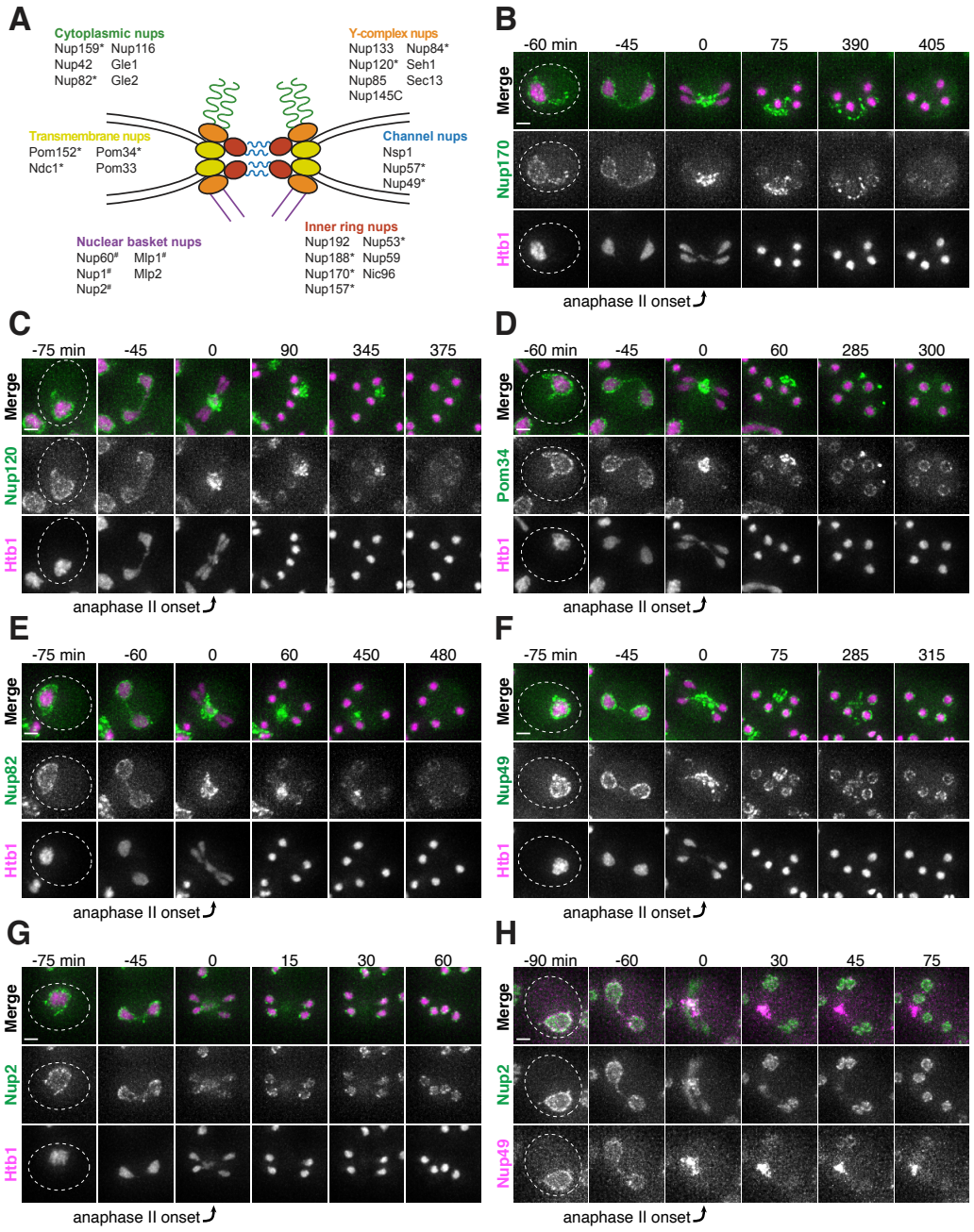

Figure 2.3. Nucleoporins from the core of the nuclear pore complex, but not the nuclear basket, are sequestered away from chromosomes during meiosis II and subsequently eliminated in young cells. **A.** A schematic depicting the different nucleoporins and subcomplexes that comprise the nuclear pore complex (NPC). Nup100 and Nup145N are not included in the schematic since they represent linkers between different subcomplexes. Nomenclature and organization are from Beck and Hurt, 2017; the schematic itself is adapted from Rajoo et al., 2018. Nucleoporins marked with an asterisk are sequestered away from chromosomes; nucleoporins marked with a pound sign return to dividing nuclei. For each nucleoporin, the observed phenotype

was observed in all tetrads examined (n ≥ 25 tetrads). **B-G.** Montages of cells with tagged nucleoporins from each subcomplex progressing through meiosis. Chromosomes were visualized with the histone marker Htb1-mCherry, and the first time point depicting anaphase II was defined as 0 minutes as indicated by the arrows. **B.** Nup170-GFP, an inner ring complex nucleoporin (UB11513) **C.** Nup120-GFP, a Y-complex nucleoporin (UB13499) **D.** Pom34-GFP, a transmembrane nucleoporin (UB13503) **E.** Nup82-GFP, a cytoplasmic nucleoporin (UB14652) **F.** Nup49-GFP, a channel nucleoporin (UB13509) **G.** Nup2-GFP, a nuclear basket nucleoporin (UB15305) **H.** Montage depicting localization of Nup2-GFP, a nuclear basket nucleoporin, and Nup49-mCherry, a channel nucleoporin (UB15672). Scale bars, 2 μm.

2.2.4 Core nucleoporins and senescence factors are excluded from developing gametes during meiosis II

The TEM analyses showed that the nuclear envelope-bound compartment localized outside of the developing gamete plasma membranes (**Figure 2.5C-D**). It remained unclear, however, how the material was sequestered into this compartment. At least two models could explain how the material was left outside of the nascent gametes: (1) the material was being 'extruded,' removed from the gamete after initial entry, or (2) 'excluded,' never entering the nascent gametes. To differentiate between these models, we analyzed the localization of a gamete-specific plasma membrane (PM) marker, yeGFP-Spo20$^{51-91}$ (Nakanishi et al., 2004), relative to NPCs and chromosomes. We found that, throughout anaphase II, a sequestered mass of nucleoporins was constrained to a region immediately outside of the nascent plasma membranes and never appeared inside **(Figure 2.6A).** The lip of the developing plasma membranes marked by Don1-GFP neatly delineated the boundary of the NPC mass **(Figure 2.6A-B).** Live-cell microscopy confirmed that the NPCs remained outside of nascent plasma membranes throughout their development, supporting 'exclusion' as the means by which nuclear material remained outside of the developing gametes (**Figure A1.5.1-2**).

To determine if senescence factors were similarly excluded, we monitored the localization of protein aggregates and nucleolar material relative to the gamete plasma membranes. This analysis revealed that age-induced damage almost never entered into the newly forming gametes **(Figure 2.6C, Figure A1.5.3)**. Only one out of several hundred gametes inherited the Hsp104-associated protein aggregates **(Figure 2.6D)**; strikingly, this Hsp104 punctum persisted after gamete maturation, suggesting that the elimination of age-associated damage is dependent on its prior exclusion. These results highlight the existence of an active mechanism in meiotic cells that precludes the inheritance of NPCs and senescence factors by the nascent gametes.

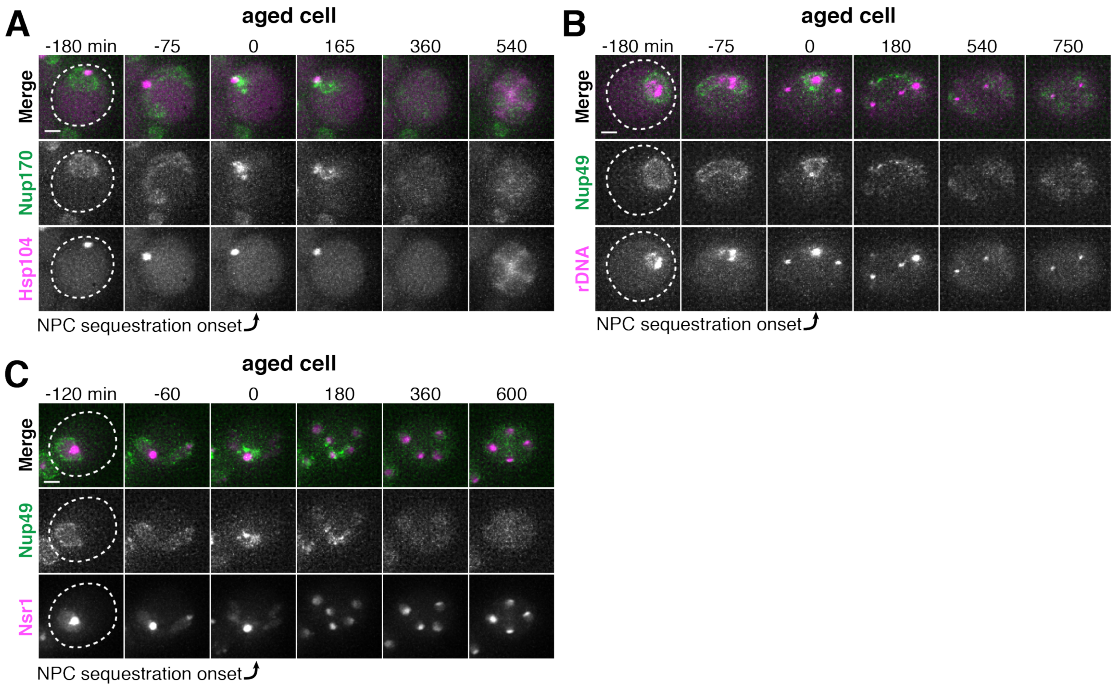

Figure 2.4. Age-dependent nuclear damage is sequestered with disposed NPCs during anaphase II. A. Montage of an aged cell (7 generations old) with protein aggregates, labeled with Hsp104-mCherry, and NPCs, labeled Nup170-GFP, progressing through meiosis (UB12975). **B.** Montage of an aged cell (9 generations old) with rDNA circles, marked by TetR-GFP binding to tetO arrays in the rDNA repeats, and NPCs, labeled with Nup49-mCherry, progressing through meiosis (UB17532). **C.** Montage of an aged cell (7 generations old) with abnormal nucleolar material, marked by Nsr1-GFP, and NPCs, marked by Nup49-mCherry, progressing through meiosis (UB16708). The first time point depicting NPC sequestration was defined as 0 minutes as indicated by the arrows. Scale bar, 2 μm.

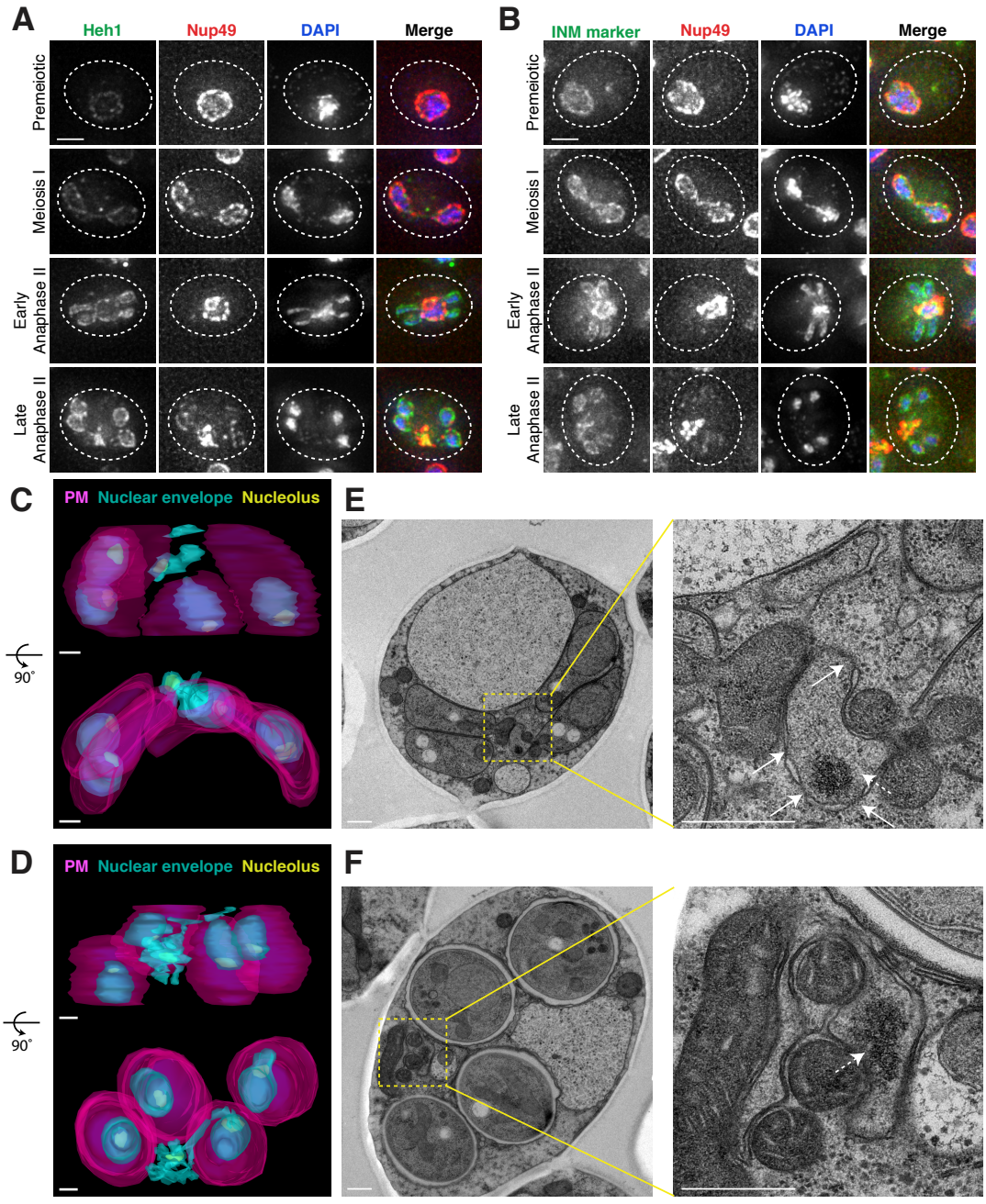

Figure 2.5. Nucleoporins are sequestered to a nuclear envelope-bound compartment during meiosis II. A-B. Maximum intensity projections of fixed young cells depicting the localization of inner nuclear membrane proteins – **A.** Heh1-3xeGFP (UB14391) and **B.** the synthetic construct eGFP-h2NLS-L-TM from (Meinema et al., 2011; UB12932) – relative to the nucleoporin Nup49-mCherry and DAPI. Scale bars, 2 µm. **C-D.** Reconstructions of **C.** a young late anaphase II cell and **D.** a young post-meiosis II cell from 70 nm serial TEM

micrographs (UB11513). Gamete plasma membranes are depicted in magenta, the nuclear envelope is depicted in cyan, and nucleoli are depicted in yellow. Scale bars, 0.5 µm. **E-F.** Electron micrographs of **E.** a young late anaphase II cell and **F.** a young post-meiosis II cell with insets depicting the nuclear envelope-bound region outside the gamete plasma membranes (UB11513). Solid arrows indicate NPCs; dashed arrows indicate nucleolar mass. Note that the electron micrographs in panel F come from the cell reconstructed in panel D. Scale bars, 0.5 µm.

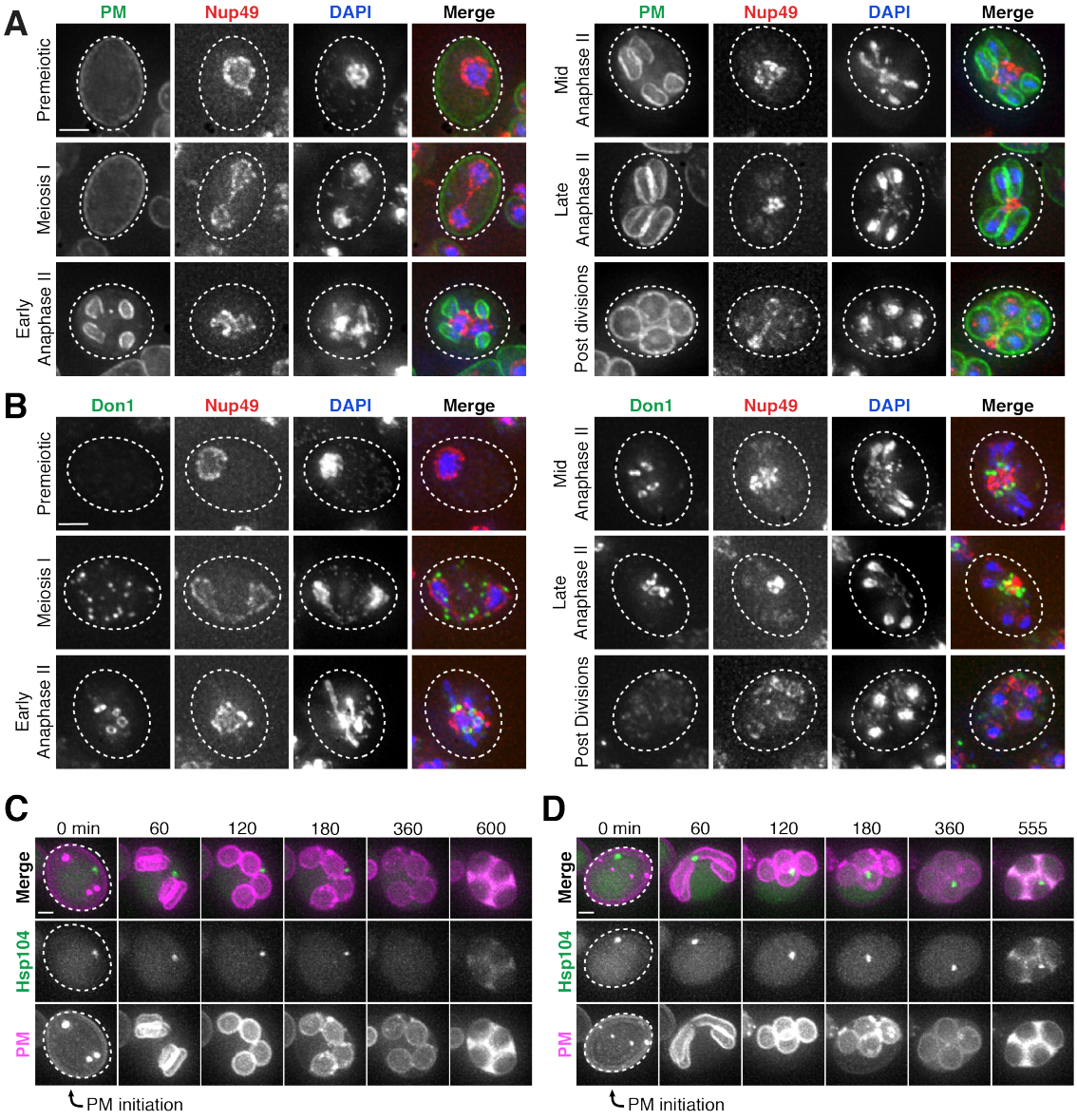

Figure 2.6. Core nucleoporins and age-dependent damage are excluded from developing gametes during meiosis II. A. Maximum intensity projections over 6 µm of fixed young cells depicting localization of the gamete plasma membrane marker yeGFP-Spo20$^{51-91}$ relative to the nucleoporin Nup49-mCherry and DAPI (UB12342). **B.** Maximum intensity projections over 8 µm of fixed young cells depicting localization of the leading edge complex tag Don1-GFP relative to the nucleoporin Nup49-mCherry and DAPI (UB12436). **C-D.** Montages of cells with a protein aggregate tag, Hsp104-mCherry, and a marker of the gamete plasma membrane, yeGFP-Spo20$^{51-91}$ (UB11821). **C.** An aged cell (6 generations old) that excluded its protein aggregate from developing gametes. **D.** An aged cell (6 generations old) that failed to exclude its protein aggregate from developing gametes. The first time point depicting gamete plasma membrane nucleation was defined as 0 minutes as indicated by the arrows. Scale bars, 2 µm.

2.2.5 Elimination of excluded nuclear material coincides with vacuolar lysis

Following gamete formation, permeabilization of the precursor cell's vacuolar membrane causes the release of proteases, which degrade the cellular contents left in the precursor cell cytosol in a process termed mega-autophagy (Eastwood et al., 2012; Eastwood and Meneghini, 2015). To determine whether mega-autophagy was responsible for the degradation of the excluded nuclear material, we monitored the disappearance of NPCs and age-associated protein aggregates relative to the lysis of the vacuolar membrane as monitored by either Vph1-eGFP or Vph1-mCherry. We found that both events coincided with the onset of vacuolar lysis **(Figure 2.7A-D)**. To further assess nucleoporin degradation, we measured the protein levels of GFP-tagged Nup84 and Nup170 by immunoblotting **(Figure 2.7E-F**). Since GFP is relatively resistant to vacuolar proteases, degradation of tagged proteins leads to the accumulation of free GFP (Kanki and Klionsky, 2008). We found that free GFP accumulated in wild-type cells 12 hours after meiosis induction, consistent with vacuolar proteases driving the elimination of Nup84 and Nup170 **(Figure 2.7E-F)** Importantly, we confirmed that the degradation of both nucleoporins depends on the meiotic transcription factor Ndt80. Ndt80 is a master transcription factor necessary for the meiotic divisions and gamete maturation (Xu et al., 1995). In the absence of *NDT80*, cells exhibit a prolonged arrest during prophase I and fail to undergo vacuolar lysis (Eastwood et al., 2012). Altogether, these analyses highlight mega-autophagy as the probable degradation mechanism for NPCs and nuclear senescence factors.

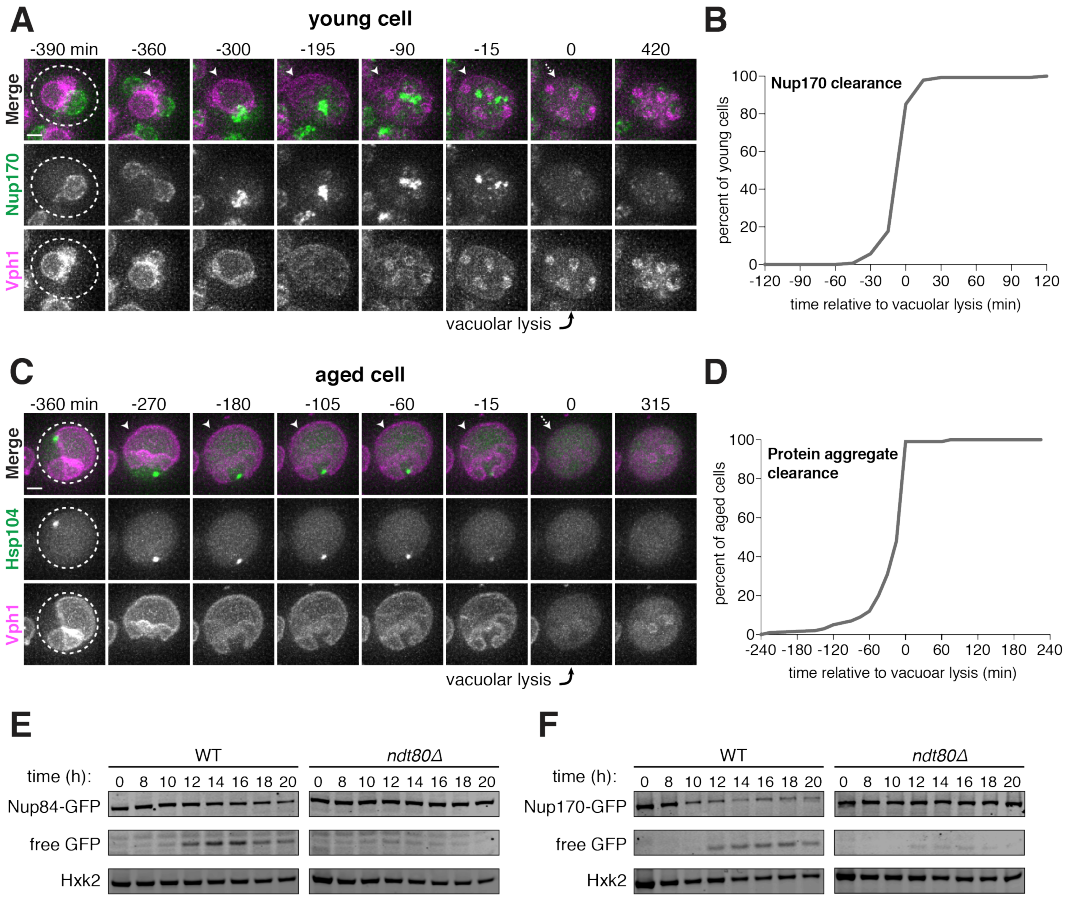

Figure 2.7. Core nucleoporins and protein aggregates are turned over coincident with vacuolar lysis. A. Montage of a young cell with an inner ring complex nucleoporin tag, Nup170-GFP, and a marker for the vacuole, Vph1-mCherry (UB15890). Images are maximum intensity projections over 6 µm; the first time point depicting vacuolar lysis was defined as 0 minutes as indicated by the arrow. **B.** Quantification of the experiment in panel A. Timing of the excluded Nup170-GFP clearance relative to vacuolar lysis (n = 141 cells). **C.** Montage of an aged cell (8 generations old) with a protein aggregate tag, Hsp104-mCherry, and a marker for the vacuolar membrane, Vph1-eGFP (UB12163). Images are maximum intensity projections over 8µm; the first time point depicting vacuolar lysis was defined as 0 minutes as indicated by the arrow. **D.** Quantification of the experiment in panel C. Timing of excluded Hsp104-mCherry clearance relative to vacuolar lysis (median replicative age = 6, mean replicative age = 5.9 ± 1.5, n = 100 cells). For panels A and C, solid arrows indicate the intact vacuolar membrane of mother cell and dashed arrows indicate vacuolar permeabilization. For panels B and D, vacuolar lysis was scored as the time of vacuolar membrane disappearance. Scale bars, 2 µm. Immunoblot assay measuring degradation of **E.** Nup84-GFP in wild type (UB13497) and *ndt80Δ* cells (UB19929) **F.** Nup170-GFP in wild type

(UB11513) and *ndt80Δ* cells (UB19927). Hxk2 levels were measured as a loading control.

2.2.6 Sequestration of nuclear pore complexes requires gamete plasma membrane development

What drives the nuclear remodeling event in meiotic cells? Given that the boundaries of the excluded NPC mass co-localize with the rims of developing gamete plasma membranes **(Figure 2.6B)**, we posited that plasma membrane development itself was required for NPC sequestration. To test this hypothesis, we monitored NPC localization in mutants with disrupted plasma membrane formation. Plasma membrane development is initiated from the cytoplasmic face of the spindle pole body, which is converted from a microtubule-nucleation center to a membrane-nucleation center during meiosis II (Knop and Strasser, 2000). *SPO21* (also known as *MPC70*) is required for this conversion event, and its deletion completely inhibits de novo plasma membrane formation (Knop and Strasser, 2000). We found that, in *spo21Δ* cells, nucleoporins remained around chromosomes during anaphase II instead of being sequestered away **(Figure 2.8A-B**).

As an independent test of the role of plasma membrane development in NPC remodeling, we perturbed plasma membrane development by an orthogonal method. The formation of fewer than four plasma membranes can be induced by low carbon conditions, since carbon concentration affects the conversion of the spindle pole body into a membrane nucleator (Davidow et al., 1980; Okamoto and Iino, 1981; Taxis et al., 2005). Under such conditions, we found that the gamete nuclei displayed reciprocal localization of plasma membranes and NPCs: only the nuclei that were devoid of plasma membranes were enriched for NPCs **(Figure 2.8C–E)**. This was consistent with the observation that, even in high carbon conditions, cells fated to form three or two mature gametes would often have one or two nuclei enriched for NPCs, respectively (**Figure 2.8B).**

Finally, we examined how defects in leading edge complex formation, the structure that forms at the rim of the developing plasma membranes, affect NPC sequestration. Specifically, the absence of the organizing member Ssp1 or simultaneous deletion of the Ady3 and Irc10 subunits results in the formation of misshapen plasma membranes (Lam et al., 2014; Moreno-Borchart et al., 2001). We found that both *ssp1Δ* and *ady3Δ irc10Δ* cells had defective NPC sequestration, with NPCs often remaining partially around anaphase II nuclei **(Figure 2.8F; Figure A1.6.1-2).** The boundary of NPC removal from the nuclei was marked by constrictions in the DAPI or histone signal and corresponded to the extent of plasma membrane formation **(Figure 2.8F; Figure A1.6.1-2).** Taken together, these data support the conclusion that NPC sequestration and

exclusion are driven by the development of plasma membranes around nascent gamete nuclei.

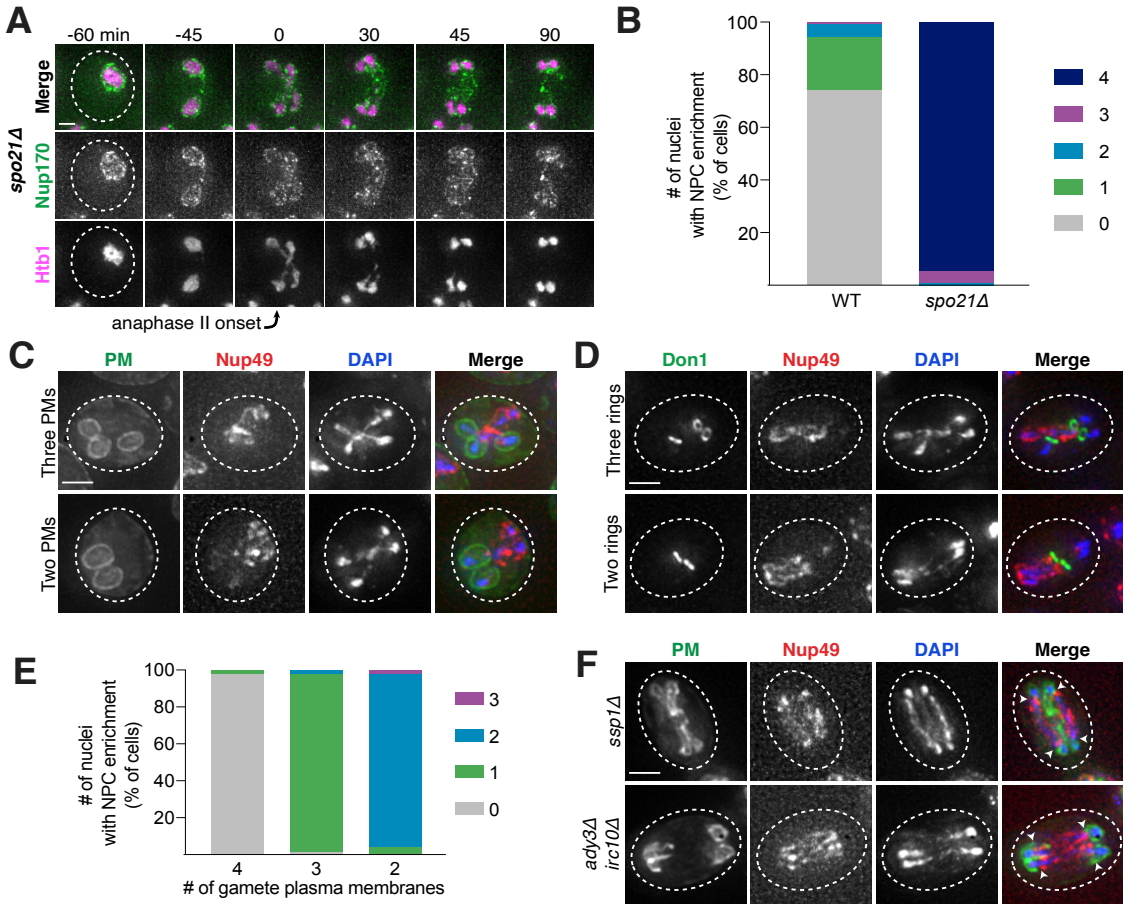

Figure 2.8. Gamete plasma membrane development is necessary for nucleoporin sequestration. A. Montage of inner ring complex nucleoporin Nup170-GFP localization relative to Htb1-mCherry in a young *spo21Δ* cell (UB13377). The first time point depicting anaphase II was defined as 0 minutes as indicated by the arrow. **B.** Quantification of the experiment in panel A for *spo21Δ* and Figure 2.3B for WT. Number of nuclei enriched for nucleoporins following anaphase II in WT or *spo21Δ* cells (n = 108 cells for WT, n = 118 cells *spo21Δ*). **C-D.** Maximum intensity projections of fixed young cells depicting **C.** gamete plasma membrane yeGFP-Spo20$^{51-91}$ (UB12342) or **D.** leading edge Don1-GFP (UB12436) localization relative to nucleoporin Nup49-mCherry localization in low-carbon conditions that promoted the formation of fewer than four gamete plasma membranes. **E.** Quantification of the experiment in panel C. Number of nuclei enriched for nucleoporins following anaphase II in cells with variable numbers of gamete plasma membranes (4 PSMs: n = 48; 3 PSMs: n = 80; 2 PSMs: n = 46). **F.** Maximum intensity projections of fixed

young cells showing gamete plasma membrane (yeGFP-Spo20$^{51-91}$) and nucleoporin (Nup49-mCherry) localization in mutants defective in leading edge complex formation, *ssp1Δ* (UB13473) or *ady3Δ irc10Δ* (UB13583). Arrowheads on merged images denote location of DAPI constrictions. Scale bars, 2 μm.

2.2.7 Sequestration of senescence factors requires proper plasma membrane development

Since the sequestration of NPCs and nuclear senescence factors were spatially and temporally coupled, we reasoned that a common mechanism could mediate both events. We therefore monitored the sequestration of protein aggregates in *spo21Δ* cells, which are defective in NPC sequestration. In comparison to wild-type cells, we found that *spo21Δ* mutants exhibited a dramatic increase in the association of protein aggregates with chromosomes during anaphase II (**48% vs. 0%; Figure 2.9A-B)**. Regardless of whether or not the protein aggregate was sequestered away from chromosomes in *spo21*Δ cells, the protein aggregates always co-localized with the nuclear envelope, as marked by NPCs (**Figure A1.7.1)**. Thus, without the nascent plasma membranes, protein aggregates appeared randomly distributed along the nuclear periphery.

We next assessed how nucleolar sequestration is affected in young *spo21Δ* cells. We found that in 39% of *spo21Δ* cells, nucleoli failed to be sequestered in meiosis II and instead co-segregated with chromosomes **(Figure 2.9C–D)**. In contrast, none of the wild-type cells displayed this behavior. Furthermore, Nsr1 remained co-localized to the nuclear envelope in *spo21Δ* cells in a similar manner to protein aggregates (**Figure A1.7.2).** Altogether, these findings support the notion that meiotic exclusion of age-induced protein aggregates and nucleolar material is coupled to a nuclear remodeling event that is driven by gamete plasma membrane formation.

2.3 Discussion

This study defines a meiotic quality control mechanism that eliminates nuclear senescence factors in budding yeast. In an aged precursor cell, many of its nuclear contents, including nuclear pore complexes, rDNA circles, nucleolar proteins and protein aggregates, are sequestered in a membranous compartment away from the chromosomes that are destined for future gametes **(Figure 2.10)**. The discarded compartment and its contents are eliminated upon programmed lysis of the vacuole, an organelle functionally equivalent to the lysosome. We further show that de novo plasma membrane growth is required for the sequestration of nuclear material **(Figure 2.10)**. Together, our findings define a meiosis-specific nuclear remodeling event that physically separates age-induced cellular damage away from gametes and highlights its role in cellular rejuvenation.

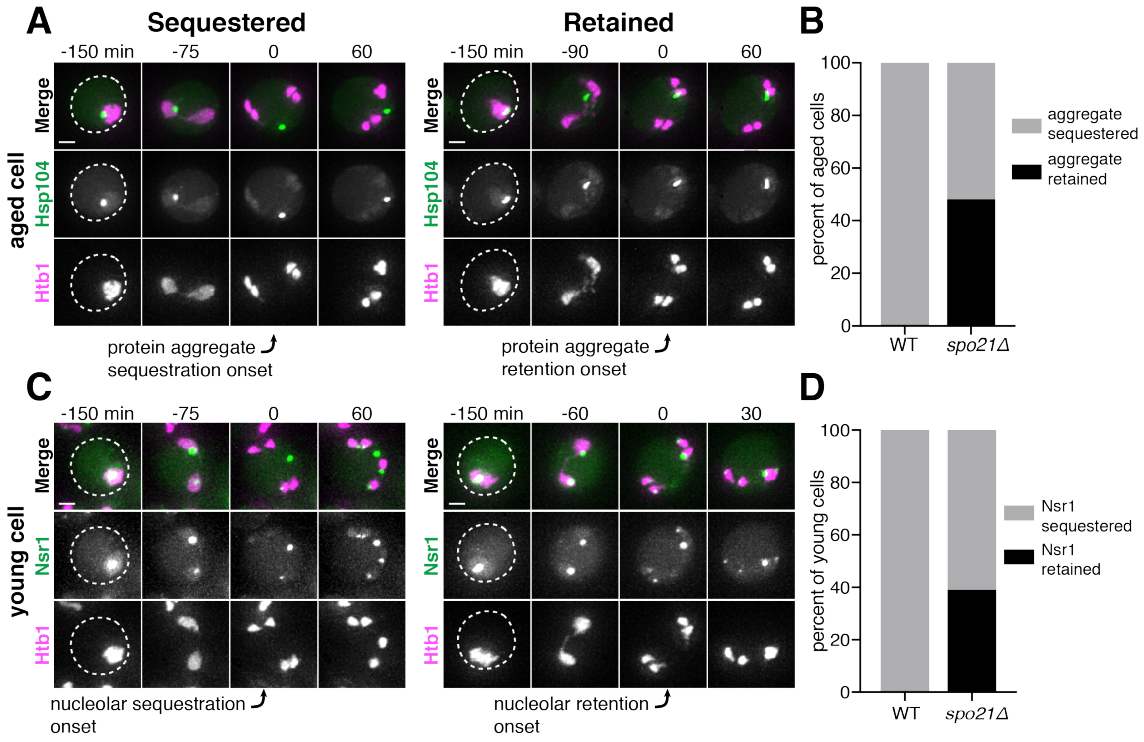

Figure 2.9. **Protein aggregate and nucleolar sequestration is coupled to NPC sequestration via gamete plasma membrane development. A.** Montages of aged *spo21Δ* cells in which protein aggregates marked by Hsp104-eGFP were either (left panel) sequestered away from (5 generations old) or (right panel) retained by (6 generations old) chromosomes during anaphase II (UB14418). **B.** Quantification of protein aggregate retention in aged WT (UB9724) and *spo21Δ* cells (UB14418). Median replicative age = 7, mean replicative age = 6.5 ± 1.5, n = 100 for WT cells; median replicative age = 6, mean replicative age = 6.2 ± 1.2, n = 100 for *spo21Δ* cells. **C.** Montages of young *spo21Δ* cells in which nucleolar material was either (left panel) sequestered away from or (right panel) retained by chromosomes during anaphase II (UB 14419). **D.** Quantification of Nsr1 retention in young WT (UB15118) and *spo21Δ* cells (UB14419). n = 100 for WT cells, n = 100 for *spo21Δ* cells. For A and C, chromosomes were visualized with the histone marker Htb1-mCherry. For A, the first time point depicting protein aggregate sequestration or retention was defined as 0 minutes as indicated by the arrows. For C, the first time point depicting nucleolar sequestration or retention was defined as 0 minutes as indicated by the arrows. Scale bars, 2 μm.

2.3.1 Selective inheritance of nuclear contents during meiotic differentiation

We found that a subset of nuclear components are sequestered away from chromosomes during anaphase II: core nucleoporins, nucleolar proteins involved in rRNA transcription and processing, extrachromosomal rDNA circles, and protein aggregates. However, other nuclear proteins – including histones, the rDNA-associated protein Cfi1, and the Ran exchange factor Prp20 – are largely retained with dividing nuclei during anaphase II (data not shown). A more thorough cataloging of nuclear components is needed to identify parameters that differentiate excluded nuclear material from retained nuclear material. Strong association with chromatin, as in the case for histones, Cfi1 and Prp20, may be one way to mediate the selective inheritance of nuclear proteins into gametes (Aebi et al., 1990; Dilworth et al., 2005; Li et al., 2003; Straight et al., 1999). On the other hand, strong association with NPCs may facilitate sequestration – for example, extrachromosomal rDNA circles have been shown to interact with NPCs in mitotic cells (Denoth-Lippuner et al., 2014).

It is currently unclear whether a mechanism exists to enrich for damaged proteins in the sequestered pool, such that any proteins remaining with the gamete nuclei are preferentially undamaged. Since some nucleoporins and nucleolar proteins are sequestered and eliminated in young cells, it is likely that undamaged proteins are destroyed during meiosis for reasons that are yet to be determined. However, the observation that the fraction of discarded nucleolar proteins is higher in aged cells than young cells is consistent with the possibility that damaged nucleolar proteins are selectively enriched in the sequestered material. Since both nucleolar proteins and NPCs have been shown to accumulate age-related damage (Denoth-Lippuner et al., 2014; Lord et al., 2015; Rempel et al., 2019; Sinclair et al., 1997; Morlot et al., 2019), selective elimination and subsequent de novo synthesis could be vital to ensuring gamete rejuvenation.

Unexpectedly, we found that nuclear basket nucleoporins dissociate from the rest of the nuclear pore complex and remain with nascent nuclei during meiosis II. Consistent with this finding, nuclear basket nucleoporins have been shown to be more dynamic than core nucleoporins (Denning et al., 2001; Dilworth et al., 2001; Niepel et al., 2013) and sub-populations of NPCs without certain nuclear basket nucleoporins are present near the nucleolus (Galy et al., 2004). We propose that the nuclear basket segregates with gamete nuclei through re-association with chromatin, which in turn facilitates the formation of new NPCs. In both the fungus *Asperilligus nidulans* and vertebrates, the nuclear basket nucleoporin Nup2 and its metazoan ortholog Nup50 associate with dividing chromatin during mitosis and contribute to the segregation of NPCs into daughter nuclei (Dultz et al., 2008; Markossian et al., 2015; Suresh et al., 2017). The nuclear basket nucleoporins Nup1 and Nup60 have innate

membrane binding and shaping capabilities, making them attractive candidates to initiate insertion of new NPCs (Mészáros et al., 2015). Indeed, deletion of non-essential nuclear basket nucleoporins results in reduced sporulation efficiency and impaired gamete viability, supporting an important functional role during the meiotic program (Chu et al., 2017).

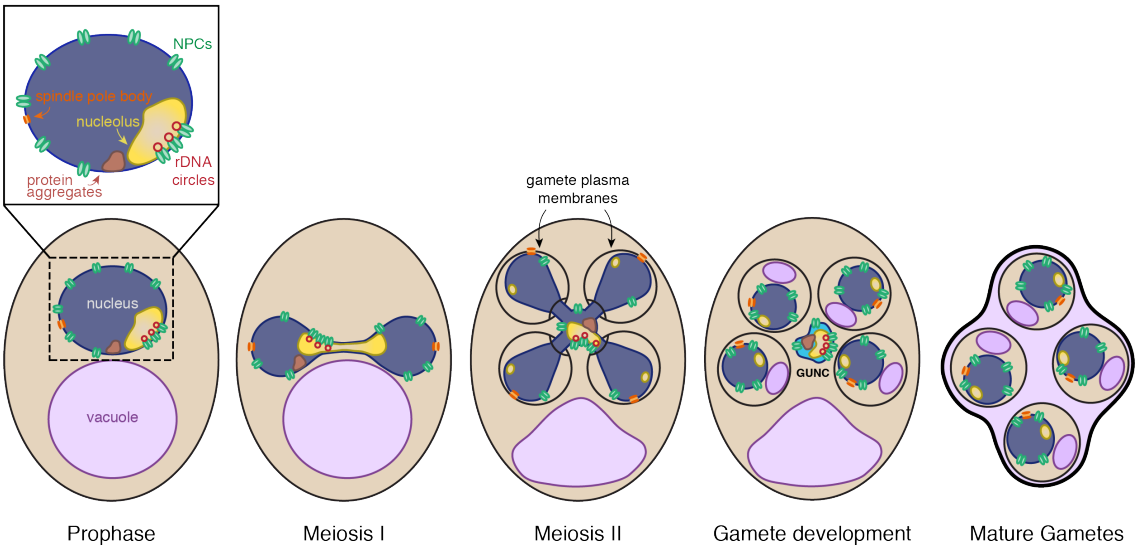

Figure 2.10. Nuclear rejuvenation during meiosis. Aged yeast cells accumulate nuclear damage including extrachromosomal rDNA circles (red), nuclear-associated protein aggregates (brown), abnormal and enlarged nucleoli (yellow), and damaged long-lived proteins including nucleoporins (green). During meiosis II, a nuclear envelope-bound compartment containing much of this age-associated damage is formed and remains outside of the developing gametes. The material in the GUNC is turned over coincident with vacuolar lysis, completing rejuvenation of the gamete nuclei. Sequestration of the age-dependent damage away from gamete nuclei requires proper gamete plasma membrane development during anaphase II.

2.3.2 Formation of gamete plasma membranes is required for the sequestration of nuclear material

We found that gamete plasma membrane formation is required for the selective sequestration of nuclear contents. When plasma membrane development is prevented, NPCs are retained and age-induced damage becomes randomly distributed along the nuclear periphery. The mechanism by which the newly forming plasma membrane creates distinct nuclear envelope domains inside

and outside of developing gametes remains unclear. A direct physical blockade, while possible, seems unlikely given that large organelles such as mitochondria enter through the rims of developing plasma membranes (Byers, 1981; Suda et al., 2007). On the other hand, the sequestration boundary at the leading edge is reminiscent of the outer nuclear envelope lateral diffusion barrier that forms at the bud neck during budding yeast mitosis (Caudron and Barral, 2009; Clay et al., 2014). In this context, septins localize to the bud neck and organize a signaling cascade, generating a sphingolipid region in the nuclear envelope that constrains the movement of nuclear envelope proteins (Clay et al., 2014). In meiosis, deletion of meiosis-specific septins (*spr3Δ* and *spr28Δ*; De Virgilio et al., 1996; Fares et al., 1996; Ozsarac et al., 1995) and leading edge complex components (*ady3Δ*, *irc10Δ*, and *don1Δ*; Knop and Strasser, 2000; Lam et al., 2014; Moreno-Borchart et al., 2001) does not grossly alter NPC or protein aggregate sequestration, beyond impacting plasma membrane morphology **(Figure 2.8F; Table A1.1).** However, an unidentified scaffold might exist to organize a nuclear envelope diffusion barrier. Determining the mechanism by which gamete plasma membranes sequester nuclear material will reveal important principles of nuclear organization and compartmentalization.

After the sequestration event, core nucleoporins begin to re-appear around nascent gamete nuclei, either by de novo synthesis or return from the sequestered mass. This raises the intriguing possibility that some core nucleoporins may be able to overcome the physical or diffusion barrier imposed by the plasma membrane. In mitosis, an active transmission mechanism involving the nucleoporin Nsp1 is required for NPCs to pass the bud neck diffusion barrier and enter into daughter cells (Colombi et al., 2013; Makio et al., 2013). Whether any factors facilitate selective NPC inheritance into gametes during meiosis II is an important direction for future studies. Further, daughter-inherited NPCs are modified by the deacetylase Hos3 as they pass through the bud neck, resulting in the formation of a daughter nucleus with distinct cell-cycle behaviors from the mother nucleus (Kumar et al., 2018). Transmission through the leading edge of the gamete plasma membrane might similarly provide an opportunity for any inherited NPCs to acquire gamete-specific modifications and functions. Further characterizing the reintegration of core nucleoporins at the gamete nuclear periphery will improve our understanding of how NPC remodeling contributes to gamete fitness.

2.3.3 A five-way nuclear division facilitates the subsequent elimination of discarded nuclear material by vacuolar lysis

The sequestration of nuclear damage into a membranous compartment outside of gametes makes it accessible to the degradation machinery active in the progenitor cell cytoplasm during gamete maturation. Due to the strong correlation between the timing of vacuolar lysis and the disappearance of sequestered material as well as the meiosis-specific vacuolar degradation of

nucleoporins, we propose that mega-autophagy is responsible for the elimination of nuclear senescence factors (Eastwood et al., 2012; Eastwood and Meneghini, 2015). The release of proteases from the vacuole could eliminate protein aggregates and other sequestered nuclear proteins, as has already been observed for unsuccessfully packaged nuclei (Eastwood et al., 2012). Another mechanism, however, is necessary for the elimination of rDNA circles. The endonuclease G homolog, Nuc1, is released from mitochondria during mega-autophagy and therefore could be responsible for the elimination of rDNA circles (Eastwood et al., 2012).

2.3.4 Nuclear remodeling as a driver of gamete health and rejuvenation

Our study highlights a mechanism that facilitates the elimination of age-induced damage during meiosis. Given that extensive nuclear remodeling occurs even in young cells, the reorganization of the nuclear periphery appears to be integral to gamete fitness. Importantly, the sequestration of NPCs in budding yeast meiosis is similar to a NPC reorganization event observed in the spermatogenesis of metazoans, including humans (Fawcett and Chemes, 1979; Ho, 2010; Troyer and Schwager, 1982). In this context, acrosome formation, potentially akin to gamete plasma membrane formation, corresponds to the redistribution of nuclear pores to the caudal end of the nucleus, coincident with chromatin condensation and elimination of un-inherited nuclear material. Whether removal of age-induced damage is also coupled to nuclear remodeling during metazoan spermatogenesis remains to be determined.

Elimination of age-induced damage during gamete maturation may also be integral to gamete rejuvenation in other organisms. In *C. elegans* gametogenesis, oocyte maturation involves the elimination of age-induced protein aggregates by lysosomal activation (Bohnert and Kenyon, 2017; Goudeau and Aguilaniu, 2010). Further determining the mechanism of age-induced damage sequestration and elimination could aid in the development of strategies to counteract cellular aging in somatic cells. The selective inheritance of distinct types of age-induced damage could provide a means of determining whether a given senescence factor is a cause or consequence of aging. In this manner, meiotic differentiation offers a unique and natural context to uncover quality control mechanisms that eliminate the determinants of cellular aging.

Chapter 3

A gamete plasma membrane proton pump facilitates programmed cellular destruction during meiotic differentiation

3.1 Introduction

Protein isoforms originate from a single gene or a set of similar genes, and can serve related, distinct or even opposing biological functions. In multicellular organisms, single gene-based protein isoforms are often generated through alternative splicing. For instance, it is estimated that ~90 % of human genes undergo splicing, and many of them with multiple exons undergo alternative splicing– estimated to be up to 95% (Matlin et al., 2005; Pan et al 2008; Sultan et al 2008; Wang et al 2008). However, alternative splicing is unlikely to generate protein isoform diversity in budding yeast, since introns are far less prevalent in this organism, where fewer than 250 of the more than 6,200 annotated genes are known to have introns (~5%), and fewer than 10 are known have more than one intron (Spingola et al, 1999). Instead, evidence suggests alternative translation or transcription initiation within a single gene are potential sources for protein isoform diversity in this organism (Pelechano et al., 2013; Zhou et al., 2017; Eisenberg et al, 2020; Chia et al., 2021). Additionally, because *Saccharomyces cerevisiae* arose from ancient whole-genome duplication, ~8% of its genes are duplicated, corresponding to 457 duplicated gene pairs, also known as paralogs (Kellis et al., 2004).

PMA1 and *PMA2* are paralogous genes that encode plasma membrane proton pumps known to regulate nutrient uptake and the cytoplasmic pH of the cell (Serrrano et al., 1986; Carmelo et al., 1996; Saliba et al., 2018). Both proteins localize to the periphery of the cell and are ~ 90% identical in amino acid sequence (**Figure 3.1;** Schlesser et al., 1988). However, Pma1 and Pma2 have a largely divergent N-terminus, with Pma2 containing a 29 amino acid extension (**Figure 3.1**). Furthermore, *PMA1* is highly expressed during vegetative growth, asymmetrically retained in mother cells and essential for organismal survival (Serrano et al., 1986; Henderson et al., 2014). In contrast, *PMA2* is a non-essential gene under the same growth conditions and is lowly expressed in mitotically dividing vegetative cells (Serrano et al., 1986; Schlesser et al., 1988).

PMA2 expression has been observed under a very limited set of growth conditions. Previous studies highlighted examples of increased *PMA2* transcription under various stress conditions (Fernandes and Sá-Correia, 2003; Andreeva et al., 2017). For example, when cells are exposed to toxic concentrations of manganese, *PMA2* mRNA levels increase approximately 10-

fold relative to unperturbed cells (Andreeva et al., 2017). Furthermore, *PMA2* contains several DNA regulatory motifs that are recognized by the Msn2 transcription factor, which regulates several hundred genes in response to cellular stress (Boy-Marcotte et al., 1998; Görner et al., 2002 ; Hasan et al., 2002 ; Fernandes and Sá-Correia, 2003; Kandror et al., 2004). However, it is unknown if Msn2 and/or other canonical stress response transcription factors induce *PMA2* expression, and what the biological role of Pma2 is during exogenous stress.

Remarkably, *PMA2* expression is upregulated during late gametogenesis, following the meiotic divisions. In parallel, many different stress response transcription factors are expressed throughout gametogenesis, most of which are upregulated during and following the meiotic divisions (Brar et al. 2012). Intriguingly, multiple modes of quality control have recently been reported to take place following the division with the ER, mitochondria, nucleus, and vacuole (**Figure 1.3**, **Figure 2.10**; Eastwood et al., 2012; Eastwood and Meneghini 2015; King and Goodman et al., 2019; Sawyer et al., 2019; Otto et al., 2021). These events are tied to removal of age-associated damage, leading to cellular rejuvenation of the gametes (Unal et al., 2011; King and Goodman et al., 2019). Whether or not *PMA2* expression in gametogenesis is regulated by stress response transcription factors and is tied to meiotic cellular rejuvenation, however, remains poorly understood.

In this study, we aimed to determine the biological significance of *PMA2* in gametogenesis. We found that Pma2 localizes to the gamete plasma membranes following the meiotic divisions and exhibited similar retention behavior to Pma1. Furthermore, we found that *PMA2* is critical to the timely destruction of the mother cell vacuole, which is responsible for the elimination of age-associated damage and other cellular material that is not inherited by the developing gametes. Under acidified media conditions, the delay in timely vacuolar lysis of *pma2Δ* cells is suppressed, indicating a pH dependency. Finally, expressing *PMA1* in place of *PMA2* completely rescues timely vacuolar lysis, highlighting the significance behind the differential expression of the two proton pump isoforms.

3.2 Results

3.2.1 *PMA2* is expressed in the gamete plasma membranes during gametogenesis

PMA1 and *PMA2* exhibit anticorrelated expression patterns in gametogenesis: Under vegetative growth conditions, *PMA1* transcription, translation and peptides levels are lower in gametogenesis in comparison to mitotically dividing vegetative cells (**Figure A2.1**, Brar et al., 2012; Cheng and Otto et al., 2018). Intriguingly, *PMA2* exhibits the opposite trend (**Figure A2.1**, Brar et al., 2012; Cheng and Otto et al., 2018). Therefore, we hypothesized that Pma2 localizes

to the gamete plasma membranes following the meiotic divisions. To assess the localization pattern, we endogenously tagged Pma2 with GFP and measured the expression timing relative to the meiotic divisions using a fluorescently labeled chromatin marker (Htb1-mCherry). As expected, we found that Pma2 levels remained low prior to the meiotic divisions, with GFP signal appearing shortly after anaphase II onset (**Figure 3.2A-B)**. In ~ 15% of cells, the GFP signal appeared 90 minutes after anaphase II onset, whereas in the remaining cell population, the GFP signal was apparent 105 to 135 minutes after anaphase II onset, suggesting that PMA2 expression is tightly regulated during the gametogenesis program (**Figure 3.2B**). Interestingly, some of the GFP signal did not appear at the gamete cortex **(Figure 3.2A)**. We attribute this to be pre-processed protein associated with secretory pathway components, or degraded protein translocated to the vacuole, a phenomenon which has been previously observed for Pma1 (Velivela and Kane, 2018). However, by the end of the gamete maturation, we found that the majority of signal was associated with periphery, indicating Pma2 localizes predominately to the gamete plasma membranes.

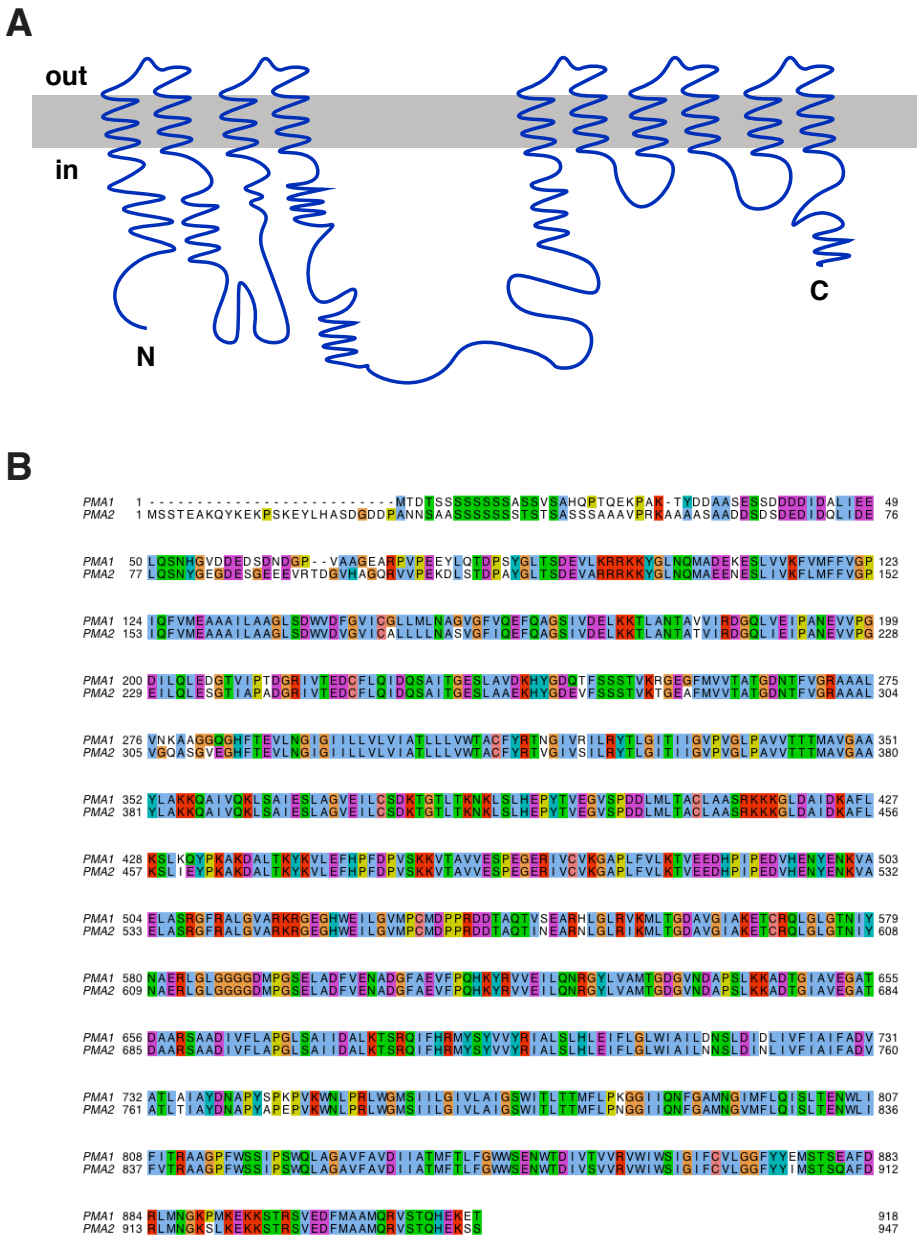

Figure 3.1. Pma2 contains a divergent N-terminus. A. Topological model of Pma1 (in blue). The protein contains 10 transmembrane domains with both termini facing the cytosol (periphery marked in grey). **B.** Pairwise sequence alignment of Pma1 and Pma2 amino acid sequences. Colored regions indicate matching amino acids between both proteins. Generated by Clustal Omega (Goujon et al., 2010; Sievers et al., 2011; McWillaim et al., 2013).

In addition to monitoring Pma2 throughout gametogenesis, we also tracked its localization dynamics in gametes undergoing germination. In the presence of synthetic defined media supplemented with glucose (SC-glucose), we found that daughter cells derived from gametes were completely devoid of GFP signal **(Figure 3.2C)**. This confirms that 1) *PMA2* expression predominantly takes place in gametogenesis and 2) highlights the similarity in localization to Pma1, which has previously been shown to be asymmetrically retained in mother cells during vegetative growth (Henderson et al., 2014). Taken together, these data support the notion that Pma2 is a gamete specific plasma membrane proton pump displaying similar localization features to its isoform, Pma1.

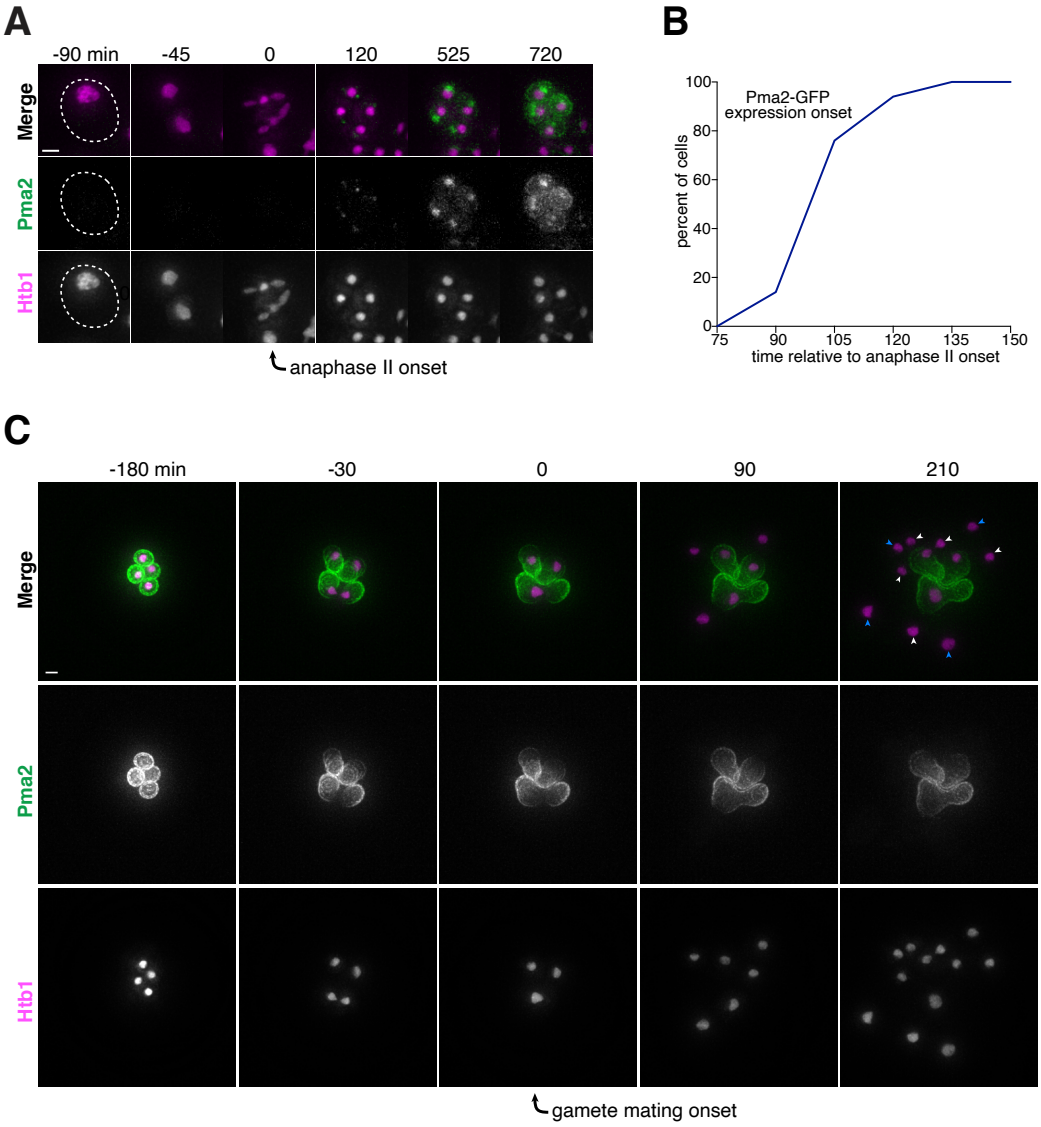

Figure 3.2. *PMA2* is expressed in the gamete plasma membranes during gametogenesis. A. Montage of a wild-type cell undergoing going gametogenesis (UB20504). **B.** Quantification of the experiment in panels A, timing of Pma2-GFP relative to anaphase II onset (in unbuffered media, N=50

meiotic cells). **C.** For montages depicted in **A** and **C**, Pma2 is labeled with Pma2-GFP and nuclei are labeled with Htb1-mCherry. The time point depicting anaphase II onset was defined as 0 minutes as indicated by the black arrow in panel **A**. The timing of gamete mating was defined as 0 minutes as indicated by the black arrow in panel **C**. Small white arrows in panel **C** indicate 1st generation daughter nuclei and the small blue arrows indicate 2nd generation daughter nuclei. Scale bars, 2 μm.

3.2.2 *PMA2* is necessary for timely vacuolar lysis during gametogenesis

Given that *PMA2* expression occurred following the meiotic divisions, we reasoned that it could play a critical role in gamete development. Therefore, we deleted *PMA2* and assessed whether gametogenesis was impaired by a variety of assays. In comparison to wild-type cells, we did not observe obvious defects in sporulation efficiency based on end point analysis.

We next performed live imaging to determine if *pma2Δ* cells exhibit subtle defects in processes that take place during gamete development. Following the meiotic divisions, several events must take place before completion of gamete maturation, including gamete cell wall (spore wall) formation and destruction of the mother cell cytoplasm (Lynn and Magee, 1970; Coluccio et al., 2004, Eastwood et al., 2012; Eastwood and Meneghini, 2015). The latter event is linked to permeabilization of the mother cell vacuole, which serves as a quality control mechanism to destroy cellular material, including age-associated damage that is not inherited by the developing gametes (Eastwood et al., 2012; Eastwood and Meneghini, 2015; King and Goodman et al., 2019). Given that vacuolar lysis occurs after *PMA2* expression, we hypothesized that *pma2Δ* cells lyse their vacuoles at a slower rate than wild-type cells. To test this, we fluorescently tagged an integral vacuolar membrane marker (Vph1-GFP) and assayed for vacuolar lysis by live-cell imaging in unbuffered sporulation media. Following completion of anaphase II, we found that the majority wild-type cells lyse their mother cell vacuoles in ~5-7 hours **(Figure 3.3A+C)** whereas the majority of *pma2Δ* cells lyse their vacuole ~12-14 hours relative to anaphase II **(Figure 3.3B-C)**. Thus, *PMA2* appears to play a role in promoting timely vacuolar lysis during gamete development.

Because Pma2 localizes to the gamete plasma membranes, we surmised that it affects timely vacuolar lysis through its proton-pumping activity. Because it is expressed many hours prior to lysis, we reasoned that Pma2 increases the pH of the gamete cytoplasm by transporting protons into the mother cell and stimulates the vacuole to permeabilize. To determine whether *PMA2*'s effect on vacuolar lysis is pH dependent, we performed additional live imaging assays using buffered sporulation media with varying pH values ranging from 7.0 to 8.0. In wild-type cells, we found that timing of vacuolar lysis does not change by varying the pH of the buffered sporulation media **(Figure 3.3D, Figure A2.2)**.

Interestingly, acidifying the gametogenesis media dramatically improved the kinetics of vacuolar lysis in *pma2Δ* cells: For cells treated with buffered media at pH 7.0, ~ 50% percent of *pma2Δ* cells undergo vacuolar lysis ~500 minutes after anaphase II, versus ~900 minutes at pH 8.0 **(Figure 3.3D, Figure A2.2)**. Altogether, these data indicate that *PMA2* facilitates vacuolar lysis in a pH dependent manner.

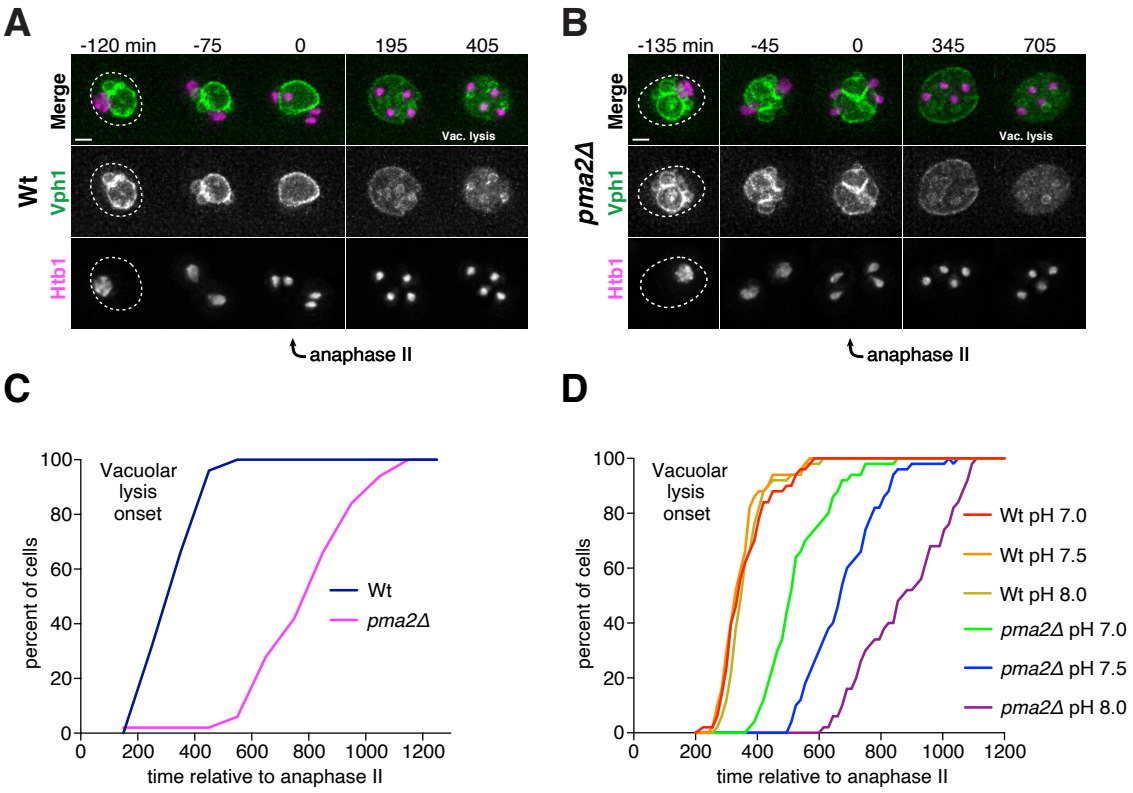

Figure 3.3. *PMA2* is necessary for timely vacuolar during gametogenesis. **A.** Montage of a wild-type cell undergoing vacuolar lysis at pH 7.0 (UB12162). **B.** Montage of a *pma2Δ* cell undergoing vacuolar lysis at pH 7.0 (UB20506). For montages depicted in A-B, the vacuole is labeled with Vph1-GFP and nuclei are labeled with Htb1-mCherry. **C.** Quantification of the experiment in panels A-B, timing of vacuolar lysis relative to anaphase II (in unbuffered media, N=50 tetrads per condition). **D.** Timing of vacuolar lysis relative to anaphase II in buffered media (SPO + 200 mM MOPS pH 7.0, SPO + 200 mM MOPS pH 7.5 or SPO + 200 mM MOPS pH 8.0, N=50 tetrads per condition). For montages depicted in A-B, the vacuole is labeled with Vph1-GFP and nuclei are labeled with Htb1-mCherry. The time point depicting anaphase II was defined as 0 minutes as indicated by the arrows. Scale bars, 2 μm.

3.2.3 *PMA1* recues timely vacuolar lysis in *pma2Δ* cells

Pma1 and Pma2 are ~90% similar in amino acid sequence (**Figure 3.1**, Schlesser et al., 1988). With the C-termini being highly homologous, the N-terminal region upstream of the first transmembrane domain is highly divergent (~50% homologous in sequence). In addition, Pma2 contains a 29 amino acid extension at its N-terminus (Schlesser et al., 1988), though the impact it has on *PMA2*'s biological function remains poorly understood.

To determine if Pma2's divergent N-terminus contributes to its function in promoting timely vacuolar lysis, we first examined if *PMA1* could complement *PMA2* in gametogenesis by generating transgenic strains lacking *PMA2* at the endogenous locus. We assessed the timing of vacuolar lysis relative to anaphase II using same fluorophores previously described and created three different strains either containing: 1) an empty vector as a negative control, 2) a *PMA2* transgene containing 1000 bp genomic region upstream of its ORF as a positive control, and 3) a *PMA1* transgene containing 1000 bp genomic region upstream of *PMA2's* ORF. We reasoned that if expressing *PMA1* under *PMA2* promoter does not rescue timely vacuolar lysis, it would imply that the difference between Pma1 and Pma2's amino acid sequence is important for carrying out timely vacuolar lysis. As expected, the timing of vacuolar lysis remained delayed when only incorporating the empty vector alone, with most cells undergoing lysis ~12-15 hours after anaphase II (**Figure 3.4A+D**). Strikingly, we found that the *PMA1* transgene rescues timely vacuolar lysis to a similar degree as the *PMA2* transgene, with most cells undergoing lysis ~6-8 hours after anaphase II (**Figure 3.4B-D**). Consequently, this indicates that *PMA1* and *PMA2* are functionally interchangeable during gametogenesis, at least under the experimental conditions and tests employed in this study. It is possible that protein-level differences between these two paralogs might be relevant in other biological contexts, such as germination or spore resistance to environmental stress. Future studies are necessary to investigate how *PMA2* expression is regulated and if it impacts other modes of quality control in gametogenesis.

3.3 Discussion

This study highlights the function of *PMA2*, a poorly characterized isoform of *PMA1*. Expression levels of *PMA2* are low during vegetive growth, but increase shortly after the onset of anaphase II. *PMA2* predominantly localizes to the gamete plasma membranes and akin to *PMA1* is asymmetrically retained during mitotic growth. *PMA2* promotes timely lysis of the mother cell vacuole in a pH dependent manner (**Figure 3.5**), which can be complemented by *PMA1*. Together, these findings define a developmental role for *PMA2*, as well as illustrate the biological significance behind the evolution of two plasma membrane proton pump isoforms.

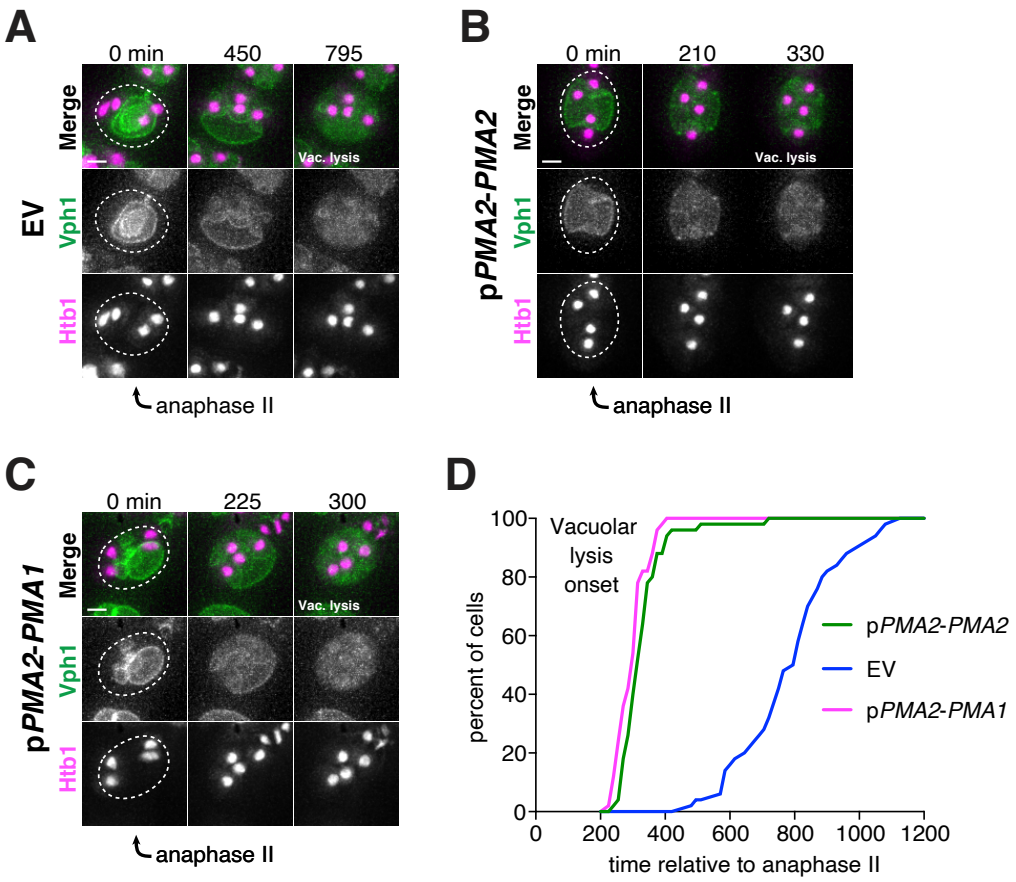

Figure 3.4. *PMA1* recues timely vacuolar lysis in *pma2Δ* cells. A. Montage of a *pma2Δ* cell with empty vector (UB27266). **B.** Montage of a *pma2Δ* cell with a *pPMA2-PMA2* transgene (UB28193). **C.** Montage of a *pma2Δ* cell with a *pPMA2-PMA1* transgene (UB27264). **D.** Quantification of the experiment in panels A-C, timing of vacuolar lysis relative to anaphase II (in unbuffered media, N=50 tetrads per condition). For montages depicted in A-C, the vacuole is labeled with Vph1-GFP and nuclei are labeled with Htb1-mCherry. The time point depicting anaphase II was defined as 0 minutes as indicated by the arrows. Scale bars, 2 μm.

3.1.1 Evolution of two plasma membrane proton pumps

Our study illustrates why two plasma membrane isoforms exist in budding yeast. *PMA1* is an essential pump that regulates cytoplasmic pH of the cell and

establishes an electrochemical gradient to promote nutrient uptake (Serrrano et al., 1986; Carmelo et al., 1996; Saliba et al., 2018). Activation of the proton pump is dependent on glucose (Serrano, 1983; Mazón et al., 2015), but the downstream signaling pathways triggered by glucose that stimulate activation remain elusive. Previous studies have suggested *PMA2* is able to partially complement *PMA1* when expressed on a CEN plasmid under the same promoter: Under normal standard yeast growth media, cells overexpressing *PMA2* are viable in the absence of *PMA1* (Supply et al. 1993). However, under acidic media conditions, *PMA2* overexpressing cells are no longer viable in the absence of *PMA1* (Supply et al., 1993). This may be attributed to the differences in the catalytic properties of both enzymes. For example, it was observed that *in vitro*, Pma2 exhibited greater affinity toward Mg^{2+}, a cofactor that facilitates its activation (Supply et al., 1993). A more thorough understanding as to how these proteins differentially behave with respect to glucose activation may indicate why these gene do not fully complement in vegetative in cells.

Intriguingly, the expression pattern of *PMA1* is downregulated in gametogenesis (**Figure A2.1**, Brar et al., 2012; Cheng and Otto et al., 2018). Under nutrient rich conditions, *PMA1* is the predominant proton pump, and its expression is essential for mitotic growth (Serrrano et al., 1986). However, gametogenesis takes place under nutrient-deprived conditions (van Werven and Amon, 2011), suggesting that it is energetically unfavorable to express a proton pump whose primary function is to uptake nutrients. Whether or not overexpressing *PMA1* causes defects in early gametogenesis stages remains to be determined. During the later stages of gametogenesis, we confirmed that *PMA2* is expressed shortly after the meiotic divisions (**Figure 3.2**). We propose that *PMA2* was maintained following whole genome duplication to carry out a similar proton pumping function to *PMA1*. The main aspect distinguishing *PMA2* from *PMA1* comes from its transient expression timing in gametogenesis, leading to vacuolar lysis (**Figure 3.3**). It would therefore be interesting to investigate whether the gene regulatory events that control *PMA2* expression is tightly coordinated with other developmental pathways that are tied to vacuolar lysis or other aspects of gamete maturation.

3.3.2. Regulation of *PMA2* expression in gametogenesis

We found that *PMA1* fully rescues timely vacuole lysis when expressed under *PMA2*'s promoter. This indicates that Pma2's divergent N-terminus is not critical for timely vacuolar lysis. Rather, our study suggests that the more intriguing feature of *PMA2* is its restricted gene expression pattern in late gametogenesis. However, little is known about the *cis* and *trans*-acting factors that regulate *PMA2* expression, in a positive or negative manner, as well as the environmental conditions that induce *PMA2* expression (Fernandes and Sá Correia, 2003; Andreeva et al., 2017). For example, *PMA2* levels increase

during stationary phase and manganese stress (Fernandes and Sá Correia, 2003; Andreeva et al., 2017). Furthermore, *PMA2* contains various DNA bindings motifs that are predicted to act as stress response promoter elements (STREs), which are recognized by the general stress response transcriptional regulator *MSN2*, which is upregulated in gametogenesis. (Boy-Marcotte et al*.,* 1998; Görner et al*.,* 2002; Hasan et al*.,* 2002; Fernandes and Sa Correia, 2003; Kandror et al., 2004; Brar et al., 2012). Whether or not removing these predicted STREs or inactivating *MSN2* has any effect on *PMA2* expression during gametogenesis remains to be determined.

Notably, other transcription factors tied to stress response are upregulated during gametogenesis (**Figure A2.3**; Brar et al., 2012). These include 1) *HAC1,* which is tied to ER stress, 2) *SKN7* and *YAP1*, which is tied to oxidative stress, 3) *GLN3*, which is tied to nutrient-deprived stress and 3) *CRZ1* and *YAP4*, which are tied to hyperosmotic stress (**Figure A2.3;** Mitchell and Magasanik, 1984; Cox and Walter, 1996; Mori et al., 1996; Mendizabal et al., 1998; Raitt et al., 2000; Okazaki et al, 2007; Hanlon et al, 2011). However, very is little is known about the genes that are regulated by these transcription factors during gametogenesis, and it is unclear whether any of these genes promote *PMA2* expression. Intriguingly, some stress response targets exhibit a similar expression profile to *PMA2* in gametogenesis, such as the catalase enzyme *CTT1*, which is targeted by *SKN7* (Grant et al., 1998; Lee et al., 1999; Brar et al., 2012). Further examination of how these canonical stress response regulators influence gene expression in gametogenesis will reveal if *PMA2* is acting as a direct target. Alternatively, there are additional upregulated transcriptional regulators that are not tied with canonical stress response pathways, including *GAT3* and *GAT4*, which target other gamete maturation genes (**Figure A2.3;** Brar et al., 2012; Lin et al, 2013). Strikingly, some of these gamete maturation genes including *DIT1* and *DIT2*, exhibit a similar expression pattern as *PMA2* late in gametogenesis (Briza et al., 1990; Briza et al., 1994; Brar et al, 2012).

In addition to understanding what positively regulates *PMA2* late in gametogenesis, the mechanism behind its repression during vegetative growth remains poorly understood. Interestingly, mRNA seq reads indicate a transcriptional product upstream of the *PMA2* transcriptional start site in vegetative cells and earlier stages of gametogenesis (**Figure A2.4;** Brar et al., 2012, Chia et al., 2021). Furthermore, a *UME6* binding site (URS1) is present ~600 bp upstream of the *PMA2* ORF, which may indicate that an intergenic transcript and/or a LUTI is being transcribed upon meiotic entry to repress *PMA2* expression (Chen and Tresenrider et al., 2017; Tresenrider, 2018; Chia et al., 2021; Tresenrider et al., 2021). A more thorough examination of what type of transcriptional products are generated upstream of the *PMA2* ORF will better characterize the nature of *PMA2*'s repression before gamete maturation. Moreover, it is unclear if there is any biological significance behind repressing *PMA2* at earlier stages of gametogenesis.

Given *PMA1* levels decrease in gametogenesis, this suggests that there may be a disadvantage for both proton pumps to be expressed during meiotic entry at or before the divisions. One reason behind this may be attributed to the regulation of nutrient uptake: *PMA1* is tied to TORC1 activation during vegetative growth, and meiotic entry is perturbed when TORC1 signaling is high (Weidberg et al., 2016; Saliba et al. 2018). Overall, understanding the factors the regulate *PMA2*'s expression will allow us to further characterize its function in gametogenesis.

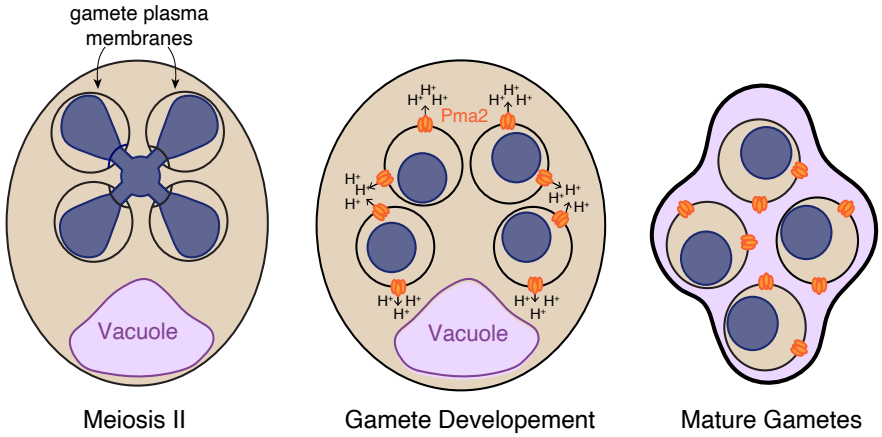

Figure 3.5. Model for *PMA2* inducing vacuolar lysis. Following meiosis, *PMA2* is expressed in the gamete plasma membranes to transport protons from the gamete cytoplasm to the mother cell cytoplasm. We hypothesize that the mother cell cytoplasm becomes acidified to promote vacuolar lysis and programmed destruction of contents that are not inherited by the gametes.

3.3.3 The pH of the mother cell cytoplasm as a likely driver of vacuolar lysis

At pH 7.0, we found that *pma2 Δ* cells undergo vacuolar lysis at a faster rate compared to pH 8.0. It is currently unclear if the mother cell cytoplasm is acidified during gamete maturation, and if so, how it leads to vacuolar lysis. One possible reason for this could be attributed to altering the activity of the enzymes which may be able to degrade the mother cell vacuolar membrane during gamete maturation. Certain lipases, including *TGL3* and *TGL4*, are up regulated during gametogenesis and have been previously reported to impact meiotic progression (Brar et al., 2012; Hsu et al., 2017). However, we found that deleting these lipases did not affect timely vacuolar lysis (**Figure A2.5**). Intriguingly, recent studies have shown that phospholipases can lead to the destruction of the lysosome (the metazoan equivalent to the vacuole) during eye differentiation in other model organisms (Morishita et al., 2021). Knocking

out phospholipases belonging to the PLAAT family in zebrafish and mice prevents complete organelle degradation in lense fibre cells, leading to the development of cataract lenses (Morishita et al., 2021). Perhaps there are yeast phospholipases, which exhibit homology to those of the PLAAT family that are expressed in gametogenesis to drive the destruction of the vacuole in a similar fashion as described in zebrafish and mice.

Alternatively, vacuolar lysis may be driven by additional enzymes that are pH dependent. Outside of other cellular differentiation contexts, lysosomal destruction has been largely observed in cells undergoing apoptosis. The nature of how apoptosis signaling triggers lysosomes to undergo destruction, however, has not been well characterized (Guicciardi et al., 2004; Johansson et al, 2010; Wang et al., 2018). Multiple caspase proteins exist in metazoans to trigger apoptosis, yet only a few apoptosis genes have been identified in budding yeast (Mazzoni and Falcone, 2008). Only one caspase enzyme, *YCA1*, has been identified to trigger cell death during prolonged stress conditions (Madeo et al., 2002), but it remained to be determined if it had a gametogenesis-specific function. Interestingly, we found that deleting *YCA1* causes a mild delay in timely vacuolar lysis in unbuffered media (**Figure A2.6A-E**). However, under buffered media conditions, *yca1Δ* cells undergo vacuolar lysis faster than *pma2Δ yca1Δ* cells at either pH 7.0 or 8.0 (**Figure A2.6F**), suggesting that *YCA1*'s effect on vacuolar lysis is likely independent of *PMA2*. Therefore, *PMA2* may take part in other signaling events that are not tied to apoptotic cell death during gamete maturation.

Although little is known about the physiological changes that take place in the mother cell cytoplasm, *PMA2's* proton pumping activity may compromise vacuolar function by perturbing the proton gradient between the cytoplasm and vacuole. It has been previously shown that V-ATPase vacuolar proton pump has been implicated in non-apoptotic cell death during prolonged ER stress in budding yeast and necrosis-mediated neurodegeneration in *C. elegans* (Syntichaki et al., 2005; Kim et al., 2012). Whether or not *PMA2* expression influences V-ATPase function remains to be determined.

Finally, *PMA2*'s involvement in facilitating vacuolar lysis may act more indirectly. As it remains unclear which events act upstream, the removal of gamete maturation genes implicated in spore wall maturation have been reported to either delay or abolish vacuolar lysis (Eastwood and Meneghini, 2015). Perhaps *PMA2* is not directly involved in triggering lysis but is instead affecting the progression of gamete cell wall (spore) formation. Altogether, better characterizing how *PMA2* facilitates vacuolar lysis will reveal how a novel mode of quality control takes place to destroy cellular material that is not inherited from the developing gametes and may shed light on analogous processes that take place during development in higher model organisms.

Chapter 4

*The following chapter contains material discussed from reviews which I am first author (Goodman and Ünal, 2020; Goodman et al., 2020).

Conclusions

This work illustrates the importance of quality control in budding yeast gametogenesis (**Figure 4.1**). During vegetative growth (i.e. asexual reproduction) mother cells gradually accumulate protein and organelle damage after every division (Sinclair et al., 1997; Sinclair and Guarente, 1997; Aguilaniu et al., 2003; Erjavec et al., 2007; Hughes and Gottschling, 2012; Morlot et al., 2019; Rempel et al., 2019). During gametogenesis, several modes of quality control take place to ensure the removal of age-associated damage and other contents not inherited by the developing gametes (Brar et al., 2012; Sawyer et al., 2019; King and Goodman et al., 2019; Otto et al., 2021). Consequently, gametes derived from old mother cells are born young (Unal et al., 2011; King and Goodman et al., 2019).

4.1 Organelle quality control in metazoan development

Quality control is an integral feature of cellular homeostasis. While most tissues gradually lose the ability to combat cellular damage with age, the germline has developed robust strategies to prevent damage from being inherited during reproduction. While we are beginning to unravel the significance behind quality control in budding yeast gametogenesis, it will be intriguing to identify similar phenomena taking place in metazoans.

4.1.1 Nuclear quality control in metazoan development

We discovered a novel mode of nuclear quality control during gametogenesis. Nuclear aged-induced damage, along with NPCs are extruded from the gamete nuclei prior to their elimination (**Figure 2.10**). A similar sequestration phenomenon with NPCs has been observed during metazoan spermiogenesis, raising the intriguing possibility that some aspects of gametogenesis-associated nuclear rejuvenation may be broadly conserved (Fawcett and Chemes, 1979; Troyer and Schwager, 1982; Russel et al., 1991; Ho, 2010). Further research is required to determine how damage is compartmentalized away from gamete nuclei during budding yeast meiosis and whether similar metazoan mechanisms exist.

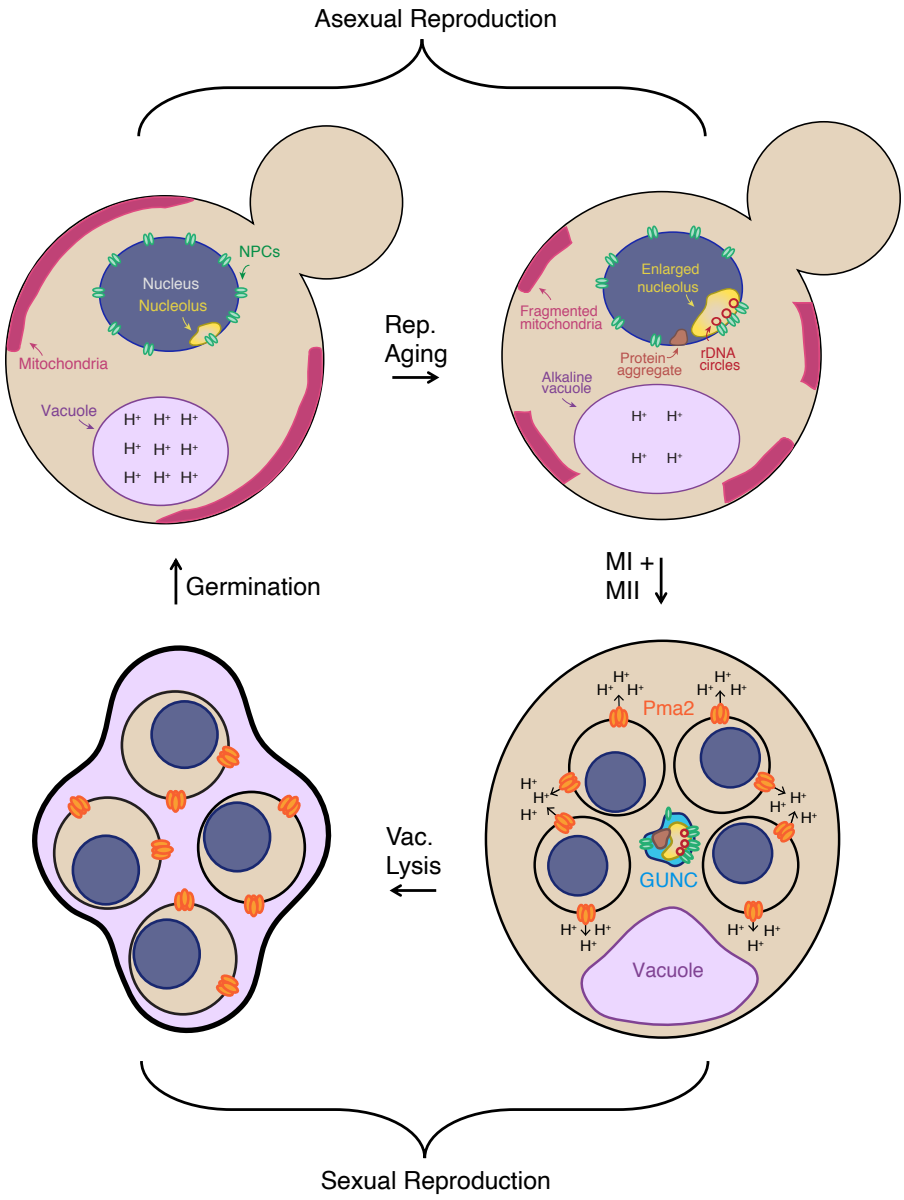

Figure 4.1. Quality control in budding yeast gametogenesis.

Though diffusion barriers at the bud neck have been implicated in preventing daughter cells from inheriting nuclear damage in mitotic budding yeast, little is known as to whether diffusion barriers truly exist in budding yeast gametogenesis, and if so, how they operate to exclude certain types of cellular material from gametes (for instance aging biomarkers). Our studies are consistent with the existence of such a barrier at the growing rim of gamete plasma membrane. However, some of the known mitotic regulators, such as *BUD6* and *SUR2* (Saarikangas et al., 2017), appear to be dispensable (J.

Schick, personal communication). Septins are indeed conserved in higher eukaryotes and have been implicated in establishing diffusion barriers for various cell types. During the late steps of mouse spermatogenesis, a region between the anterior and posterior tail for sperm, termed the annulus, generates septin rings to maintain the integrity of discrete membrane domains (Kwitny et al., 2010). In humans, septins can generate a diffusion barrier at the neck of neuronal dendritic spines, to regulate the mobility of certain postsynaptic receptors (Bloodgood and Sabatini, 2005; Ewers et al., 2014). It will therefore be interesting to determine if similar types of machinery serve a function in preventing nuclear damage from being transmitted to ensuing progeny during reproduction.

As in budding yeast, reproduction in metazoans involves nuclear rejuvenation. During cellular reprogramming to a pluripotent state as occurs in fertilization and embryogenesis, aging is reset to enable the formation of young offspring (Rando and Chang, 2012). Transient expression of pluripotency factors in aged mice and human cells is sufficient to reset nuclear dysfunction, including epigenetic defects and lamin abnormalities (Ocampo et al, 2016; Sarkar et al., 2020). Notably, nuclear age resetting takes place before the reprogramming of cell fate (Ocampo et al., 2016; Sarkar et al., 2020), suggesting that co-opting this natural age-resetting pathway may have therapeutic potential. It remains to be determined, however, whether eliminating nuclear damage directly contributes to cellular rejuvenation.

Reproduction-associated nuclear quality control events have also been observed to reverse harmful genetic changes and regulate harmful genetic elements. For example, rDNA copy number decreases in *D. melanogaster* male germline stem cells with age but is then recovered in their offspring (Lu et al., 2018). In addition, the activity of mobile genetic elements, including retrotransposons, has been implicated in oocyte nuclear quality control. Recent studies in female mice have illustrated that LINE-1 (L1) retrotransposons can instigate fetal oocyte attrition (FOA), which leads to the apoptotic destruction of oocytes during prophase I (Tharp et al., 2020; Malki et al., 2014). Perturbing L1 retrotransposon activity with a reverse transcriptase inhibitor reduces FOA (Tharp et al., 2020; Malki et al., 2014), suggesting that oocytes are selected based on their L1 activity. Whether or not L1 induced FOA results in any physiological benefit or detriment to fertility, however, remains to be determined (Laureau et al., 2021). Together, these examples highlight the importance of nuclear damage elimination during reproduction and development.

4.1.2 Lysosomal quality control in metazoan development

Our work additionally highlights a quality control event that takes place in the vacuole during gamete maturation. The mother cell vacuole is not inherited by the gametes and subsequently lyse, leading to degradation of age-induced

damage and uninherited cellular material that is left outside of the gametes (**Figure 2.7 + 2.10;** Eastwood et al., 2012; Eastwood and Meneghini, 2015; King and Goodman et al., 2019). Interestingly, *C. elegans* accumulates protein aggregates in oocytes during aging and employs a lysosomal acidification process, which depends on the V-ATPase proton pump, to clear age-induced damage following fertilization (Goudeau and Aguilaniu, 2010; David et al., 2010; Bohnert and Kenyon, 2017; Goudeau et al., 2020). Surprisingly, lysosome-mediated aggregate clearance does not appear to depend on canonical autophagy machinery but depends on male sperm protein (MSP) signaling. Identifying factors that act downstream of the MSP signal to stimulate V-ATPase activity will provide increased insight into how fertilization leads to the elimination of age-induced damage.

While the mechanism behind vacuolar destruction remains poorly understood, we discovered that *PMA2*, a gamete plasma membrane proton pump, facilitates vacuolar lysis in a pH dependent manner (**Figure 3.3 + 3.5**). Recent studies in *D. melanogaster* have revealed a similar phenomenon. Follicle stem cells (FSCs), which are derived from the epithelium to provide maintenance to germ cells, recruit proton-pumping machinery to the plasma membrane to acidify adjacent nurse cells (Mondragon et al., 2019), leading to their destruction. Additionally, FSCs can export lysosomal proteases in an exocytosis-dependent manner to fragment nuclear DNA that is not partitioned into the developing oocyte. Indeed, reducing the expression of lysosomal protease and proton-pumping machinery in FSCs is sufficient to prolong nuclear fragmentation in nurse cells during oocyte maturation. How FSCs are triggered to stimulate nurse cell acidification, what additional factors are degraded in nurse cells, and the functional significance it plays in oogenesis all remain to be determined.

Other metazoan cell types eliminate age-induced damage using similar lysosomal quality control mechanisms. Lysosomes are more abundant in mouse quiescent neural stem cells (qNSCs) compared to activated neural stem cells (Leeman et al., 2018; Kobayashi et al., 2019). As such, protein aggregates accumulate in lysosomes with age in mouse qNSCs, making the NSCs less able to proliferate (Leeman et al., 2018). Enhancing lysosomal activity in aged qNCSs, both by TFEB overexpression or nutrient deprivation, promotes protein aggregate clearance and restores NSC activation. However, it remains unclear if the driving force behind NSC activation is the reduction of age-induced protein aggregates or simply the increased function of lysosomes. Nevertheless, the degradative machinery of lysosomes is integral in eliminating age-induced damage during gametogenesis and development.

4.1.3 Mitochondrial quality control in metazoan development

Regulated mitochondrial inheritance during gametogenesis may also contribute to gamete fitness in budding yeast. Ime2 phosphorylates mitochondrial-plasma membrane tethers to induce mitochondrial collapse (Sawyer et al., 2019).

Consequently, some of the mitochondria is inherited by the nascent gametes, while the remaining pool is degraded with other cellular components present in the GUNC (Gorsich and Shaw, 2004; Neiman, 2011; King and Goodman et al, 2019;). This raises the interesting possibility that gametes may preferentially inherit healthy mitochondria over damaged mitochondria to maximize their longevity. Indeed, mitochondria that are not partitioned into the gametes are more depolarized, but it remains unclear if depolarization is a consequence of pre-existing damage in the mother cell or if mitochondria become depolarized during the meiotic program (Eastwood and Meneghini, 2015). More thorough studies examining mitochondrial dynamics in aged meiotic cells will shed light on whether mitochondrial inheritance strongly influences the cellular rejuvenation process.

Several studies have illustrated that mitochondria undergo a unique mode of inheritance in metazoan oogenesis. Female germline stem cells of most animals differentiate into cystocytes, which in turn act as precursor cells that generate oocytes (Bastock and Johnson 2008). Cystocytes undergo incomplete cytokinesis and remain interconnected to supply the developing oocyte with a portion of their cellular contents. In *D. melanogaster*, mitochondria derived from cystocytes are transported to the oocyte by the fusome, which is a germline specific organelle that establishes germ cell polarity in a microtubule-dependent manner (Grieder et al., 2000; Cox and Spradling 2003; Cox and Spradling, 2006;). Mitochondria in cystocytes condense with the Golgi apparatus, ER membranes, and RNA granules to form what is known as the Balbiani body (Cox and Spradling, 2003; Pepling et al., 2007; Lei and Spradling, 2016;). The oocyte eventually receives Balbiani bodies to inherit organelle contents from nurse cells. In mouse oocytes, mitochondria initially exhibit perinuclear localization before they disperse throughout the entire cell (Lei and Spradling, 2016). Intriguingly, mitochondria in budding yeast gametes establish transient contact with the nuclear envelope prior to gamete maturation (Miyakawa et al., 1984; Sawyer et al., 2019;), suggesting that perinuclear localization may be a conserved feature of mitochondrial inheritance.

Evidence suggests that healthy mitochondria are preferentially inherited over damaged mitochondria during metazoan oogenesis. Recent electron microscopy work revealed oocytes preferentially inherit healthy mitochondria over damaged mitochondria in the insect *Thermobia domestica*. In this study, Balbiani bodies were found to contain mitochondria with a high membrane potential but exclude mitochondria with a low potential and damaged morphology (Tworzydlo et al., 2016). Additionally, oocytes have quality control mechanisms to distinguish between wild type and mutant mitochondrial DNA (mtDNA) in the germarium (Hill et al., 2014; Lieber et al., 2019;). This occurs through the downregulation of Mitofusin, which results in the physical separation of mitochondrial genomes into individual mitochondrial fragments. If a mitochondrion carries mutations in its mtDNA, this manifests itself in reduced ATP production and elimination by mitophagy (Lieber et al., 2019). Importantly, inhibiting mitochondrial fragmentation in the germline prevents oocytes from

selecting against mutant mtDNA, while inducing mitochondrial fragmentation in the soma is sufficient to block amplification of mutant mtDNA (Lieber et al., 2019). Further elucidating the consequences of blocking mtDNA selection during oogenesis will reveal the importance of mitochondrial quality control in gamete fitness.

Regulated mitochondrial inheritance occurs in other metazoan developmental contexts, most notably the elimination of paternal mitochondria during fertilization to ensure that new progeny only receive maternal mitochondria. In *D. melanogaster*, maternal mitochondrial inheritance depends on *Oskar*, a gene required for germ plasm assembly (Ephrussi and Lehmann, 1992; Hurd et al., 2016;). Specifically, the long isoform of *Oskar*, which is dispensable for generating the germ plasm, facilitates maternal mitochondrial localization to the posterior region of the embryo in an actin-dependent fashion (Hurd et al., 2016). However, it remains to be determined how the long isoform of *Oskar* promotes actin-mediated partitioning of mitochondria to the posterior region of the embryo and if *Oskar*-mediated mitochondrial inheritance affects the development of ensuing germ cells.

Elimination of paternal mitochondria can occur through multiple degradation mechanisms. In a variety of metazoans, paternal mitochondrial proteins are sequestered into autophagosomes and are degraded in the lysosome shortly after fertilization (Al Rawi et al., 2011; Sato and Sato, 2011; Politi et al., 2014; Rojansky et al., 2016). In contrast, paternal mitochondrial nucleoids in metazoans are eliminated by endonuclease G. While paternal nucleoid destruction in *D. melanogaster* occurs prior to fertilization, *C. elegans* degrade their paternal nucleoids after fertilization (DeLuca and O'Farrell, 2012; Zhou et al., 2016). Strikingly, inhibiting paternal nucleoid destruction in *C. elegans* causes minor embryonic lethality, though it is unclear if this is similarly observed in other metazoans (Zhou et al., 2016). Current evidence suggests endonucleases are also activated in yeast during meiotic differentiation to cleave and eliminate uninherited nuclear DNA (Eastwood et al., 2012; Eastwood and Meneghini, 2015; Nishimura et al., 2020) Whether or not these endonucleases are able to prevent deleterious mtDNA from being inherited into budding yeast gametes remains to be determined. Overall, mitochondria exhibit unique modes of quality control and inheritance during gametogenesis, though how mitochondria influence gamete fitness is still a largely unexplored question.

4.2 Outlook for future studies

How is nuclear material sequestered away from the gamete nuclei in anaphase II and how does *PMA2* trigger vacuolar lysis? Answering these questions along with studying other quality control events will better reveal how cellular rejuvenation is achieved in gametogenesis.

4.2.1 Stress response activation in gametogenesis

It is unclear whether stress pathway activation in gametogenesis is tied to cellular rejuvenation. Many different transcription factors involved in specific stress response pathways are upregulated at discrete stages of gametogenesis (**A2.3;** Brar et al., 2012), though it remains to be determined by what degree their canonical targets are expressed to alleviate cellular damage. It will be interesting to test if depleting these transcription factors will prevent the expression of their canonical target and impede ensuing gamete health. Furthermore, as these stress response genes are transiently expressed, it will be intriguing to quantify the natural levels of expression that pertain to these transcription factors and determine if increasing expression exhibits a positive or negative impact on meiotic quality control. The latter possibility would exemplify how only moderate stress response activation (i.e. hormesis) can provide a beneficial effect on cellular health (Le Bourg, 2009; Zimmermann et al., 2014).

Outside of budding yeast, little work has been done in studying stress response pathways, including the UPR, in other developmental contexts. *C. elegans* larvae arrested in the quiescent L1 stage acquire damage similar to that observed during aging, such as fragmented mitochondria and protein aggregation, but revert back to their youthful state when exposed to bacterial nutrients (Roux et al., 2016). The ability to restore youthfulness in developmentally arrested animals requires the IRE1/XBP1 pathway of the ER UPR. Though *Ire1* null animals are unable to recover after quiescence, *Xbp1* null animals show only a modest defect in recovery, suggesting that *Ire1* activates other genes outside of its canonical UPR regulon to promote cellular rejuvenation. In addition, *Xbp1* can actively regulate genes without *Ire1* during development. An *Xbp1* homologue in *Xenopus laevis* has been shown to play a role in regulating mesodermal and neural development during gastrulation (Cao et al., 2006). Remarkably, the *Xbp1* homologue is alternatively spliced by an unconventional mechanism independent of IRE1 function. Additional *in vitro* and *in vivo* studies indicated that the XBP1 homologue protein associates with transcriptional co-activators implicated in BMP4 and TGFβ signaling. It will therefore be intriguing to investigate if the UPR in budding yeast utilizes transcriptional machinery not implicated with canonical UPR induction to regulate other aspects of gametogenesis.

The HSR may also play a role in protein quality control during gametogenesis in other model organisms. In mice, HSF1 induces transcription of *Hsp90* along with other chaperones during oogenesis (Metchat et al., 2009). Inhibiting HSP90 causes oocytes to exhibit delays in the G2/M transition and defects in cytokinesis during meiosis I. It has yet to be determined, however, if *Hsf1* activation in mouse oogenesis is similar to its activation during heat shock-induced stress and if other chaperones contribute to these meiotic phenotypes. In budding yeast, some Hsps are upregulated during meiosis,

though their functional roles in meiosis remain to be determined (Brar et al., 2012). In parallel Hsf1 synthesis increases during budding yeast gametogenesis, though it remains unclear if its main function is to alleviate proteotoxic stress or to induce meiotic genes that are not part of the canonical HSR (Brar et al., 2012).

In other developmental contexts, HSF1 can transcriptionally target genes outside the HSR. Under stress conditions, HSF1 engages with cis-acting promoter motifs called heat shock elements (HSEs) to initiate the HSR (Liu et al., 1997). Interestingly, *C. elegans* larvae utilize HSF1 and HSEs to transcriptionally activate developmental genes (Li et al., 2017). Unlike canonical HSR genes, these developmental genes contain other *cis* promoter elements adjacent to HSEs that facilitate the binding of additional co-activators, including the E2F/DP heterodimer (Li et al., 2016). How these co-activators engage with HSF1 to promote transcriptional specificity in larval development remains to be determined. In a similar manner, *D. melanogaster* expresses *Hsf1* during oogenesis to activate genes that are implicated in meiotic progression, including factors required for DNA recombination, cohesin assembly, and synaptonemal complex formation (Le Masson et al., 2011). The nature by which HSF1 can differentially regulate canonical HSR genes and developmental genes requires further investigation.

4.2.2 The mysteries behind meiotic cellular rejuvenation

While many asymmetric cell division studies have been done in mitosis, this work shows the need of partitioning damage during meiotic development in budding yeast. Interestingly, genes that are normally implicated in retaining aging determinants in mother cells during replicative aging are dispensable for their sequestration and elimination during meiotic differentiation (J. Schick, personal communication). This suggests that factors specific to the gametogenesis program may be driving the rejuvenation process. Along with *PMA2*, there are many poorly characterized genes that are expressed late in gametogenesis (**Table A2.1;** Brar et al., 2012). Furthermore, the fundamental processes that take place during gamete differentiation remain poorly understood. For example, little is known as to how organelle compartments, including NPCs and the vacuole, are generated *de novo* in developing gametes (Roeder and Shaw, 1996; King and Ünal, 2019). Likewise, it is unclear if gametes can selectively inherit healthy organelle contents from the ER and mitochondria, while leaving behind damaged material for ensuing elimination.

Expressing *NDT80* in vegetative cells increases replicative longevity but does not eliminate all types of nuclear age-associated damage (Unal et al., 2011). However, it remains unclear if *NDT80* alters the ability of mother cells to retain age-associated damage. Monitoring the asymmetric segregation pattern of age-induced damage in mitotic cells expressing *NDT80* may reveal different partitioning patterns of age-associated damage in vegetative cells that are tied

to an increase in replicative longevity. Alternatively, monitoring if other types of organelle damage, including increased mitochondrial oxidation and reduced vacuolar acidity, are reverted in the presence of Ndt80 would shed light on additional pathways in meiosis that counteract replicative aging. Altogether, further dissecting these novel processes occurring in gametogenesis may reveal therapeutic strategies that combat somatic aging or other diseases that are tied to a decline in quality control.

References

1. Aebi, M., Clark, M. W., Vijayraghavan, U. & Abelson, J. A yeast mutant, PRP20, altered in mRNA metabolism and maintenance of the nuclear structure, is defective in a gene homologous to the human gene RCC1 which is involved in the control of chromosome condensation. *Mol Gen Genet* **224**, 72–80 (1990).
2. Aguilaniu, H., Gustafsson, L., Rigoulet, M. & Nystrom, T. Asymmetric inheritance of oxidatively damaged proteins during cytokinesis. *Science (New York, N.Y.)* **299**, 1751–1753 (2003).
3. Al Rawi, S. *et al.* Postfertilization autophagy of sperm organelles prevents paternal mitochondrial DNA transmission. *Science* **334**, 1144–1147 (2011).
4. Andreeva, N. *et al.* Transcriptome profile of yeast reveals the essential role of PMA2 and uncharacterized gene YBR056W-A (MNC1) in adaptation to toxic manganese concentration. *Metallomics* **9**, 175–182 (2017).
5. Bastock, R. & St Johnston, D. Drosophila oogenesis. *Curr Biol* **18**, R1082-1087 (2008).
6. Beck, M. & Hurt, E. The nuclear pore complex: understanding its function through structural insight. *Nat Rev Mol Cell Biol* **18**, 73–89 (2017).
7. Ben-Zvi, A., Miller, E. A. & Morimoto, R. I. Collapse of proteostasis represents an early molecular event in Caenorhabditis elegans aging. *Proc Natl Acad Sci U S A* **106**, 14914–14919 (2009).
8. Benjamin, K. R., Zhang, C., Shokat, K. M. & Herskowitz, I. Control of landmark events in meiosis by the CDK Cdc28 and the meiosis-specific kinase Ime2. *Genes Dev* **17**, 1524–1539 (2003).
9. Berchowitz, L. E. *et al.* A developmentally regulated translational control pathway establishes the meiotic chromosome segregation pattern. *Genes Dev* **27**, 2147–2163 (2013).
10. Berchowitz, L. E. *et al.* Regulated Formation of an Amyloid-like Translational Repressor Governs Gametogenesis. *Cell* **163**, 406–418 (2015).
11. Bloodgood, B. L. & Sabatini, B. L. Neuronal activity regulates diffusion across the neck of dendritic spines. *Science* **310**, 866–869 (2005).
12. Bohnert, K. A. & Kenyon, C. A lysosomal switch triggers proteostasis renewal in the immortal C. elegans germ lineage. *Nature* (2017).
13. Boselli, M., Rock, J., Unal, E., Levine, S. S. & Amon, A. Effects of age on meiosis in budding yeast. *Dev Cell* **16**, 844–855 (2009).
14. Boy-Marcotte, E., Perrot, M., Bussereau, F., Boucherie, H. & Jacquet, M. Msn2p and Msn4p Control a Large Number of Genes Induced at the Diauxic Transition Which Are Repressed by Cyclic AMP in Saccharomyces cerevisiae. *J Bacteriol* **180**, 1044–1052 (1998).
15. Brar, G. A. *et al.* High-resolution view of the yeast meiotic program revealed by ribosome profiling. *Science (New York, N.Y.)* **335**, 552–557 (2012).

16. Brewer, B. J., Zakian, V. A. & Fangman, W. L. Replication and meiotic transmission of yeast ribosomal RNA genes. *Proc Natl Acad Sci U S A* **77**, 6739–6743 (1980).
17. Briza, P., Eckerstorfer, M. & Breitenbach, M. The sporulation-specific enzymes encoded by the DIT1 and DIT2 genes catalyze a two-step reaction leading to a soluble LL-dityrosine-containing precursor of the yeast spore wall. *Proc Natl Acad Sci U S A* **91**, 4524–4528 (1994).
18. Briza, P., Ellinger, A., Winkler, G. & Breitenbach, M. Chemical composition of the yeast ascospore wall. The second outer layer consists of chitosan. *J Biol Chem* **263**, 11569–11574 (1988).
19. Briza, P., Ellinger, A., Winkler, G. & Breitenbach, M. Characterization of a DL-dityrosine-containing macromolecule from yeast ascospore walls. *J Biol Chem* **265**, 15118–15123 (1990).
20. Byers, B. Cytology of the yeast life cycle. in *The Molecular Biology of the Yeast Saccharomyces: Life Cycle and Inheritance* (eds. Strathern, J. N., Jones, E. W. & Broach, J. R.) 59–96 (Cold Spring Harbor Laboratory Press, 1981).
21. Cabrera, M., Novarina, D., Rempel, I. L., Veenhoff, L. M. & Chang, M. A simple microfluidic platform to study age-dependent protein abundance and localization changes in Saccharomyces cerevisiae. *Microbial cell (Graz, Austria)* **4**, 169–174 (2017).
22. Cao, Y. *et al.* XBP1 forms a regulatory loop with BMP-4 and suppresses mesodermal and neural differentiation in Xenopus embryos. *Mech Dev* **123**, 84–96 (2006).
23. Carlile, T. M. & Amon, A. Meiosis I is established through division-specific translational control of a cyclin. *Cell* **133**, 280–291 (2008).
24. Carmelo, V., Bogaerts, P. & Sá-Correia, I. Activity of plasma membrane H+-ATPase and expression of PMA1 and PMA2 genes in Saccharomyces cerevisiae cells grown at optimal and low pH. *Arch Microbiol* **166**, 315–320 (1996).
25. Carpenter, K., Bell, R. B., Yunus, J., Amon, A. & Berchowitz, L. E. Phosphorylation-Mediated Clearance of Amyloid-like Assemblies in Meiosis. *Dev Cell* **45**, 392-405.e6 (2018).
26. Caudron, F. & Barral, Y. Septins and the lateral compartmentalization of eukaryotic membranes. *Dev Cell* **16**, 493–506 (2009).
27. Chen, J. *et al.* Kinetochore inactivation by expression of a repressive mRNA. *eLife* **6**, e27417 (2017).
28. Cheng, Z. & Brar, G. A. Global translation inhibition yields condition-dependent de-repression of ribosome biogenesis mRNAs. *Nucleic Acids Research* **47**, 5061–5073 (2019).
29. Cheng, Z. *et al.* Pervasive, Coordinated Protein-Level Changes Driven by Transcript Isoform Switching during Meiosis. *Cell* **172**, 910-923.e16 (2018).
30. Chia, M. *et al.* High-resolution analysis of cell-state transitions in yeast suggests widespread transcriptional tuning by alternative starts. *Genome Biology* **22**, 34 (2021).

31. Chu, D. B., Gromova, T., Newman, T. A. C. & Burgess, S. M. The Nucleoporin Nup2 Contains a Meiotic-Autonomous Region that Promotes the Dynamic Chromosome Events of Meiosis. *Genetics* **206**, 1319–1337 (2017).
32. Chu, S. *et al.* The transcriptional program of sporulation in budding yeast. *Science* **282**, 699–705 (1998).
33. Chu, S. & Herskowitz, I. Gametogenesis in yeast is regulated by a transcriptional cascade dependent on Ndt80. *Molecular Cell* **1**, 685–696 (1998).
34. Clay, L. *et al.* A sphingolipid-dependent diffusion barrier confines ER stress to the yeast mother cell. *eLife* **3**, e01883 (2014).
35. Colacurcio, D. J. & Nixon, R. A. Disorders of lysosomal acidification-The emerging role of v-ATPase in aging and neurodegenerative disease. *Ageing Res Rev* **32**, 75–88 (2016).
36. Colombi, P., Webster, B. M., Frohlich, F. & Lusk, C. P. The transmission of nuclear pore complexes to daughter cells requires a cytoplasmic pool of Nsp1. *The Journal of cell biology* **203**, 215–232 (2013).
37. Coluccio, A. *et al.* Morphogenetic pathway of spore wall assembly in Saccharomyces cerevisiae. *Eukaryot Cell* **3**, 1464–1475 (2004).
38. Covitz, P. A., Herskowitz, I. & Mitchell, A. P. The yeast RME1 gene encodes a putative zinc finger protein that is directly repressed by a1-alpha 2. *Genes Dev* **5**, 1982–1989 (1991).
39. Cox, J. S. & Walter, P. A novel mechanism for regulating activity of a transcription factor that controls the unfolded protein response. *Cell* **87**, 391–404 (1996).
40. Cox, R. T. & Spradling, A. C. A Balbiani body and the fusome mediate mitochondrial inheritance during Drosophila oogenesis. *Development* **130**, 1579–1590 (2003).
41. Cox, R. T. & Spradling, A. C. Milton controls the early acquisition of mitochondria by Drosophila oocytes. *Development* **133**, 3371–3377 (2006).
42. Cuervo, A. M. Autophagy and aging: keeping that old broom working. *Trends Genet* **24**, 604–612 (2008).
43. David, D. C. *et al.* Widespread Protein Aggregation as an Inherent Part of Aging in C. elegans. *PLOS Biology* **8**, e1000450 (2010).
44. Davidow, L. S., Goetsch, L. & Byers, B. Preferential Occurrence of Nonsister Spores in Two-Spored Asci of SACCHAROMYCES CEREVISIAE: Evidence for Regulation of Spore-Wall Formation by the Spindle Pole Body. *Genetics* **94**, 581–595 (1980).
45. De Craene, J.-O. *et al.* Rtn1p Is Involved in Structuring the Cortical Endoplasmic Reticulum. *Mol Biol Cell* **17**, 3009–3020 (2006).
46. de Hoon, M. J. L., Imoto, S., Nolan, J. & Miyano, S. Open source clustering software. *Bioinformatics* **20**, 1453–1454 (2004).
47. De Virgilio, C., DeMarini, D. J. & Pringle, J. R. SPR28, a sixth member of the septin gene family in Saccharomyces cerevisiae that is expressed

specifically in sporulating cells. *Microbiology* **142 (Pt 10)**, 2897–2905 (1996).
48. Defossez, P. A. *et al.* Elimination of replication block protein Fob1 extends the life span of yeast mother cells. *Molecular cell* **3**, 447–455 (1999).
49. DeLuca, S. Z. & O'Farrell, P. H. Barriers to male transmission of mitochondrial DNA in sperm development. *Dev Cell* **22**, 660–668 (2012).
50. Denning, D. *et al.* The nucleoporin Nup60p functions as a Gsp1p-GTP-sensitive tether for Nup2p at the nuclear pore complex. *J Cell Biol* **154**, 937–950 (2001).
51. Denoth Lippuner, A., Julou, T. & Barral, Y. Budding yeast as a model organism to study the effects of age. *FEMS microbiology reviews* **38**, 300–325 (2014).
52. Denoth-Lippuner, A., Krzyzanowski, M. K., Stober, C. & Barral, Y. Role of SAGA in the asymmetric segregation of DNA circles during yeast ageing. *eLife* **2014**, 1–33 (2014).
53. Dilworth, D. J. *et al.* Nup2p dynamically associates with the distal regions of the yeast nuclear pore complex. *J Cell Biol* **153**, 1465–1478 (2001).
54. Dilworth, D. J. *et al.* The mobile nucleoporin Nup2p and chromatin-bound Prp20p function in endogenous NPC-mediated transcriptional control. *J Cell Biol* **171**, 955–965 (2005).
55. Dultz, E. *et al.* Systematic kinetic analysis of mitotic dis- and reassembly of the nuclear pore in living cells. *J Cell Biol* **180**, 857–865 (2008).
56. Eastwood, M. D., Cheung, S. W. T., Lee, K. Y., Moffat, J. & Meneghini, M. D. Developmentally Programmed Nuclear Destruction during Yeast Gametogenesis. *Developmental Cell* **23**, 35–44 (2012).
57. Eastwood, M. D. & Meneghini, M. D. Developmental coordination of gamete differentiation with programmed cell death in sporulating yeast. *Eukaryotic Cell* **14**, 858–867 (2015).
58. Eisen, M. B., Spellman, P. T., Brown, P. O. & Botstein, D. Cluster analysis and display of genome-wide expression patterns. *PNAS* **95**, 14863–14868 (1998).
59. Eisenberg, A. R. *et al.* Translation Initiation Site Profiling Reveals Widespread Synthesis of Non-AUG-Initiated Protein Isoforms in Yeast. *cels* **11**, 145-160.e5 (2020).
60. Ephrussi, A. & Lehmann, R. Induction of germ cell formation by oskar. *Nature* **358**, 387–392 (1992).
61. Erjavec, N., Larsson, L., Grantham, J. & Nyström, T. Accelerated aging and failure to segregate damaged proteins in Sir2 mutants can be suppressed by overproducing the protein aggregation-remodeling factor Hsp104p. *Genes & development* **21**, 2410–2421 (2007).
62. Erjavec, N. & Nyström, T. Sir2p-dependent protein segregation gives rise to a superior reactive oxygen species management in the progeny of Saccharomyces cerevisiae. *Proc Natl Acad Sci U S A* **104**, 10877–10881 (2007).
63. Ewers, H. *et al.* A Septin-Dependent Diffusion Barrier at Dendritic Spine Necks. *PLoS One* **9**, e113916 (2014).

64. Fares, H., Goetsch, L. & Pringle, J. R. Identification of a developmentally regulated septin and involvement of the septins in spore formation in Saccharomyces cerevisiae. *J Cell Biol* **132**, 399–411 (1996).
65. Fawcett, D. W. & Chemes, H. E. Changes in distribution of nuclear pores during differentiation of the male germ cells. *Tissue and Cell* **11**, 147–162 (1979).
66. Fernandes, A. R. & Sá-Correia, I. Transcription patterns of PMA1 and PMA2 genes and activity of plasma membrane H+-ATPase in Saccharomyces cerevisiae during diauxic growth and stationary phase. *Yeast* **20**, 207–219 (2003).
67. Fuchs, J. & Loidl, J. Behaviour of nucleolus organizing regions (NORs) and nucleoli during mitotic and meiotic divisions in budding yeast. *Chromosome research : an international journal on the molecular, supramolecular and evolutionary aspects of chromosome biology* **12**, 427–438 (2004).
68. Fuller, M. T. & Spradling, A. C. Male and female Drosophila germline stem cells: two versions of immortality. *Science* **316**, 402–404 (2007).
69. Galy, V. *et al.* Nuclear retention of unspliced mRNAs in yeast is mediated by perinuclear Mlp1. *Cell* **116**, 63–73 (2004).
70. Gao, J. *et al.* Meiotic viral attenuation through an ancestral apoptotic pathway. *Proc Natl Acad Sci U S A* **116**, 16454–16462 (2019).
71. Glover, J. R. & Lindquist, S. Hsp104, Hsp70, and Hsp40: a novel chaperone system that rescues previously aggregated proteins. *Cell* **94**, 73–82 (1998).
72. Goodman, J. S., King, G. A. & Ünal, E. Cellular quality control during gametogenesis. *Exp Cell Res* **396**, 112247 (2020).
73. Goodman, J. S. & Ünal, E. Asymmetric Segregation of Age-Induced Damage in Budding Yeast. in *eLS* 1–7 (American Cancer Society, 2020). doi:10.1002/9780470015902.a0021856.
74. Görner, W. *et al.* Acute glucose starvation activates the nuclear localization signal of a stress-specific yeast transcription factor. *EMBO J* **21**, 135–144 (2002).
75. Gorsich, S. W. & Shaw, J. M. Importance of mitochondrial dynamics during meiosis and sporulation. *Molecular biology of the cell* **15**, 4369–4381 (2004).
76. Goudeau, J. & Aguilaniu, H. Carbonylated proteins are eliminated during reproduction in C. elegans. *Aging cell* **9**, 991–1003 (2010).
77. Goudeau, J., Samaddar, M., Bohnert, K. A. & Kenyon, C. Addendum: A lysosomal switch triggers proteostasis renewal in the immortal C. elegans germ lineage. *Nature* **580**, E5 (2020).
78. Goujon, M. *et al.* A new bioinformatics analysis tools framework at EMBL–EBI. *Nucleic Acids Research* **38**, W695–W699 (2010).
79. Grant, C. M., Perrone, G. & Dawes, I. W. Glutathione and catalase provide overlapping defenses for protection against hydrogen peroxide in the yeast Saccharomyces cerevisiae. *Biochem Biophys Res Commun* **253**, 893–898 (1998).

80. Grieder, N. C., de Cuevas, M. & Spradling, A. C. The fusome organizes the microtubule network during oocyte differentiation in Drosophila. *Development* **127**, 4253–4264 (2000).
81. Guicciardi, M. E., Leist, M. & Gores, G. J. Lysosomes in cell death. *Oncogene* **23**, 2881–2890 (2004).
82. Hanlon, S. E., Rizzo, J. M., Tatomer, D. C., Lieb, J. D. & Buck, M. J. The stress response factors Yap6, Cin5, Phd1, and Skn7 direct targeting of the conserved co-repressor Tup1-Ssn6 in S. cerevisiae. *PLoS One* **6**, e19060 (2011).
83. Hasan, R. *et al.* The control of the yeast H2O2 response by the Msn2/4 transcription factors. *Mol Microbiol* **45**, 233–241 (2002).
84. Henderson, K. A., Hughes, A. L. & Gottschling, D. E. Mother-daughter asymmetry of pH underlies aging and rejuvenation in yeast. *eLife* **3**, e03504 (2014).
85. Hetz, C. The unfolded protein response: controlling cell fate decisions under ER stress and beyond. *Nature Reviews Molecular Cell Biology* **13**, 89–102 (2012).
86. Higuchi, R. *et al.* Actin Dynamics Affect Mitochondrial Quality Control and Aging in Budding Yeast. *Current Biology* **23**, 2417–2422 (2013).
87. Hill, J. H., Chen, Z. & Xu, H. Selective propagation of functional mitochondrial DNA during oogenesis restricts the transmission of a deleterious mitochondrial variant. *Nat Genet* **46**, 389–392 (2014).
88. Ho, H. C. Redistribution of nuclear pores during formation of the redundant nuclear envelope in mouse spermatids. *J Anat* **216**, 525–532 (2010).
89. Homann, O. R. & Johnson, A. D. MochiView: versatile software for genome browsing and DNA motif analysis. *BMC Biol* **8**, 49 (2010).
90. Hsu, A.-L., Murphy, C. T. & Kenyon, C. Regulation of aging and age-related disease by DAF-16 and heat-shock factor. *Science* **300**, 1142–1145 (2003).
91. Hsu, T.-H., Chen, R.-H., Cheng, Y.-H. & Wang, C.-W. Lipid droplets are central organelles for meiosis II progression during yeast sporulation. *Mol Biol Cell* **28**, 440–451 (2017).
92. Hu, J. *et al.* Membrane proteins of the endoplasmic reticulum induce high-curvature tubules. *Science* **319**, 1247–1250 (2008).
93. Hughes, A. L. & Gottschling, D. E. An early age increase in vacuolar pH limits mitochondrial function and lifespan in yeast. *Nature* **492**, 261–265 (2012).
94. Hughes, C. E. *et al.* Cysteine Toxicity Drives Age-Related Mitochondrial Decline by Altering Iron Homeostasis. *Cell* **180**, 296-310.e18 (2020).
95. Hurd, T. R. *et al.* Long Oskar Controls Mitochondrial Inheritance in Drosophila melanogaster. *Developmental Cell* **39**, 560–571 (2016).
96. Janke, C. *et al.* A versatile toolbox for PCR-based tagging of yeast genes: new fluorescent proteins, more markers and promoter substitution cassettes. *Yeast* **21**, 947–962 (2004).
97. Janssens, G. E. *et al.* Protein biogenesis machinery is a driver of replicative aging in yeast. *eLife* **4**, e08527 (2015).

98. Johansson, A.-C. *et al.* Regulation of apoptosis-associated lysosomal membrane permeabilization. *Apoptosis* **15**, 527–540 (2010).
99. Kaeberlein, M. Lessons on longevity from budding yeast. *Nature* **464**, 513–519 (2010).
100. Kaeberlein, M., McVey, M. & Guarente, L. The SIR2/3/4 complex and SIR2 alone promote longevity in Saccharomyces cerevisiae by two different mechanisms. *Genes & development* **13**, 2570–2580 (1999).
101. Kandror, O., Bretschneider, N., Kreydin, E., Cavalieri, D. & Goldberg, A. L. Yeast adapt to near-freezing temperatures by STRE/Msn2,4-dependent induction of trehalose synthesis and certain molecular chaperones. *Mol Cell* **13**, 771–781 (2004).
102. Kanki, T. & Klionsky, D. J. Mitophagy in yeast occurs through a selective mechanism. *J Biol Chem* **283**, 32386–32393 (2008).
103. Kassir, Y., Granot, D. & Simchen, G. IME1, a positive regulator gene of meiosis in S. cerevisiae. *Cell* **52**, 853–862 (1988).
104. Kellis, M., Patterson, N., Birren, B., Berger, B. & Lander, E. S. Methods in comparative genomics: genome correspondence, gene identification and regulatory motif discovery. *J Comput Biol* **11**, 319–355 (2004).
105. Kim, H., Kim, A. & Cunningham, K. W. Vacuolar H+-ATPase (V-ATPase) promotes vacuolar membrane permeabilization and nonapoptotic death in stressed yeast. *J Biol Chem* **287**, 19029–19039 (2012).
106. Kim, S. J. *et al.* Integrative structure and functional anatomy of a nuclear pore complex. *Nature* **555**, 475–482 (2018).
107. King, G. A. *et al.* Meiotic cellular rejuvenation is coupled to nuclear remodeling in budding yeast. *eLife* **8**, 1–32 (2019).
108. King, G. A. & Ünal, E. The dynamic nuclear periphery as a facilitator of gamete health and rejuvenation. *Curr Genet* **66**, 487–493 (2020).
109. King, M. C., Lusk, C. P. & Blobel, G. Karyopherin-mediated import of integral inner nuclear membrane proteins. *Nature* **442**, 1003–1007 (2006).
110. Knop, M. & Strasser, K. Role of the spindle pole body of yeast in mediating assembly of the prospore membrane during meiosis. *The EMBO journal* **19**, 3657–3667 (2000).
111. Kobayashi, T. *et al.* Enhanced lysosomal degradation maintains the quiescent state of neural stem cells. *Nat Commun* **10**, 5446 (2019).
112. Kremer, J. R., Mastronarde, D. N. & McIntosh, J. R. Computer visualization of three-dimensional image data using IMOD. *J Struct Biol* **116**, 71–76 (1996).
113. Kumar, A. *et al.* Daughter-cell-specific modulation of nuclear pore complexes controls cell cycle entry during asymmetric division. *Nat Cell Biol* **20**, 432–442 (2018).
114. Kwitny, S., Klaus, A. V. & Hunnicutt, G. R. The annulus of the mouse sperm tail is required to establish a membrane diffusion barrier that is engaged during the late steps of spermiogenesis. *Biol Reprod* **82**, 669–678 (2010).
115. Labbadia, J. & Morimoto, R. I. The biology of proteostasis in aging and disease. *Annu Rev Biochem* **84**, 435–464 (2015).

116. Lam, C. *et al.* A Visual Screen of Protein Localization during Sporulation Identifies New Components of Prospore Membrane-Associated Complexes in Budding Yeast. *Eukaryotic Cell* **13**, 383 LP – 391 (2014).
117. Laureau, R. *et al.* Meiotic Cells Counteract Programmed Retrotransposon Activation via RNA-Binding Translational Repressor Assemblies. *Developmental Cell* **56**, 22-35.e7 (2021).
118. Le Bourg, E. Hormesis, aging and longevity. *Biochim Biophys Acta* **1790**, 1030–1039 (2009).
119. Le Masson, F. *et al.* Identification of Heat Shock Factor 1 Molecular and Cellular Targets during Embryonic and Adult Female Meiosis. *Molecular and Cellular Biology* **31**, 3410–3423 (2011).
120. Lee, J. *et al.* Yap1 and Skn7 control two specialized oxidative stress response regulons in yeast. *J Biol Chem* **274**, 16040–16046 (1999).
121. Lee, W. C., Zabetakis, D. & Melese, T. NSR1 is required for pre-rRNA processing and for the proper maintenance of steady-state levels of ribosomal subunits. *Mol Cell Biol* **12**, 3865–3871 (1992).
122. Leeman, D. S. *et al.* Lysosome activation clears aggregates and enhances quiescent neural stem cell activation during aging. *Science* **359**, 1277–1283 (2018).
123. Lei, L. & Spradling, A. C. Mouse oocytes differentiate through organelle enrichment from sister cyst germ cells. *Science* **352**, 95–99 (2016).
124. Lewinska, A., Miedziak, B., Kulak, K., Molon, M. & Wnuk, M. Links between nucleolar activity, rDNA stability, aneuploidy and chronological aging in the yeast Saccharomyces cerevisiae. *Biogerontology* **15**, 289–316 (2014).
125. Li, H. Y., Wirtz, D. & Zheng, Y. A mechanism of coupling RCC1 mobility to RanGTP production on the chromatin in vivo. *J Cell Biol* **160**, 635–644 (2003).
126. Li, J., Chauve, L., Phelps, G., Brielmann, R. M. & Morimoto, R. I. E2F coregulates an essential HSF developmental program that is distinct from the heat-shock response. *Genes Dev.* **30**, 2062–2075 (2016).
127. Li, J., Labbadia, J. & Morimoto, R. I. Rethinking HSF1 in Stress, Development, and Organismal Health. *Trends in Cell Biology* **27**, 895–905 (2017).
128. Li, P., Jin, H., Hoang, M. L. & Yu, H. G. Tracking chromosome dynamics in live yeast cells: coordinated movement of rDNA homologs and anaphase disassembly of the nucleolus during meiosis. *Chromosome Res* **19**, 1013–1026 (2011).
129. Lieber, T., Jeedigunta, S. P., Palozzi, J. M., Lehmann, R. & Hurd, T. R. Mitochondrial fragmentation drives selective removal of deleterious mtDNA in the germline. *Nature* **570**, 380–384 (2019).
130. Lin, C. P.-C., Kim, C., Smith, S. O. & Neiman, A. M. A highly redundant gene network controls assembly of the outer spore wall in S. cerevisiae. *PLoS Genet* **9**, e1003700 (2013).
131. Liu, B. *et al.* The polarisome is required for segregation and retrograde transport of protein aggregates. *Cell* **140**, 257–267 (2010).

132. Liu, X.-D., Liu, P. C. C., Santoro, N. & Thiele, D. J. Conservation of a stress response: human heat shock transcription factors functionally substitute for yeast HSF. *The EMBO Journal* **16**, 6466–6477 (1997).
133. Longo, V. D., Shadel, G. S., Kaeberlein, M. & Kennedy, B. Replicative and chronological aging in Saccharomyces cerevisiae. *Cell metabolism* **16**, 18–31 (2012).
134. Longtine, M. S. *et al.* Additional modules for versatile and economical PCR-based gene deletion and modification in Saccharomyces cerevisiae. *Yeast* **14**, 953–961 (1998).
135. Lord, C. L., Timney, B. L., Rout, M. P. & Wente, S. R. Altering nuclear pore complex function impacts longevity and mitochondrial function in S. cerevisiae. *J Cell Biol* **208**, 729–744 (2015).
136. Lu, K. L., Nelson, J. O., Watase, G. J., Warsinger-Pepe, N. & Yamashita, Y. M. Transgenerational dynamics of rDNA copy number in Drosophila male germline stem cells. *eLife* **7**, e32421 (2018).
137. Lynn, R. R. & Magee, P. T. Development of the spore wall during ascospore formation in Saccharomyces cerevisiae. *J Cell Biol* **44**, 688–692 (1970).
138. Madeo, F. *et al.* A Caspase-Related Protease Regulates Apoptosis in Yeast. *Molecular Cell* **9**, 911–917 (2002).
139. Makio, T., Lapetina, D. L. & Wozniak, R. W. Inheritance of yeast nuclear pore complexes requires the Nsp1p subcomplex. *The Journal of cell biology* **203**, 187–196 (2013).
140. Malki, S., van der Heijden, G. W., O'Donnell, K. A., Martin, S. L. & Bortvin, A. A Role for Retrotransposon LINE-1 in Fetal Oocyte Attrition in Mice. *Developmental Cell* **29**, 521–533 (2014).
141. Markossian, S., Suresh, S., Osmani, A. H. & Osmani, S. A. Nup2 requires a highly divergent partner, NupA, to fulfill functions at nuclear pore complexes and the mitotic chromatin region. *Mol Biol Cell* **26**, 605–621 (2015).
142. Matlin, A. J., Clark, F. & Smith, C. W. J. Understanding alternative splicing: towards a cellular code. *Nat Rev Mol Cell Biol* **6**, 386–398 (2005).
143. Matos, J. *et al.* Dbf4-dependent CDC7 kinase links DNA replication to the segregation of homologous chromosomes in meiosis I. *Cell* **135**, 662–678 (2008).
144. Mazón, M. J., Eraso, P. & Portillo, F. Specific phosphoantibodies reveal two phosphorylation sites in yeast Pma1 in response to glucose. *FEMS Yeast Research* **15**, (2015).
145. Mazzoni, C. & Falcone, C. Caspase-dependent apoptosis in yeast. *Biochimica et Biophysica Acta (BBA) - Molecular Cell Research* **1783**, 1320–1327 (2008).
146. McDonald, K. L. Out with the old and in with the new: rapid specimen preparation procedures for electron microscopy of sectioned biological material. *Protoplasma* **251**, 429–448 (2014).
147. McDonald, K. L. & Webb, R. I. Freeze substitution in 3 hours or less. *J Microsc* **243**, 227–233 (2011).

148. McDonald, K. & Muller-Reichert, T. Cryomethods for thin section electron microscopy. *Methods Enzymol* **351**, 96–123 (2002).
149. McMurray, M. A. & Thorner, J. Septin stability and recycling during dynamic structural transitions in cell division and development. *Curr Biol* **18**, 1203–1208 (2008).
150. McWilliam, H. *et al.* Analysis Tool Web Services from the EMBL-EBI. *Nucleic Acids Research* **41**, W597–W600 (2013).
151. Meinema, A. C. *et al.* Long unfolded linkers facilitate membrane protein import through the nuclear pore complex. *Science* **333**, 90–93 (2011).
152. Mendizabal, I., Rios, G., Mulet, J. M., Serrano, R. & de Larrinoa, I. F. Yeast putative transcription factors involved in salt tolerance. *FEBS Lett* **425**, 323–328 (1998).
153. Mészáros, N. *et al.* Nuclear pore basket proteins are tethered to the nuclear envelope and can regulate membrane curvature. *Developmental cell* **33**, 285–298 (2015).
154. Metchat, A. *et al.* Mammalian Heat Shock Factor 1 Is Essential for Oocyte Meiosis and Directly Regulates Hsp90α Expression. *J Biol Chem* **284**, 9521–9528 (2009).
155. Mitchell, A. P. & Herskowitz, I. Activation of meiosis and sporulation by repression of the RME1 product in yeast. *Nature* **319**, 738–742 (1986).
156. Mitchell, A. P. & Magasanik, B. Regulation of glutamine-repressible gene products by the GLN3 function in Saccharomyces cerevisiae. *Mol Cell Biol* **4**, 2758–2766 (1984).
157. Miyakawa, I., Aoi, H., Sando, N. & Kuroiwa, T. Fluorescence microscopic studies of mitochondrial nucleoids during meiosis and sporulation in the yeast, Saccharomyces cerevisiae. *Journal of cell science* **66**, 21–38 (1984).
158. Moens, P. B. Fine structure of ascospore development in the yeast Saccharomyces cerevisiae. *Can J Microbiol* **17**, 507–510 (1971).
159. Moens, P. B. & Rapport, E. Spindles, spindle plaques, and meiosis in the yeast Saccharomyces cerevisiae (Hansen). *J Cell Biol* **50**, 344–361 (1971).
160. Mondragon, A. A. *et al.* Lysosomal Machinery Drives Extracellular Acidification to Direct Non-apoptotic Cell Death. *Cell Reports* **27**, 11-19.e3 (2019).
161. Moreno-Borchart, A. C. *et al.* Prospore membrane formation linked to the leading edge protein (LEP) coat assembly. *The EMBO journal* **20**, 6946–6957 (2001).
162. Mori, K., Kawahara, T., Yoshida, H., Yanagi, H. & Yura, T. Signalling from endoplasmic reticulum to nucleus: transcription factor with a basic-leucine zipper motif is required for the unfolded protein-response pathway. *Genes Cells* **1**, 803–817 (1996).
163. Morishita, H. *et al.* Organelle degradation in the lens by PLAAT phospholipases. *Nature* **592**, 634–638 (2021).

164. Morlot, S. *et al.* Excessive rDNA Transcription Drives the Disruption in Nuclear Homeostasis during Entry into Senescence in Budding Yeast. *Cell reports* **28**, 408-422.e4 (2019).
165. Mortimer, R. K. & Johnston, J. R. Life span of individual yeast cells. *Nature* **183**, 1751–1752 (1959).
166. Nakanishi, H., de los Santos, P. & Neiman, A. M. Positive and negative regulation of a SNARE protein by control of intracellular localization. *Mol Biol Cell* **15**, 1802–1815 (2004).
167. Neiman, A. M. Prospore membrane formation defines a developmentally regulated branch of the secretory pathway in yeast. *J Cell Biol* **140**, 29–37 (1998).
168. Neiman, A. M. Sporulation in the budding yeast Saccharomyces cerevisiae. *Genetics* **189**, 737–765 (2011).
169. Niepel, M. *et al.* The nuclear basket proteins Mlp1p and Mlp2p are part of a dynamic interactome including Esc1p and the proteasome. *Mol Biol Cell* **24**, 3920–3938 (2013).
170. Nishimura, Y., Shikanai, T., Kawamoto, S. & Toh-e, A. Step-wise elimination of α-mitochondrial nucleoids and mitochondrial structure as a basis for the strict uniparental inheritance in Cryptococcus neoformans. *Sci Rep* **10**, 2468 (2020).
171. Ocampo, A. *et al.* In Vivo Amelioration of Age-Associated Hallmarks by Partial Reprogramming. *Cell* **167**, 1719-1733.e12 (2016).
172. Okamoto, S. & Iino, T. Selective abortion of two nonsister nuclei in a developing ascus of the hfd-1 mutant in Saccharomyces cerevisiae. *Genetics* **99**, 197–209 (1981).
173. Okazaki, S., Tachibana, T., Naganuma, A., Mano, N. & Kuge, S. Multistep disulfide bond formation in Yap1 is required for sensing and transduction of H2O2 stress signal. *Mol Cell* **27**, 675–688 (2007).
174. Otto, G. M., Cheunkarndee, T., Leslie, J. M. & Brar, G. A. Programmed ER fragmentation drives selective ER inheritance and degradation in budding yeast meiosis. *bioRxiv* 2021.02.12.430990 (2021) doi:10.1101/2021.02.12.430990.
175. Ozsarac, N., Bhattacharyya, M., Dawes, I. W. & Clancy, M. J. The SPR3 gene encodes a sporulation-specific homologue of the yeast CDC3/10/11/12 family of bud neck microfilaments and is regulated by ABFI. *Gene* **164**, 157–162 (1995).
176. Pablo-Hernando, M. E. *et al.* Septins localize to microtubules during nutritional limitation in Saccharomyces cerevisiae. *BMC Cell Biol* **9**, 55 (2008).
177. Pan, Q., Shai, O., Lee, L. J., Frey, B. J. & Blencowe, B. J. Deep surveying of alternative splicing complexity in the human transcriptome by high-throughput sequencing. *Nat Genet* **40**, 1413–1415 (2008).
178. Pelechano, V., Wei, W. & Steinmetz, L. M. Extensive transcriptional heterogeneity revealed by isoform profiling. *Nature* **497**, 127–131 (2013).

179. Pepling, M. E., Wilhelm, J. E., O'Hara, A. L., Gephardt, G. W. & Spradling, A. C. Mouse oocytes within germ cell cysts and primordial follicles contain a Balbiani body. *Proc Natl Acad Sci U S A* **104**, 187–192 (2007).
180. Politi, Y. *et al.* Paternal mitochondrial destruction after fertilization is mediated by a common endocytic and autophagic pathway in Drosophila. *Dev Cell* **29**, 305–320 (2014).
181. Raitt, D. C. *et al.* The Skn7 response regulator of Saccharomyces cerevisiae interacts with Hsf1 in vivo and is required for the induction of heat shock genes by oxidative stress. *Mol Biol Cell* **11**, 2335–2347 (2000).
182. Rajoo, S., Vallotton, P., Onischenko, E. & Weis, K. Stoichiometry and compositional plasticity of the yeast nuclear pore complex revealed by quantitative fluorescence microscopy. *Proc Natl Acad Sci U S A* **115**, E3969-e3977 (2018).
183. Rando, T. A. & Chang, H. Y. Aging, Rejuvenation, and Epigenetic Reprogramming: Resetting the Aging Clock. *Cell* **148**, 46–57 (2012).
184. Rempel, I. L. *et al.* Age-dependent deterioration of nuclear pore assembly in mitotic cells decreases transport dynamics. *eLife* **8**, (2019).
185. Reynolds, E. S. The use of lead citrate at high pH as an electron-opaque stain in electron microscopy. *J Cell Biol* **17**, 208–212 (1963).
186. Roeder, A. D. & Shaw, J. M. Vacuole Partitioning during Meiotic Division in Yeast. *Genetics* **144**, 445–458 (1996).
187. Rojansky, R., Cha, M.-Y. & Chan, D. C. Elimination of paternal mitochondria in mouse embryos occurs through autophagic degradation dependent on PARKIN and MUL1. *eLife* **5**, e17896 (2016).
188. Roux, A. E., Langhans, K., Huynh, W. & Kenyon, C. Reversible Age-Related Phenotypes Induced during Larval Quiescence in C. elegans. *Cell Metab* **23**, 1113–1126 (2016).
189. Russell, L. D., Russell, J. A., MacGregor, G. R. & Meistrich, M. L. Linkage of manchette microtubules to the nuclear envelope and observations of the role of the manchette in nuclear shaping during spermiogenesis in rodents. *American Journal of Anatomy* **192**, 97–120 (1991).
190. Saarikangas, J. *et al.* Compartmentalization of ER-Bound Chaperone Confines Protein Deposit Formation to the Aging Yeast Cell. *Current biology : CB* **27**, 773–783 (2017).
191. Saliba, E. *et al.* The yeast H+-ATPase Pma1 promotes Rag/Gtr-dependent TORC1 activation in response to H+-coupled nutrient uptake. *eLife* **7**, e31981 (2018).
192. Sarkar, T. J. *et al.* Transient non-integrative expression of nuclear reprogramming factors promotes multifaceted amelioration of aging in human cells. *Nat Commun* **11**, 1545 (2020).
193. Sato, M. & Sato, K. Degradation of paternal mitochondria by fertilization-triggered autophagy in C. elegans embryos. *Science* **334**, 1141–1144 (2011).
194. Sawyer, E. M. *et al.* Developmental regulation of an organelle tether coordinates mitochondrial remodeling in meiosis. *Journal of Cell Biology* **218**, 559–579 (2019).

195. Scarcelli, J. J., Hodge, C. A. & Cole, C. N. The yeast integral membrane protein Apq12 potentially links membrane dynamics to assembly of nuclear pore complexes. *The Journal of cell biology* **178**, 799–812 (2007).
196. Schindelin, J. *et al.* Fiji: an open-source platform for biological-image analysis. *Nat Methods* **9**, 676–682 (2012).
197. Schlesser, A., Ulaszewski, S., Ghislain, M. & Goffeau, A. A second transport ATPase gene in Saccharomyces cerevisiae. *J Biol Chem* **263**, 19480–19487 (1988).
198. Serrano, R. In vivo glucose activation of the yeast plasma membrane ATPase. *FEBS Letters* **156**, 11–14 (1983).
199. Serrano, R., Kielland-Brandt, M. C. & Fink, G. R. Yeast plasma membrane ATPase is essential for growth and has homology with (Na + + K +), K + - and Ca 2+ -ATPases. *Nature* **319**, 689–693 (1986).
200. Settembre, C., Fraldi, A., Medina, D. L. & Ballabio, A. Signals from the lysosome: a control centre for cellular clearance and energy metabolism. *Nat Rev Mol Cell Biol* **14**, 283–296 (2013).
201. Sheff, M. A. & Thorn, K. S. Optimized cassettes for fluorescent protein tagging in Saccharomyces cerevisiae. *Yeast* **21**, 661–670 (2004).
202. Sievers, F. *et al.* Fast, scalable generation of high-quality protein multiple sequence alignments using Clustal Omega. *Molecular Systems Biology* **7**, 539 (2011).
203. Sinclair, D. A. & Guarente, L. Extrachromosomal rDNA circles–a cause of aging in yeast. *Cell* **91**, 1033–1042 (1997).
204. Sinclair, D. A., Mills, K. & Guarente, L. Accelerated aging and nucleolar fragmentation in yeast sgs1 mutants. *Science (New York, N.Y.)* **277**, 1313–1316 (1997).
205. Smeal, T., Claus, J., Kennedy, B., Cole, F. & Guarente, L. Loss of transcriptional silencing causes sterility in old mother cells of S. cerevisiae. *Cell* **84**, 633–642 (1996).
206. Smits, G. J., van den Ende, H. & Klis, F. M. Differential regulation of cell wall biogenesis during growth and development in yeast. *Microbiology (Reading)* **147**, 781–794 (2001).
207. Spingola, M., Grate, L., Haussler, D. & Ares, M. Genome-wide bioinformatic and molecular analysis of introns in Saccharomyces cerevisiae. *RNA* **5**, 221–234 (1999).
208. Stevens, B. Mitochondrial structure. in *Molecular Biology of the Yeast Saccharomyces* (eds. Strathern, J. N., Jones, E. W. & Broach, J. R.) 471–505 (Cold Spring Harbor Laboratory Press, 1981).
209. Straight, A. F. *et al.* Net1, a Sir2-associated nucleolar protein required for rDNA silencing and nucleolar integrity. *Cell* **97**, 245–256 (1999).
210. Suda, Y., Nakanishi, H., Mathieson, E. M. & Neiman, A. M. Alternative modes of organellar segregation during sporulation in Saccharomyces cerevisiae. *Eukaryot Cell* **6**, 2009–2017 (2007).
211. Sultan, M. *et al.* A global view of gene activity and alternative splicing by deep sequencing of the human transcriptome. *Science* **321**, 956–960 (2008).

212. Sun, N., Youle, R. J. & Finkel, T. The Mitochondrial Basis of Aging. *Mol Cell* **61**, 654–666 (2016).
213. Supply, P., Wach, A. & Goffeau, A. Enzymatic properties of the PMA2 plasma membrane-bound H(+)-ATPase of Saccharomyces cerevisiae. *J Biol Chem* **268**, 19753–19759 (1993).
214. Supply, P., Wach, A., Thinès-Sempoux, D. & Goffeau, A. Proliferation of intracellular structures upon overexpression of the PMA2 ATPase in Saccharomyces cerevisiae. *J Biol Chem* **268**, 19744–19752 (1993).
215. Suresh, S., Markossian, S., Osmani, A. H. & Osmani, S. A. Mitotic nuclear pore complex segregation involves Nup2 in Aspergillus nidulans. *The Journal of cell biology* **216**, 2813–2826 (2017).
216. Syntichaki, P., Samara, C. & Tavernarakis, N. The Vacuolar H+-ATPase Mediates Intracellular Acidification Required for Neurodegeneration in C. elegans. *Current Biology* **15**, 1249–1254 (2005).
217. Takagi, T., Osumi, M. & Shinohara, A. Nuclear bundle/cable containing actin during yeast meiosis. *bioRxiv* 778100 (2021) doi:10.1101/778100.
218. Taxis, C. *et al.* Spore number control and breeding in Saccharomyces cerevisiae: a key role for a self-organizing system. *J Cell Biol* **171**, 627–640 (2005).
219. Taylor, R. C. & Dillin, A. XBP-1 is a cell-nonautonomous regulator of stress resistance and longevity. *Cell* **153**, 1435–1447 (2013).
220. Tharp, M. E., Malki, S. & Bortvin, A. Maximizing the ovarian reserve in mice by evading LINE-1 genotoxicity. *Nat Commun* **11**, 330 (2020).
221. Tiku, V. *et al.* Small nucleoli are a cellular hallmark of longevity. *Nature Communications* **8**, 16083 (2017).
222. Tresenrider, A. *et al.* Integrated genomic analysis reveals key features of long undecoded transcript isoform-based gene repression. *Mol Cell* **81**, 2231-2245.e11 (2021).
223. Tresenrider, A. & Ünal, E. One-two punch mechanism of gene repression: a fresh perspective on gene regulation. *Curr Genet* **64**, 581–588 (2018).
224. Troyer, D. & Schwager, P. *Evidence for nuclear membrane fluidity: Proacrosome migration and nuclear pore redistribution during grasshopper spermiogenesis*. *Cell Motility* vol. 2 (Wiley-Blackwell, 1982).
225. Tworzydlo, W., Kisiel, E., Jankowska, W., Witwicka, A. & Bilinski, S. M. Exclusion of dysfunctional mitochondria from Balbiani body during early oogenesis of Thermobia. *Cell Tissue Res* **366**, 191–201 (2016).
226. Ünal, E. & Amon, A. Gamete formation resets the aging clock in yeast. *Cold Spring Harbor symposia on quantitative biology* **76**, 73–80 (2011).
227. Unal, E., Kinde, B. & Amon, A. Gametogenesis eliminates age-induced cellular damage and resets life span in yeast. *Science (New York, N.Y.)* **332**, 1554–1557 (2011).
228. Van Dalfsen, K. M. *et al.* Global Proteome Remodeling during ER Stress Involves Hac1-Driven Expression of Long Undecoded Transcript Isoforms. *Developmental Cell* **46**, 219-235.e8 (2018).
229. van Werven, F. J. & Amon, A. Regulation of entry into gametogenesis. *Philos Trans R Soc Lond B Biol Sci* **366**, 3521–3531 (2011).

230. Veatch, J. R., McMurray, M. A., Nelson, Z. W. & Gottschling, D. E. Mitochondrial dysfunction leads to nuclear genome instability via an iron-sulfur cluster defect. *Cell* **137**, 1247–1258 (2009).
231. Velivela, S. D. & Kane, P. M. Compensatory Internalization of Pma1 in V-ATPase Mutants in Saccharomyces cerevisiae Requires Calcium- and Glucose-Sensitive Phosphatases. *Genetics* **208**, 655–672 (2018).
232. Verbeke, P., Fonager, J., Clark, B. F. & Rattan, S. I. Heat shock response and ageing: mechanisms and applications. *Cell Biol Int* **25**, 845–857 (2001).
233. Vilchez, D. *et al.* RPN-6 determines C. elegans longevity under proteotoxic stress conditions. *Nature* **489**, 263–268 (2012).
234. Voeltz, G. K., Prinz, W. A., Shibata, Y., Rist, J. M. & Rapoport, T. A. A Class of Membrane Proteins Shaping the Tubular Endoplasmic Reticulum. *Cell* **124**, 573–586 (2006).
235. Wang, E. T. *et al.* Alternative isoform regulation in human tissue transcriptomes. *Nature* **456**, 470–476 (2008).
236. Wang, F., Gómez-Sintes, R. & Boya, P. Lysosomal membrane permeabilization and cell death. *Traffic* **19**, 918–931 (2018).
237. Webster, B. M., Colombi, P., Jager, J. & Lusk, C. P. Surveillance of nuclear pore complex assembly by ESCRT-III/Vps4. *Cell* **159**, 388–401 (2014).
238. Weidberg, H., Moretto, F., Spedale, G., Amon, A. & Werven, F. J. van. Nutrient Control of Yeast Gametogenesis Is Mediated by TORC1, PKA and Energy Availability. *PLOS Genetics* **12**, e1006075 (2016).
239. Xu, L., Ajimura, M., Padmore, R., Klein, C. & Kleckner, N. NDT80, a meiosis-specific gene required for exit from pachytene in Saccharomyces cerevisiae. *Mol Cell Biol* **15**, 6572–6581 (1995).
240. Zhou, Q. *et al.* Mitochondrial endonuclease G mediates breakdown of paternal mitochondria upon fertilization. *Science* **353**, 394–399 (2016).
241. Zhou, S., Sternglanz, R. & Neiman, A. M. Developmentally regulated internal transcription initiation during meiosis in budding yeast. *PLoS One* **12**, e0188001 (2017).
242. Zimmermann, A., Bauer, M. A., Kroemer, G., Madeo, F. & Carmona-Gutierrez, D. When less is more: hormesis against stress and disease. *Microb Cell* **1**, 150–153.

Appendix A

Additional Results

A.1 Supplemental data for Chapter 2: Nuclear envelope remodeling drives the removal of age-induced damage during meiotic differentiation.

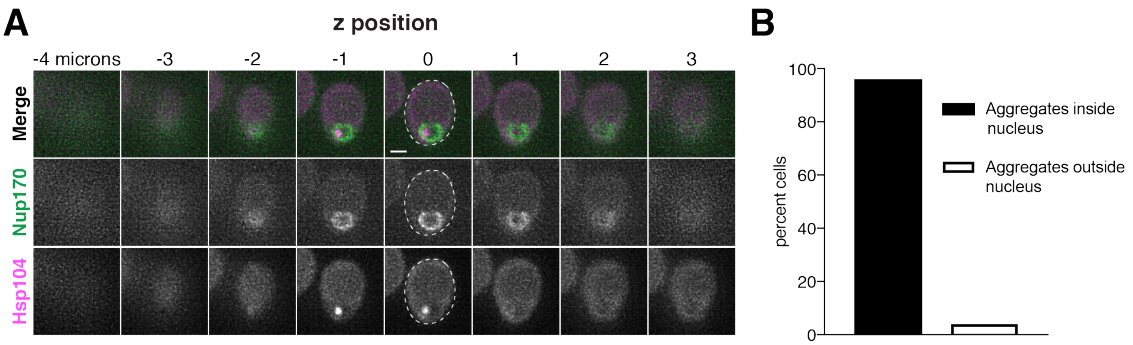

Figure A1.1.1. Age-induced protein aggregates are localized inside the nucleus prior to the meiotic divisions. A. Z-slices of an aged prophase I cell (7 generations old) depicting localization of NPCs, marked by Nup170-GFP, and protein aggregates, marked by Hsp104-mCherry (UB12975). **B.** Quantification depicting frequency of pre-meiotic cells with protein aggregates inside the nucleus (median replicative age = 6, mean replicative age = 6.2 ± 2.1, n =100 cells). Scale bars, 2 μm.

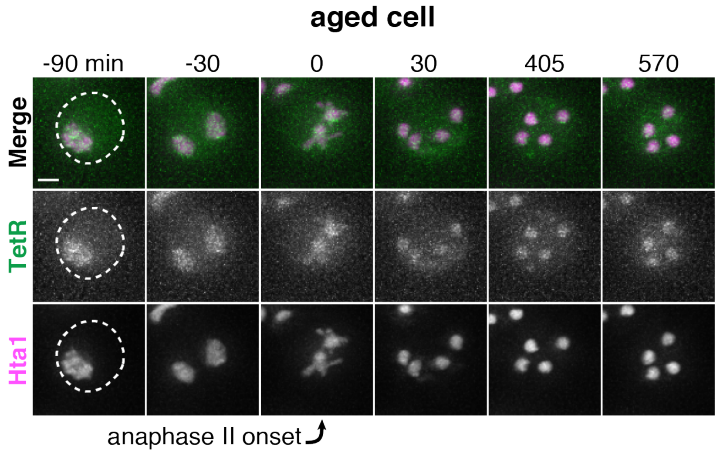

Figure A1.1.2. TetR-GFP is not sequestered in aged cells lacking the rDNA-tetO array. Montage of an aged cell (9 generations old) containing TetR-GFP but lacking the tetO array (UB17509). Chromosomes were visualized with histone marker Hta1-mApple, and the time point depicting anaphase II onset was defined as 0 minutes as indicated by the arrow. Scale bars, 2 μm.

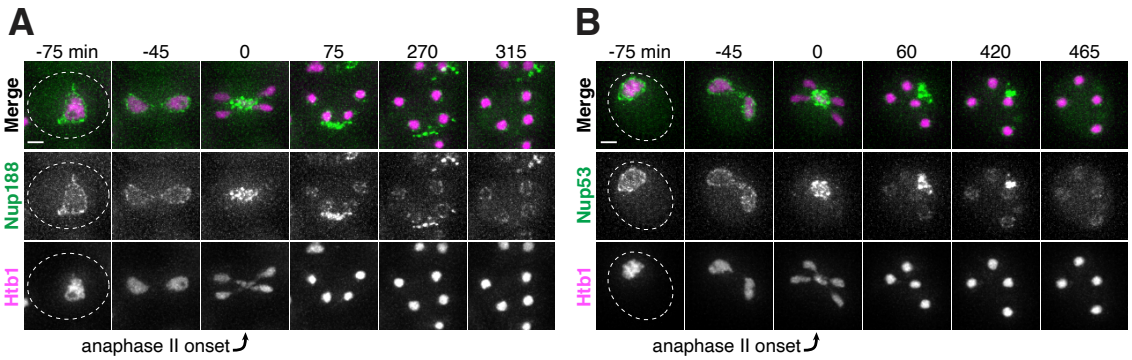

Figure A1.2.1. The inner ring complex nucleoporins Nup188 and Nup53 are sequestered away from chromosomes and subsequently eliminated. A-B. Montages of young cells with **A.** Nup188-GFP (UB13505) and **B.** Nup53-eGFP (UB3810) progressing through meiosis. Chromosomes were visualized with the histone marker Htb1-mCherry, and the time point depicting anaphase II onset was defined as 0 minutes as indicated by the arrows. Scale bars, 2 μm.

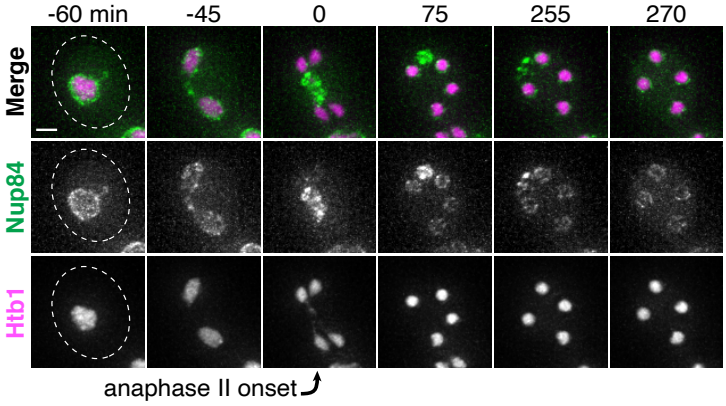

Figure A1.2.2. The Y-complex nucleoporin Nup84 is sequestered away from chromosomes and subsequently eliminated. Montages of a young cell with Nup84-GFP (UB13497) progressing through meiosis. Chromosomes were visualized with the histone marker Htb1-mCherry, and the time point depicting anaphase II onset was defined as 0 minutes as indicated by the arrow. Scale bar, 2 μm.

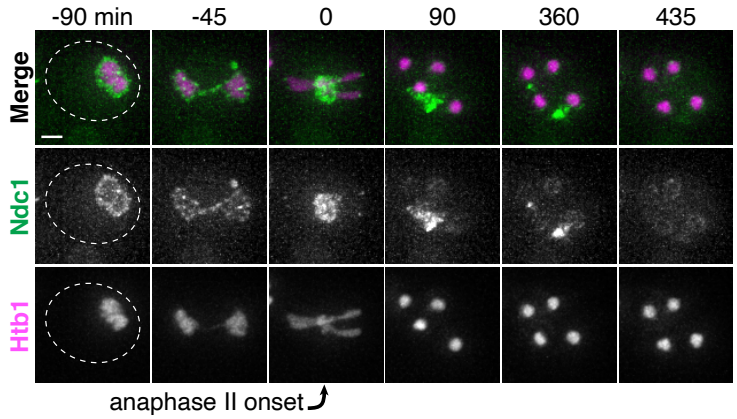

Figure A1.2.3. The transmembrane nucleoporin Ndc1 is sequestered away from chromosomes and subsequently eliminated. Montages of a young cell with Ndc1-GFP (UB15301) progressing through meiosis. Chromosomes were visualized with the histone marker Htb1-mCherry, and the time point depicting anaphase II onset was defined as 0 minutes as indicated by the arrow. Note Ndc1 is also known to localize to spindle pole bodies, consistent with the data shown above (https://www.yeastgenome.org/locus/NDC1). Scale bar, 2 μm.

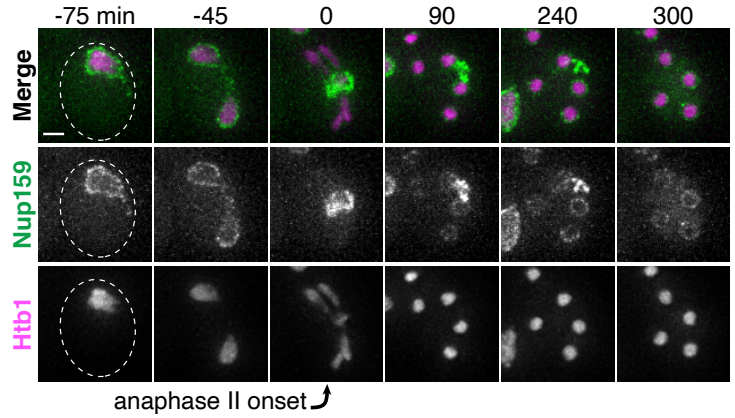

Figure A1.2.4. The cytoplasmic nucleoporin Nup159 is sequestered away from chromosomes and subsequently eliminated. Montages of a young cell with Nup159-GFP (UB14650) progressing through meiosis. Chromosomes were visualized with the histone marker Htb1-mCherry, and the time point depicting anaphase II onset was defined as 0 minutes as indicated by the arrow. Scale bar, 2 μm.

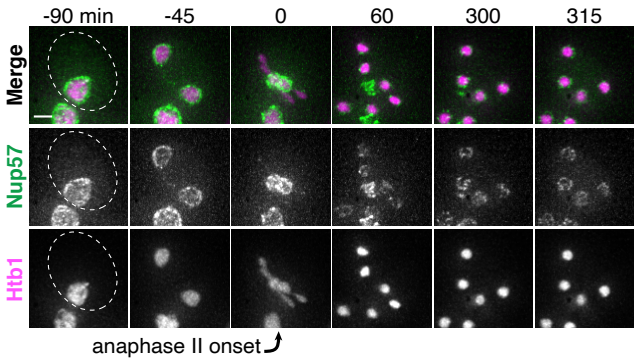

Figure A1.2.5. The channel nucleoporin Nup57 is sequestered away from chromosomes and subsequently eliminated. Montages of a young cell with Nup57-GFP (UB14654) progressing through meiosis. Chromosomes were visualized with the histone marker Htb1-mCherry, and the time point depicting anaphase II onset was defined as 0 minutes as indicated by the arrow. Scale bar, 2 μm.

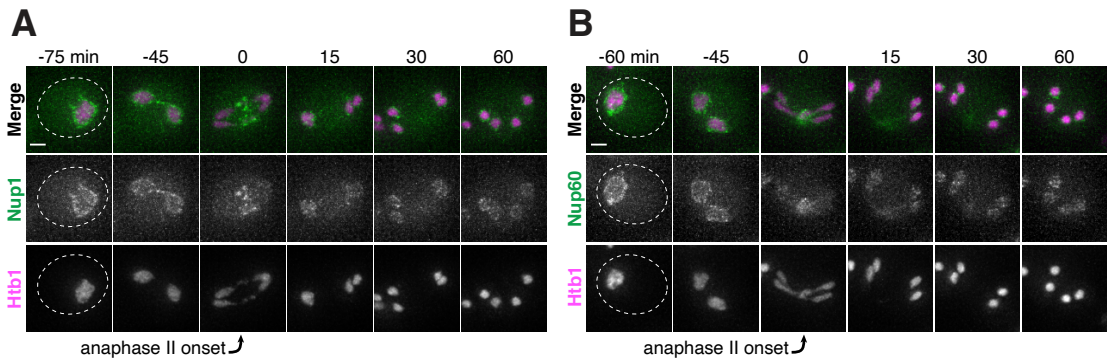

Figure A1.2.6. The nuclear basket nucleoporins Nup1 and Nup60 return to dividing nuclei during and after anaphase II. A-B. Montages of young cells with **A.** Nup1-GFP (UB15303) and **B.** Nup60-GFP (UB14646) progressing through meiosis. Chromosomes were visualized with the histone marker Htb1-mCherry, and the time point depicting anaphase II onset was defined as 0 minutes as indicated by the arrows. Scale bars, 2 μm.

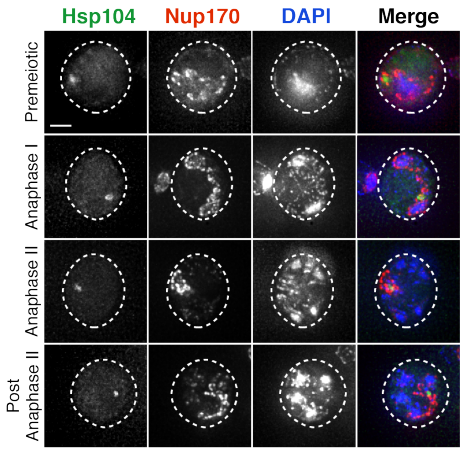

Figure A1.3.1. Protein aggregates are sequestered with disposed NPCs in fixed cells. Maximum intensity projections (derived from fifty 0.2 µm Z slices of fixed premeiotic and meiotic cells depicting localization of NPCs, marked by Nup170-GFP, and protein aggregates, marked by Hsp104-mCherry (UB12975). Scale bar, 2 µm.

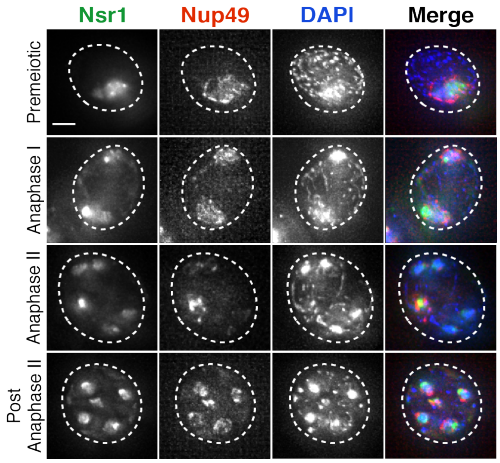

Figure A1.3.2. Nucleolar material is sequestered with disposed NPCs in fixed cells. Maximum intensity projections (derived from fifty 0.2 µm Z slices of fixed premeiotic and meiotic cells depicting localization of NPCs, marked by Nup49-mCherry, and nucleolar material, marked by Nsr1-GFP (UB16708). Scale bar, 2 µm.

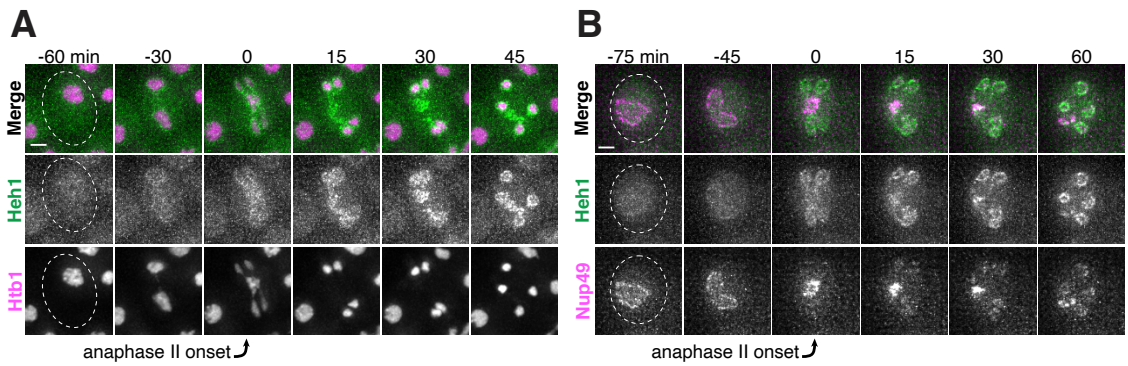

Figure A1.4.1. The inner nuclear envelope protein Heh1 localizes to the dividing nuclei and nucleoporin mass during anaphase II. A-B. Montages of young cells with a fluorescently-tagged inner nuclear membrane protein Heh1-3xeGFP and either **A.** Htb1-mCherry, a histone marker (UB14393), or **B.** Nup49-mCherry, a nucleoporin (UB14391). The time point depicting anaphase II onset was defined as 0 minutes as indicated by the arrows. Scale bars, 2 μm.

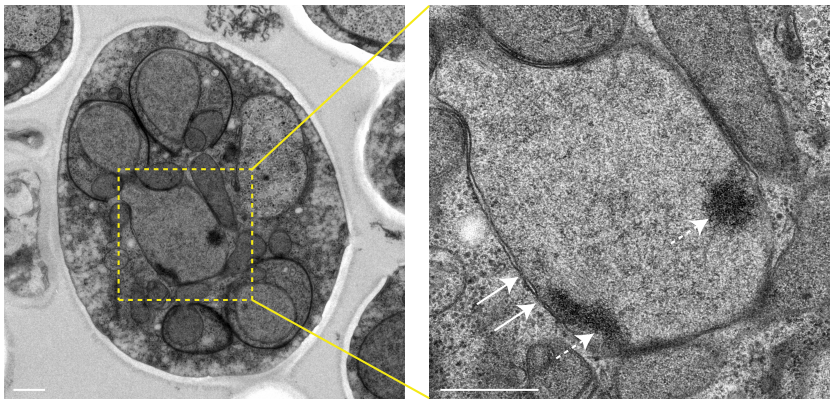

Figure A1.4.2. The nuclear envelope region outside of gamete plasma membranes contains NPCs and nucleolar material during early anaphase II. Electron micrographs of a young early anaphase II cell and an inset of the nuclear envelope-bound region outside the gamete plasma membranes (UB11513). Solid arrows indicate NPCs; dashed arrows indicate nucleolar mass. Scale bars, 0.5 μm.

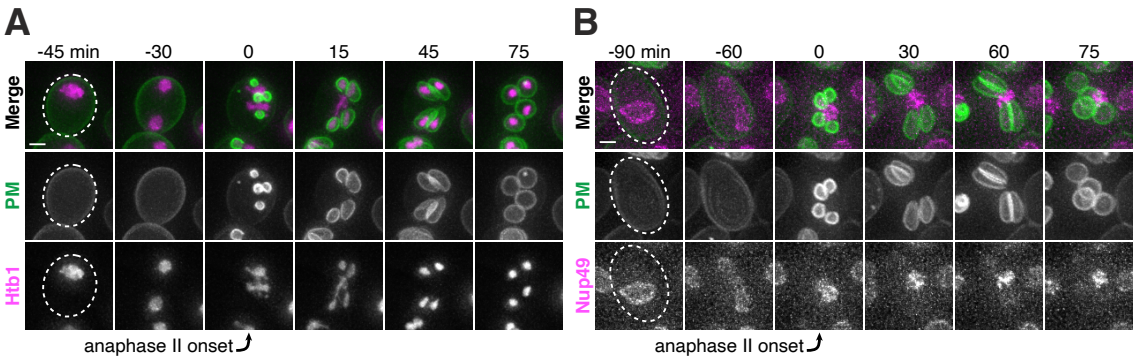

Figure A1.5.1. Dynamic localization of sequestered nucleoporins relative to gamete plasma membranes. A-B. Montages of young cells progressing through the meiotic divisions with a gamete plasma membrane marker yeGFP-Spo20$^{51-91}$ and either **A.** a histone marker Htb1-mCherry (UB12434), or **B.** a nucleoporin marker Nup49-mCherry (UB12342). The time point depicting anaphase II onset was defined as 0 minutes as indicated by the arrows. Scale bars, 2 μm.

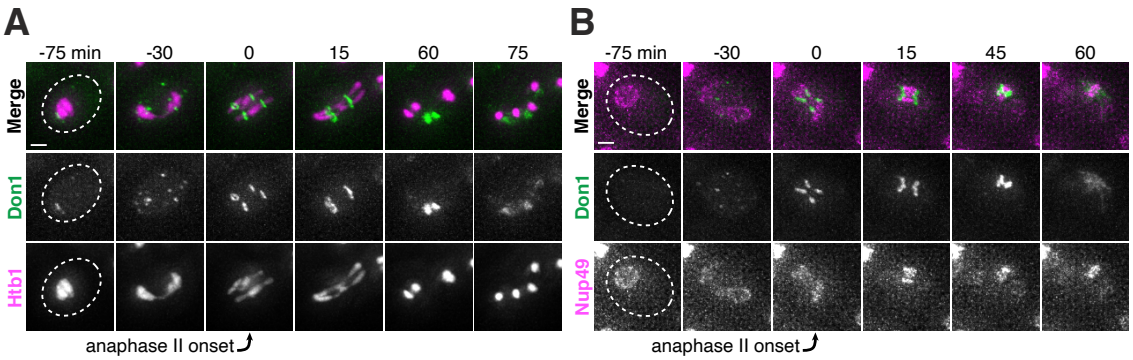

Figure A1.5.2 Dynamic localization of sequestered nucleoporins relative to the leading edge of gamete plasma membranes. A-B. Montages of young cells progressing through the meiotic divisions with the leading edge marker Don1-GFP and either **A.** a histone marker Htb1-mCherry (UB12438), or **B.** a nucleoporin marker Nup49-mCherry (UB12436). The time point depicting anaphase II onset was defined as 0 minutes as indicated by the arrows. Scale bars, 2 μm.

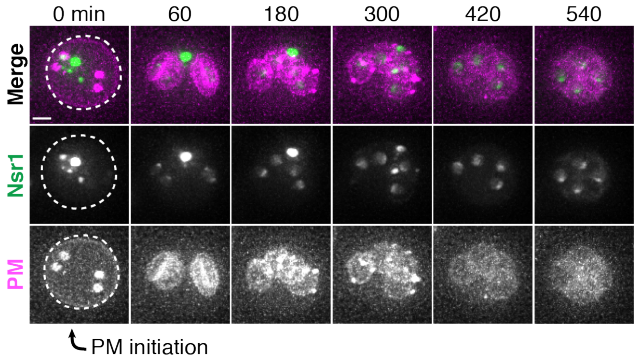

Figure A1.5.3. Nucleolar material in aged cells is excluded from the developing gametes. Montage of an aged cell (7 generations old) excluding nucleolar material marked by Nsr1-GFP during meiosis II (UB16710). Gamete plasma membranes were marked by mKate-Spo20$^{51-91}$. The time point depicting anaphase II onset was defined as 0 minutes as indicated by the arrow. Scale bar, 2 μm.

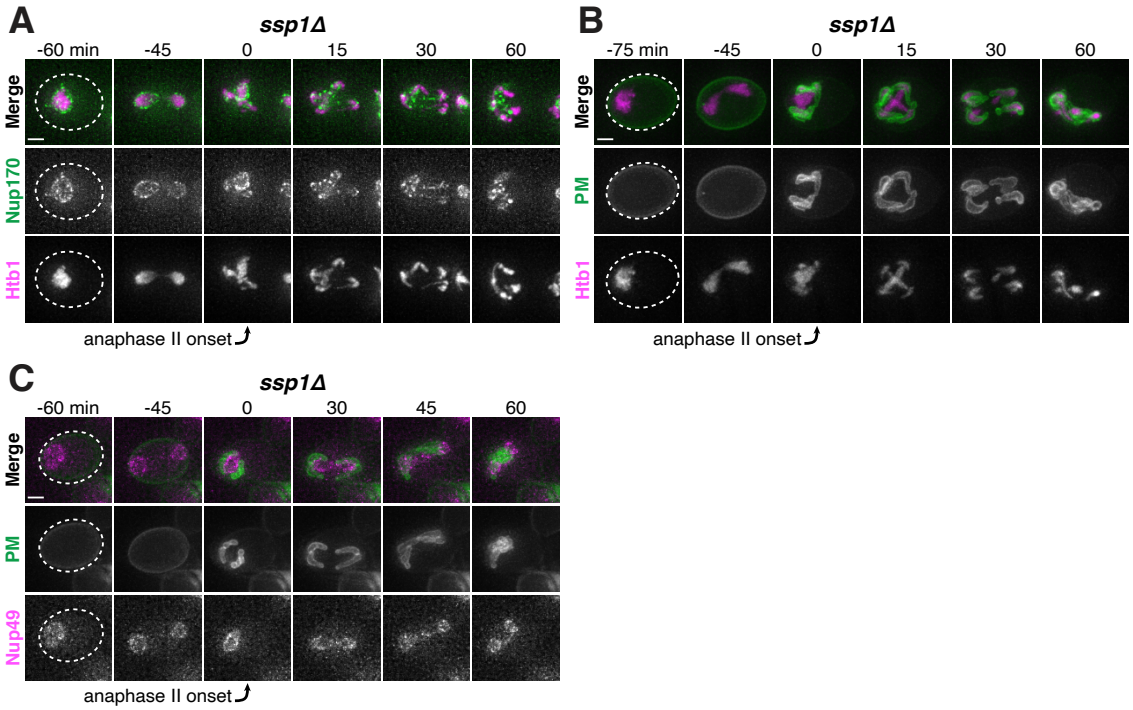

Figure A1.6.1. The leading edge complex member Ssp1 is required for proper gamete plasma membrane formation and nucleoporin sequestration. A-C. Montages of young *ssp1Δ* cells progressing through the meiotic divisions with the following tags: **A.** nucleoporin Nup170-GFP and histone Htb1-mCherry (UB13373); **B.** gamete plasma membrane yeGFP-Spo20$^{51-91}$ and histone Htb1-mCherry (UB13475); **C.** and gamete plasma

membrane yeGFP-Spo20$^{51-91}$ and nucleoporin Nup49-mCherry (UB13473). The time point depicting anaphase II onset was defined as 0 minutes as indicated by the arrows. Scale bars, 2 μm.

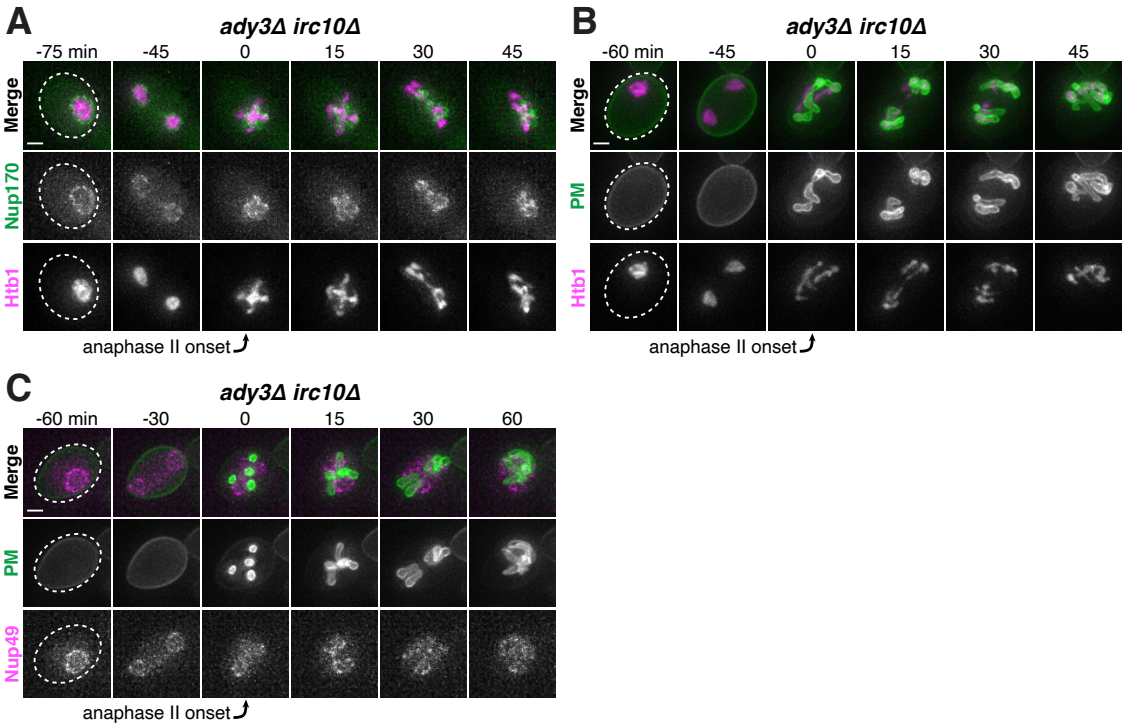

Figure A1.6.2. The leading-edge complex members Ady3 and Irc10 are required for proper gamete plasma membrane formation and nucleoporin sequestration. A-C. Montages of young *ady3Δ irc10Δ* cells progressing through the meiotic divisions with the following tags: **A.** nucleoporin Nup170-GFP and histone Htb1-mCherry (UB12465); **B.** gamete plasma membrane yeGFP-Spo20$^{51-91}$ and histone Htb1-mCherry (UB13585); **C.** and gamete plasma membrane yeGFP-Spo20$^{51-91}$ and nucleoporin Nup49-mCherry (UB13583). The time point depicting anaphase II onset was defined as 0 minutes as indicated by the arrows. Scale bars, 2 μm.

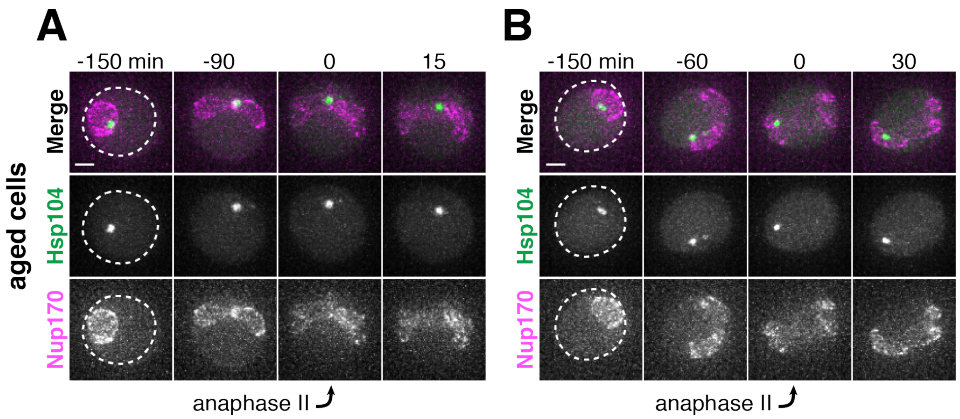

Figure A1.7.1. Protein aggregates co-localize with NPCs during anaphase II in *spo21Δ* cells. **(A-B)** Montages of aged *spo21Δ* cells with protein aggregates labeled with Hsp104-mCherry and NPCs labeled with Nup170-GFP (UB13568). **A.** Montage of a cell that sequesters protein aggregates during meiosis II (7 generations old). **B.** Montage of a cell that retains protein aggregates during meiosis II (6 generations old). The time point depicting anaphase II was defined as 0 minutes as indicated by the arrows. Scale bars, 2 μm.

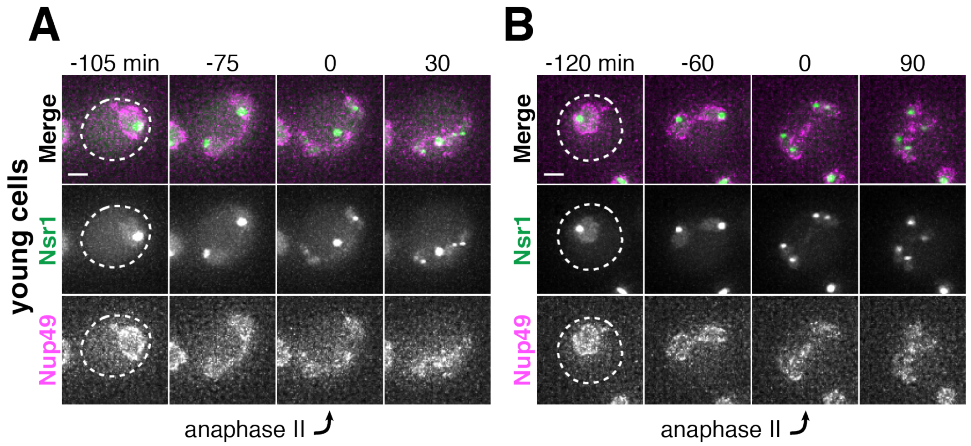

Figure A1.7.2. Nucleolar material co-localizes with NPCs during anaphase II in *spo21Δ* cells. A-B. Montages of young *spo21Δ* cells with nucleolar material labeled with Nsr1-GFP and NPCs labeled with Nup49-mCherry (UB14425). **A.** Montage of a cell that sequesters an Nsr1-GFP punctum during meiosis II. **B.** Montage of a cell that retains all Nsr1-GFP during meiosis II. The time point depicting anaphase II was defined as 0 minutes as indicated by the arrows. Scale bars, 2 μm.

Table A1.1. Meiotic septin and leading edge complex genes are not required for nuclear pore complex or protein aggregate sequestration.

Function	Gene	NPC Strain (Nup170-GFP)	Protein Aggregate strain (Hsp104-GFP)
Leading edge	*ady3Δ*	UB12414	UB19758
	don1Δ	UB12461	UB19756
	irc10Δ	UB12463	UB19762
Meiotic septins	*spr3Δ*	UB15307	UB19752
	spr28Δ	UB15426	UB19754
	spr3Δspr28Δ	UB15428	UB19760

A.2 Supplemental data for Chapter 3: A gamete plasma membrane proton pump facilitates programmed cellular destruction during meiotic differentiation

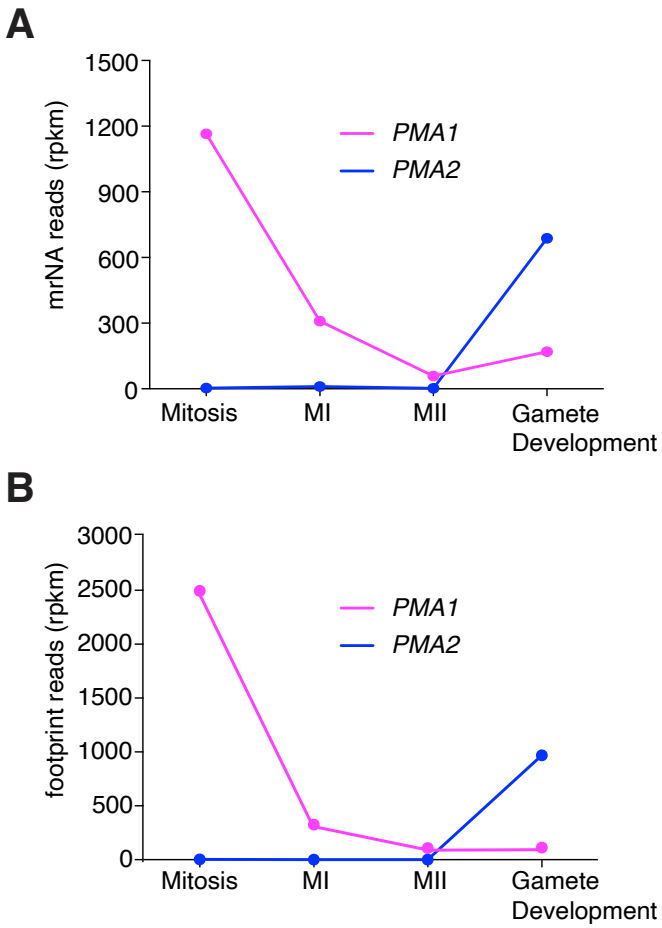

Figure A2.1. *PMA1* and *PMA2* expression during gametogenesis are anti-correlated. mRNA **(A)** and ribosome footprint levels **(B)** plotted across different time points that pertain to different stages of gametogenesis (units are in rpkm). Data obtained from Brar et al., 2012.

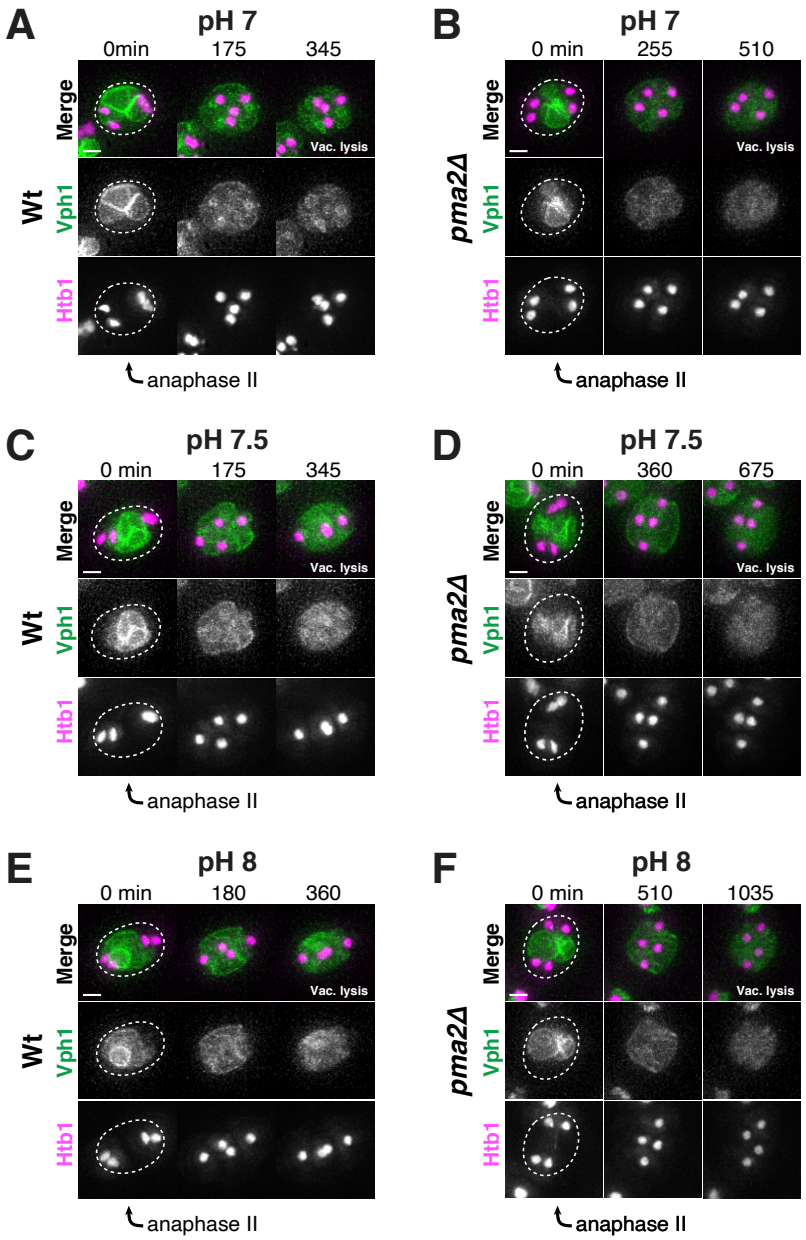

Figure A2.2. *PMA2* facilitates vacuolar lysis in a pH dependent manner. **A.** Montage of a wild-type cell undergoing vacuolar lysis at pH 7.0 (UB12162). **B.** Montage of a *pma2Δ* cell undergoing vacuolar lysis at pH 7.0 (UB20506). **C.** Montage of a wild-type cell undergoing vacuolar lysis at pH 7.5 (UB12162). **D.** Montage of a *pma2Δ* cell undergoing vacuolar lysis at pH 7.5 (UB20506). **E.** Montage of a wild-type cell undergoing vacuolar lysis at pH 8.0 (UB12162). **F.** Montage of a *pma2Δ* cell undergoing vacuolar lysis at pH 8.0 (UB20506). For montages depicted in A-F, the vacuole is labeled with Vph1-GFP and nuclei are labeled with Htb1-mCherry. The time point depicting anaphase II was defined as 0 minutes as indicated by the arrows. Scale bars, 2 μm.

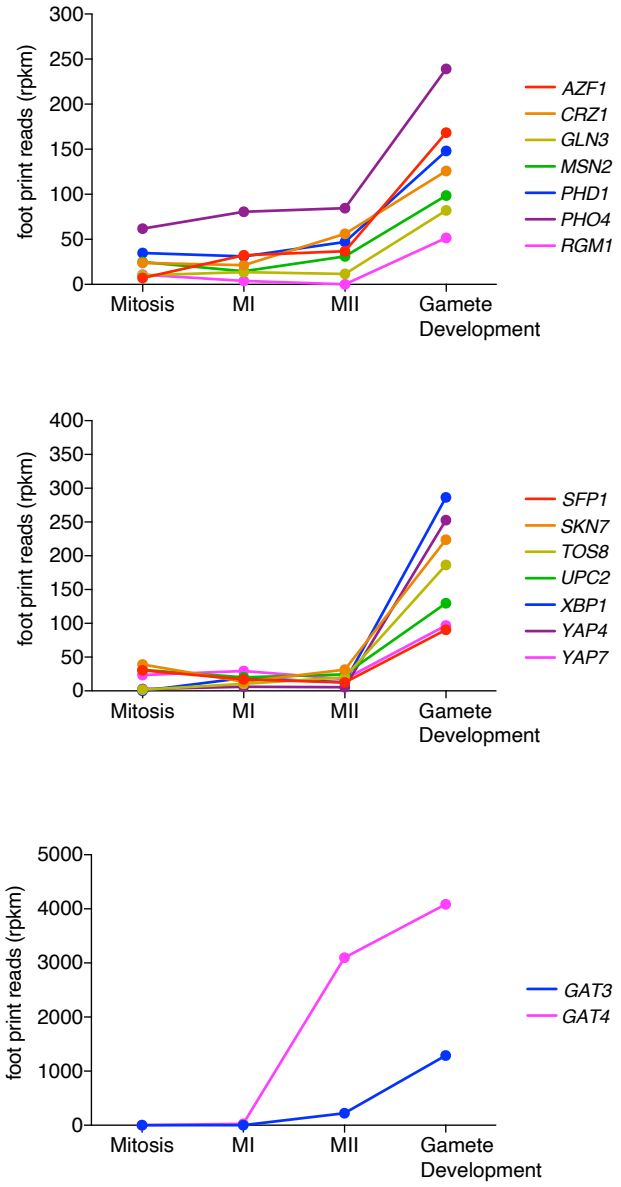

Figure A2.3. Transcription regulator candidates for *PMA2*. Ribosome footprint levels of transcription factors that are upregulated after the meiotic divisions (top, middle and bottoms graphs, units are in rpkm). Data obtained from Brar et al., 2012.

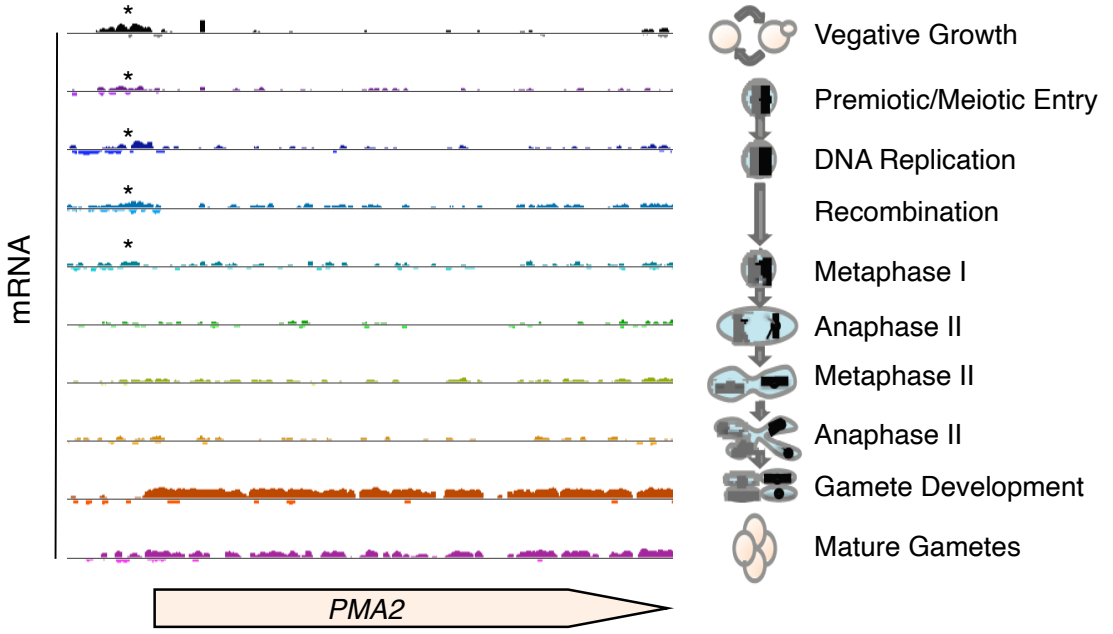

Figure A2.4. mRNA occupancy profile of *PMA2* in gametogenesis. Time points are denoted on the right. Asterisks denote presumptive non-canonical transcript expressed at early time points. Data obtained from Brar et al., 2012. Plot was generated by MochiView (Homann and Johnson, 2010).

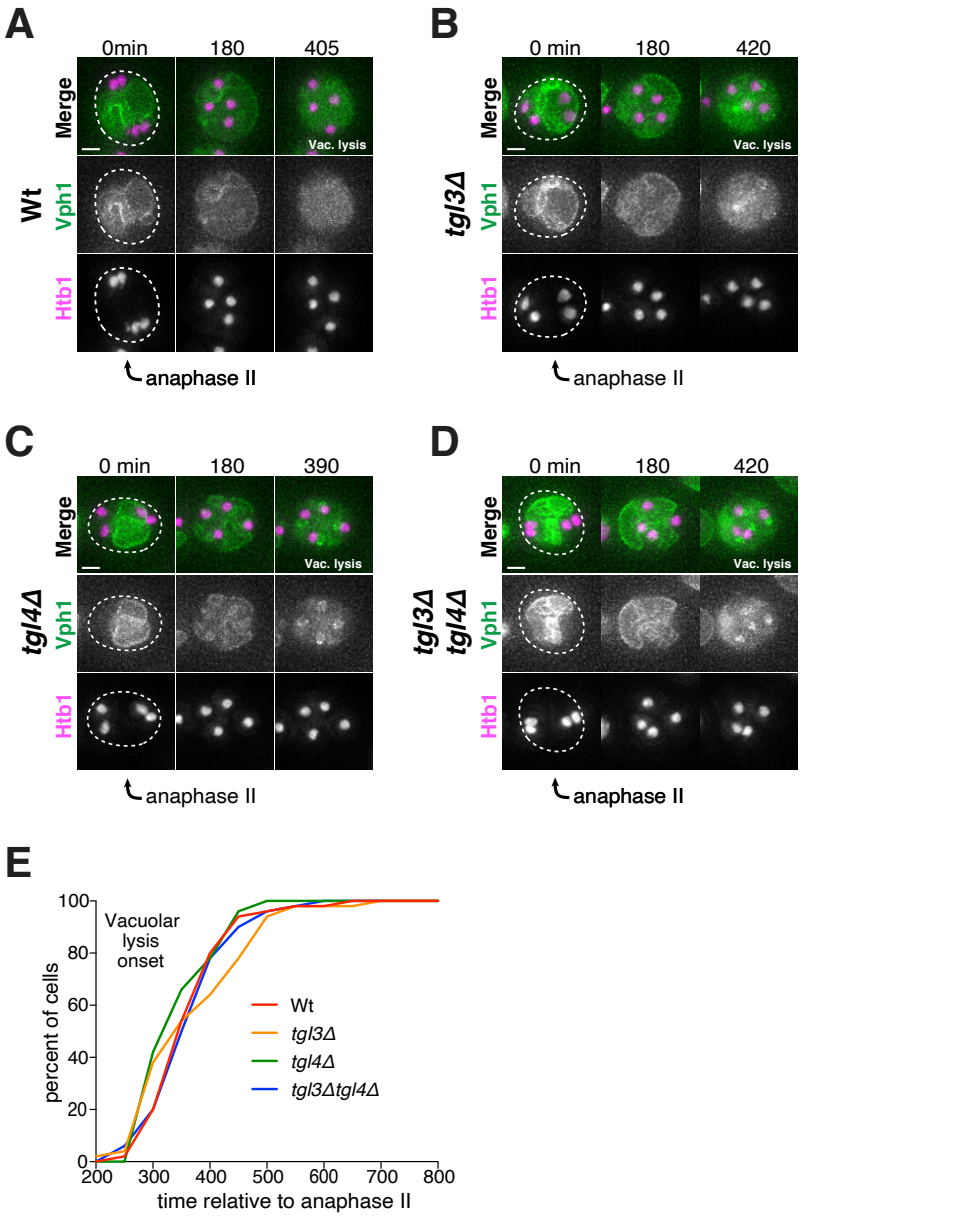

Figure A2.5. Meiotic lipases *TGL3* and *TGL4* do not affect timely vacuolar lysis. A. Montage of a wild-type cell undergoing vacuolar lysis (UB12162). **B.** Montage of a *tgl3Δ* cell undergoing vacuolar lysis (UB26367). **C.** Montage of a t*gl4Δ* cell undergoing vacuolar lysis (UB25986). **D.** Montage of a *tgl3Δtgl4Δ* cell undergoing vacuolar lysis (UB 26711). **E.** Quantification of the experiment in panels A-D, timing of vacuolar lysis relative to anaphase II (N= 50 tetrads per condition). For montages depicted in A-D, the vacuole is labeled with Vph1-GFP and nuclei are labeled with Htb1-mCherry. The time point depicting anaphase II was defined as 0 minutes as indicated by the arrows. Scale bars, 2 μm.

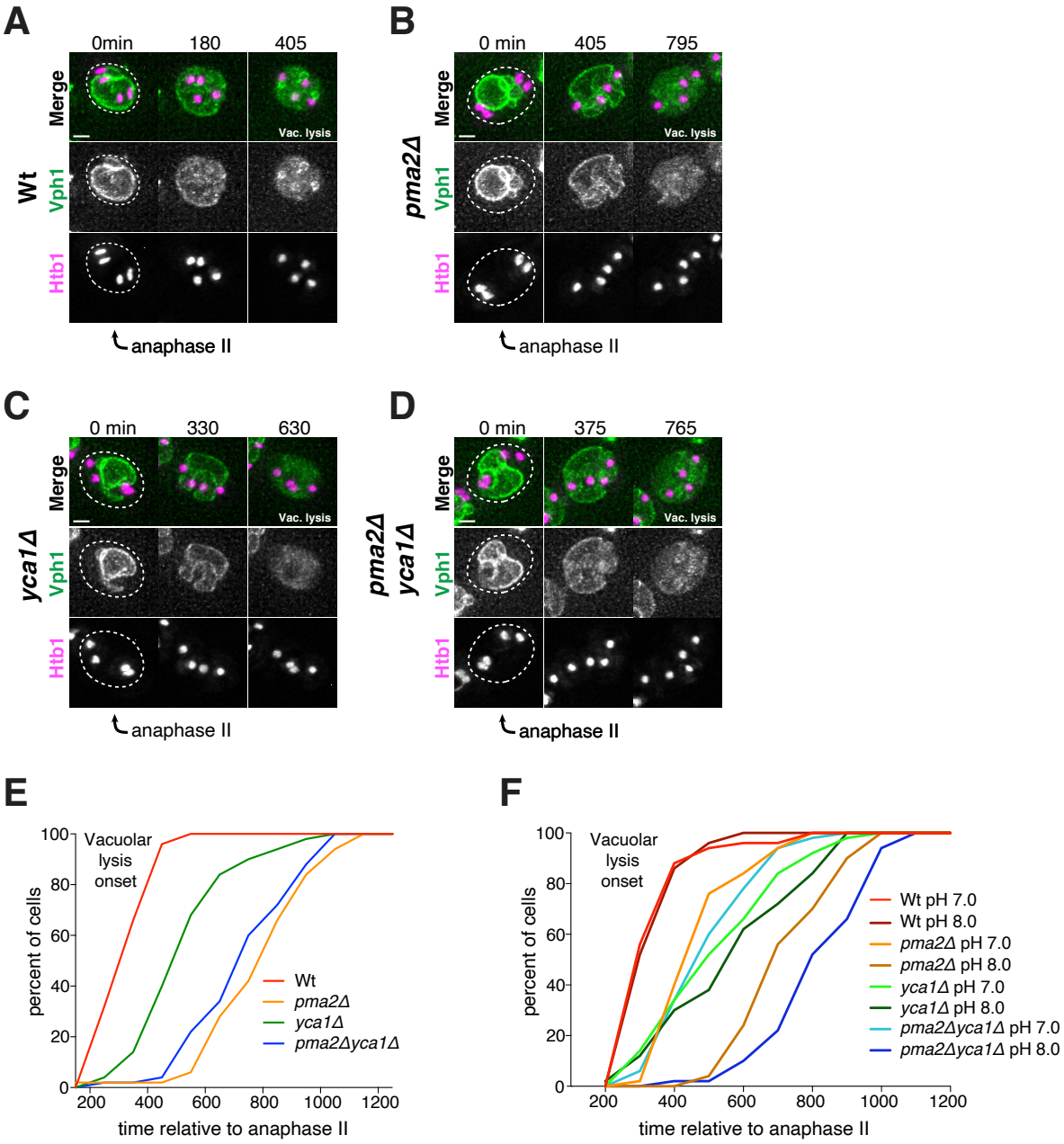

Figure A2.6. Yeast metacaspase gene *YCA1* affects timely vacuolar lysis in a pH dependent manner. A. Montage of a wild-type cell undergoing vacuolar lysis (UB12162). **B.** Montage of a *pma2Δ* cell undergoing vacuolar lysis (UB20506). **C.** Montage of a *yca1Δ* cell undergoing vacuolar lysis (UB 26366). **D.** Montage of a *pma2yca1Δ* cell undergoing vacuolar lysis (UB 26870). **E.** Quantification of the experiment in panels A-D, timing of vacuolar lysis relative to anaphase II (in unbuffered media, N=50 tetrads per condition). **F.** Quantification of wild-type, *pma2Δ*, *yca1Δ* and pma2*yca1Δ* cells undergoing

vacuolar lysis relative to anaphase II in buffered media (SPO + 200 mM MOPS pH 7.0 or SPO + 200 mM MOPS pH 8.0, N=50 tetrads per condition). For montages depicted in A-D, the vacuole is labeled with Vph1-GFP and nuclei are labeled with Htb1-mCherry. The time point depicting anaphase II was defined as 0 minutes as indicated by the arrows. Scale bars, 2 μm.

Table A2.1. List of genes that cluster with *PMA2* gene expression.

mRNA seq (Brar et al., 2012)	ribosome profiling (Brar et al., 2012)
YAL016C-A	YAL016C-A
YBR103C-A	YBL106C
YBR116C	YBR116C
YBR116C	YCL007C
YBR117C	YCR081C-A
YBR200W-A	YDL024C
YDL024C	YDL026W
YDL151C	YDR213W
YDL204W	YDR402C
YDL218W	YDR403W
YDR095C	YEL049W
YDR290W	YEL057C
YDR402C	YER067C-A
YDR403W	YER079C-A
YEL018C-A	YER096W
YEL057C	YFL020C
YER152W-A	YGL123C-A
YFL020C	YHL034W-A
YGL218W	YHR056W-A
YHR056W-A	YHR061C
YHR061C	YHR125W
YIL101C	YIL102C
YIL102C	YJR061W
YIR020C-B	YJR150C
YIR038C	YLL057C
YJL032W	YLR235C
YJL175W	YLR252W
YJR061W	YMR057C
YKL096W-A	YMR084W
YLL044W	YMR085W
YLR109W	YMR086W
YLR187W	YMR172C-A
YLR219W	YMR215W
YLR232W	YNL266W
YMR084W	YOR072W-B
YMR085W	YOR169C
YMR086W	YPL036W
YMR135W-A	YPL112C
YMR251W	YPL272C
YMR317W	YPR059C
YOL052C-A	
YOR050C	
YOR181W	
YOR225W	
YPL036W	
YPL135C-A	
YPL251W	
YPR074W-A	

Hierarchical clustering of Brar et al. 2012 datasets were done with Cluster 3.0 (Eisen et al., 1998; de Hoon et al; 2004).

Appendix B

Materials and Methods

B.1 Yeast strains, plasmids and primers

All strains in these studies are derivatives of SK1 and specified in Table B1.1. Strains UB17338, UB17509 and UB17532 are derivatives of strain HY2545 (a gift from Dr. Hong-Guo Yu). Deletion and C-terminal tagging at endogenous loci were performed using previously described PCR-based methods unless otherwise specified (Longtine et al., 1998; Janke et al., 2004; Sheff and Thorn, 2004). Deletion of *SSP1* was performed by transforming cells with a PCR amplicon of the locus from the SK1 yeast deletion collection (a gift from Dr. Lars Steinmetz). Primer sequences used for strain construction are specified in Table B1.2, and plasmids used for strain construction are specified in Table B1.3. The following strains were constructed in a previous studies: *flo8Δ* (Boselli et al., 2009), Htb1-mCherry (Matos et al., 2008), Hsp104-eGFP (Unal et al., 2011), *ndt80Δ* (Xu et al., 1995), and *spo21Δ* (Sawyer et al., 2019).

To visualize the vacuole, we used either an eGFP-tagged version of Vph1 integrated at the *HIS3* locus or a mCherry-tagged version of Vph1 at its endogenous locus. To generate the eGFP-tagged version, we amplified the W303 genomic region from 1000 bp upstream to immediately before the stop codon of *VPH1* (2520 bp after the ORF start) and fused it to yeGFP in the *HIS3* integrating plasmid pNH603 (a gift from Leon Chan). We then performed integration at the *HIS3* locus by cutting the plasmid with PmeI. To generate the mCherry-tagged version, we constructed a new *HIS3*-selectable mCherry plasmid by replacing eGFP in pYM28 (Janke et al., 2004) with mCherry. We then tagged the locus via traditional PCR-based methods.

To visualize the nuclear envelope, we generated an inner nuclear membrane-localizing reporter (eGFP-h2NLS-L-TM) by fusing eGFP and amino acids 93 to 378 of Heh2 (Gene ID: 852069; Meinema et al., 2011) under control of pARO10 in the *LEU2* integrating plasmid pLC605 (a gift from Leon Chan). To visualize the gamete plasma membranes, we used a reporter consisting of amino acids 51 to 91 from Spo20 fused to the C terminus of link-yeGFP under control of pATG8 in a *LEU2* integrating plasmid (Sawyer et al., 2019). We also constructed a new variant with mKate2 in place of yeGFP. All *LEU2* integration constructs were integrated into the genome by cutting the plasmids with PmeI.

To assemble the *PMA1* and *PMA2* transgenes, we amplified the SK1 genomic region from 1000 bp upstream of the *PMA2* start site along with the ORF of each gene (2757 bp for *PMA1*; 2844 bp for *PMA2*) and fused to a *TRP1*

integrating plasmid pNH604 (a gift from Leon Chan). We then performed integration at the *TRP1* locus by cutting both integrating plasmids with PmeI.

Table B1.1. Strain table.

Strain	Genotype
SK1 wild-type	*ho::LYS2 lys2 ura3 leu2::hisG his3::hisG trp1::hisG*
UB3810	*MAT**a** /MATalpha Htb1-mCherry::HISMX6/Htb1-mCherry::HISMX6 Nup53-eGFP:KanMX6/Nup53-eGFP:KanMX6*
UB9724	*MAT**a** /MATalpha Htb1-mCherry::HISMX6/Htb1-mCherry::HISMX6 Hsp104-eGFP::KanMX6/Hsp104-eGFP::KanMX6 flo8::KanMX6/ flo8::KanMX6*
UB11513	*MAT**a** /MATalpha Htb1-mCherry::HISMX6/Htb1-mCherry::HISMX6 Nup170-GFP::KanMX6/Nup170-GFP::KanMX6*
UB11821	*MAT**a** /MATalpha Hsp104-mCherry::NatMX6/Hsp104-mCherry::NatMX6 leu2::pATG8-link-yeGFP-SPO20(51-91)::LEU2/leu2::pATG8-link-yeGFP-SPO20(51-91)::LEU2 flo8::KanMX6/flo8::KanMX6*
UB12162	*MAT**a** /MATalpha Htb1-mCherry::HISMX6/Htb1-mCherry::HISMX6 his3::VPH1-eGFP::HIS3/ his3::VPH1-eGFP::HIS3*
UB12163	*MAT**a** /MATalpha flo8::KanMX6/flo8::KanMX6 Hsp104-mCherry::NatMX6/Hsp104-mCherry::NatMX6 his3::VPH1-eGFP::HIS3/ his3::VPH1-eGFP::HIS3*
UB12342	*MAT**a** /MATalpha leu2::pATG8-link-yeGFP-SPO20(51-91)::LEU2/ leu2::pATG8-link-yeGFP-SPO20(51-91)::LEU2 Nup49-mCherry::KanMX6/ Nup49-mCherry::KanMX6*
UB12414	*MAT**a** /MATalpha Ady3::HygB/Ady3::HygB Htb1-mCherry::HISMX6/ Htb1-mCherry::HISMX6 Nup170-GFP::KanMX6/Nup170-GFP::KanMX6*
UB12434	*MAT**a** /MATalpha leu2::pATG8-link-yeGFP-SPO20(51-91)::LEU2/ leu2::pATG8-link-yeGFP-SPO20(51-91)::LEU2 Htb1-mCherry::HISMX6/Htb1-mCherry::HISMX6*
UB12436	*MAT**a** /MATalpha Don1-GFP::KanMX6/Don1-GFP::KanMX6 Nup49-mCherry::KanMX6/Nup49-mCherry::KanMX6*
UB12438	*MAT**a** /MATalpha Don1-GFP::KanMX6/Don1-GFP::KanMX6 Htb1-mCherry::HISMX6/Htb1-mCherry::HISMX6*
UB12461	*MAT**a** /MATalpha Don1::HygB/Don1::HygB Nup170-GFP::KanMX6/Nup170-GFP::KanMX6 Htb1-mCherry::HISMX6/Htb1-mCherry::HISMX6*

UB12463	*MAT**a** /MATalpha Irc10::HygB/Irc10::HygB Nup170-GFP::KanMX6/Nup170-GFP::KanMX6 Htb1-mCherry::HISMX6/Htb1-mCherry::HISMX6*
UB12465	*MAT**a** /MATalpha ady3::HygB/ady3::HygB irc10::HygB/irc10::HygB Nup170-GFP::KanMX6/Nup170-GFP::KanMX6 Htb1-mCherry::HISMX6/ Htb1-mCherry::HISMX6*
UB12932	*MAT**a** /MATalpha leu2::pARO10-eGFP-h2NLS-L-TM::LEU2/leu2::pARO10-eGFP-h2NLS-L-TM::LEU2 Nup49-mCherry::KanMX6/ Nup49-mCherry::KanMX6*
UB12975	*MAT**a** /MATalpha Nup170-GFP::KanMX6/ Nup170-GFP::KanMX6 Hsp104-mCherry::NatMX6/Hsp104-mCherry::NatMX6 flo8::KanMX6/flo8::KanMX6*
UB13299	*MAT**a** /MATalpha Nsr1-GFP::KanMX6/ Nsr1-GFP::KanMX6 Hsp104-mCherry::NatMX6/Hsp104-mCherry::NatMX6 flo8::KanMX6/flo8::KanMX6*
UB13373	*MAT**a** /MATalpha ssp1::KanMX6/ ssp1::KanMX6 Nup170-GFP::KanMX6/Nup170-GFP::KanMX6 Htb1-mCherry::HISMX6/Htb1-mCherry::HISMX6*
UB13377	*MAT**a** /MATalpha spo21::HygB/spo21::HygB Nup170-GFP::KanMX6/Nup170-GFP::KanMX6 Htb1-mCherry::HISMX6/Htb1-mCherry::HISMX6*
UB13473	*MAT**a** /MATalpha ssp1::KanMX6/ ssp1::KanMX6 leu2::pATG8-link-yeGFP-SPO20(51-91)::LEU2/ leu2::pATG8-link-yeGFP-SPO20(51-91)::LEU2 Nup49-mCherry::KanMX6/ Nup49-mCherry::KanMX6*
UB13475	*MAT**a** /MATalpha ssp1::KanMX6/ ssp1::KanMX6 leu2::pATG8-link-yeGFP-SPO20(51-91)::LEU2/ leu2::pATG8-link-yeGFP-SPO20(51-91)::LEU2 Htb1-mCherry::HISMX6/Htb1-mCherry::HISMX6*
UB13497	*MAT**a** /MATalpha Nup84-GFP::KanMX6/ Nup84-GFP::KanMX6 Htb1-mCherry::HISMX6/Htb1-mCherry::HISMX6*
UB13499	*MAT**a** /MATalpha Nup120-GFP::KanMX6/Nup120-GFP::KanMX6 Htb1-mCherry::HISMX6/Htb1-mCherry::HISMX6*
UB13503	*MAT**a** /MATalpha Pom34-GFP::KanMX6/Pom34-GFP::KanMX6 Htb1-mCherry::HISMX6/Htb1-mCherry::HISMX6*
UB13505	*MAT**a** /MATalpha Nup188-GFP::KanMX6/Nup188-GFP::KanMX6 Htb1-mCherry::HISMX6/Htb1-mCherry::HISMX6*
UB13509	*MAT**a** /MATalpha Nup49-GFP::KanMX6/Nup49::KanMX6 Htb1-mCherry::HISMX6/Htb1-mCherry::HISMX6*
UB13568	*MAT**a** /MATalpha spo21::HygB/spo21::HygB Hsp104-mCherry::NatMX6/ Hsp104-mCherry::NatMX6 Nup170-GFP::KanMX6/Nup170-GFP::KanMX6 flo8::KanMX6/flo8::KanMX6*
UB13583	*MAT**a** /MATalpha ady3::HygB/ady3::HygB Irc10::HygB/Irc10::HygB leu2::pATG8-link-yeGFP-SPO20(51-91)::LEU2/ leu2::pATG8-link-yeGFP-SPO20(51-91)::LEU2 Nup49-mCherry::KanMX6/ Nup49-mCherry::KanMX6*

UB13585	*MAT**a** /MATalpha ady3::HygB/ady3::HygB Irc10::HygB/Irc10::HygB leu2::pATG8-link-yeGFP-SPO20(51-91)::LEU2/ leu2::pATG8-link-yeGFP-SPO20(51-91)::LEU2 Htb1-mCherry::HISMX6/Htb1-mCherry::HISMX6*
UB14391	*MAT**a** /MATalpha Heh1-3xeGFP::KanMX6/Heh1-3xeGFP::KanMX6 Nup49-mCherry::KanMX6/ Nup49-mCherry::KanMX6*
UB14393	*MAT**a** /MATalpha Heh1-3xeGFP::KanMX6/Heh1-3xeGFP::KanMX6 Htb1-mCherry::HISMX6/ Htb1-mCherry::HISMX6*
UB14418	*MAT**a** /MATalpha Htb1-mCherry::HISMX6/Htb1-mCherry::HISMX6 Hsp104-eGFP::KanMX6/Hsp104-eGFP::KanMX6 flo8::KanMX6/ flo8::KanMX6 spo21::HygB/spo21::HygB*
UB14419	*MAT**a** /MATalpha Htb1-mCherry::HISMX6/Htb1-mCherry::HISMX6 Nsr1-GFP::KanMX6/ Nsr1-GFP::KanMX6 spo21::HygB/spo21::HygB*
UB14425	*MAT**a** /MATalpha Nsr1-GFP::KanMX6/ Nsr1-GFP::KanMX6 Nup49-mCherry::KanMX6/ Nup49-mCherry::KanMX6 spo21::HygB/spo21::HygB*
UB14646	*MAT**a** /MATalpha Nup60-GFP::KanMX6/ Nup60-GFP::KanMX6 Htb1-mCherry::HISMX6/Htb1-mCherry::HISMX6*
UB14650	*MAT**a** /MATalpha Nup159-GFP::KanMX6/ Nup159-GFP::KanMX6 Htb1-mCherry::HISMX6/Htb1-mCherry::HISMX6*
UB14652	*MAT**a** /MATalpha Nup82-GFP::KanMX6/ Nup82-GFP::KanMX6 Htb1-mCherry::HISMX6/Htb1-mCherry::HISMX6*
UB14654	*MAT**a** /MATalpha Nup57-GFP::KanMX6/Nup57-GFP::KanMX6 Htb1-mCherry::HISMX6/Htb1-mCherry::HISMX6*
UB15118	*MAT**a** /MATalpha Nsr1-GFP::KanMX6/ Nsr1-GFP::KanMX6 Htb1-mCherry::HISMX6/Htb1-mCherry::HISMX6*
UB15301	*MAT**a** /MATalpha Ndc1-GFP::KanMX6/ Ndc1-GFP::KanMX6 Htb1-mCherry::HISMX6/Htb1-mCherry::HISMX6*
UB15303	*MAT**a** /MATalpha Nup1-GFP::KanMX6/ Nup1-GFP::KanMX6 Htb1-mCherry::HISMX6/Htb1-mCherry::HISMX6*
UB15305	*MAT**a** /MATalpha Nup2-GFP::KanMX6/ Nup2-GFP::KanMX6 Htb1-mCherry::HISMX6/Htb1-mCherry::HISMX6*
UB15307	*MAT**a** /MATalpha spr3::HygB/ spr3::HygB Nup170-GFP::KanMX6/ Nup170-GFP::KanMX6 Htb1-mCherry::HISMX6/ Htb1-mCherry::HISMX6*
UB15426	*MAT**a** /MATalpha spr28::HygB/ spr28::HygB Nup170-GFP::KanMX6/ Nup170-GFP::KanMX6 Htb1-mCherry::HISMX6/ Htb1-mCherry::HISMX6*
UB15428	*MAT**a** /MATalpha spr3::HygB/ spr3::HygB spr28::HygB/ spr28::HygB Nup170-GFP::KanMX6/ Nup170-GFP::KanMX6 Htb1-mCherry::HISMX6/ Htb1-mCherry::HISMX6*
UB15672	*MAT**a** /MATalpha Nup2-GFP::KanMX6/ Nup2-GFP::KanMX6 Nup49-mCherry::KanMX6/ Nup49-mCherry::KanMX6*

UB15890	*MAT**a** /MATalpha Nup170-GFP::KanMX6/Nup170-GFP::KanMX6 Vph1-mCherry::HisMX6/Vph1-mCherry::HisMX6*
UB16708	*MAT**a** /MATalpha Nsr1-GFP::KanMX6/ Nsr1-GFP::KanMX6 Nup49-mCherry::KanMX6/ Nup49-mCherry::KanMX6 flo8/flo8*
UB16710	*MAT**a** /MATalpha Nsr1-GFP::KanMX6/ Nsr1-GFP::KanMX6 leu2::pATG8-link-mKate-SPO20(51-91)::LEU2/leu2::pATG8-link-mKate-SPO20(51-91)::LEU2 flo8/flo8*
UB16712	*MAT**a** /MATalpha Nsr1-GFP::KanMX6/ Nsr1-GFP::KanMX6 Htb1-mCherry::HISMX6/ Htb1-mCherry::HISMX6 flo8/flo8*
UB17338	*MAT**a** /MATalpha Hta1-mApple::HIS5/ Hta1-mApple::HIS5 rDNA-5xtetO/rDNA pREC8-TetR-GFP::LEU2/ pREC8-TetR-GFP::LEU2 flo8/flo8 * Derived from HY2545*
UB17509	*MAT**a** /MATalpha Hta1-mApple::HIS5/ Hta1-mApple::HIS5 pREC8-TetR-GFP::LEU2/ pREC8-TetR-GFP::LEU2 flo8/flo8 * Derived from HY2545*
UB17532	*MAT**a** /MATalpha Nup49-mCherry::KanMX6/ Nup49-mCherry::KanMX6 rDNA-5xtetO/+ pREC8-TetR-GFP::LEU2/ pREC8-TetR-GFP::LEU2 flo8/flo8 * Derived from HY2545*
UB19927	*MAT**a** /MATalpha Htb1-mCherry::HISMX6/Htb1-mCherry::HISMX6 Nup170-GFP::KanMX6/Nup170-GFP::KanMX6 ndt80::LEU2/ndt80::LEU2*
UB19229	*MAT**a** /MATalpha Nup84-GFP::KanMX6/ Nup84-GFP::KanMX6 Htb1-mCherry::HISMX6/Htb1-mCherry::HISMX6 ndt80::LEU2/ndt80::LEU2*
UB19752	*MAT**a** /MATalpha Hsp104-mCherry::NatMX6/Hsp104-mCherry::NatMX6 leu2::pATG8-link-yeGFP-SPO20(51-91)::LEU2/leu2::pATG8-link-yeGFP-SPO20(51-91)::LEU2 flo8::KanMX6/flo8::KanMX6 spr3::HygB/ spr3::HygB*
UB19754	*MAT**a** /MATalpha Hsp104-mCherry::NatMX6/Hsp104-mCherry::NatMX6 leu2::pATG8-link-yeGFP-SPO20(51-91)::LEU2/leu2::pATG8-link-yeGFP-SPO20(51-91)::LEU2 flo8::KanMX6/flo8::KanMX6 spr28::HygB/ spr28::HygB*
UB19756	*MAT**a** /MATalpha Hsp104-mCherry::NatMX6/Hsp104-mCherry::NatMX6 leu2::pATG8-link-yeGFP-SPO20(51-91)::LEU2/leu2::pATG8-link-yeGFP-SPO20(51-91)::LEU2 flo8::KanMX6/flo8::KanMX6 don1::HygB/ don1::HygB*
UB19758	*MAT**a** /MATalpha Hsp104-mCherry::NatMX6/Hsp104-mCherry::NatMX6 leu2::pATG8-link-yeGFP-SPO20(51-91)::LEU2/leu2::pATG8-link-yeGFP-SPO20(51-91)::LEU2 flo8::KanMX6/flo8::KanMX6 ady3::HygB/ ady3::HygB*
UB19760	*MAT**a** /MATalpha Hsp104-mCherry::NatMX6/Hsp104-mCherry::NatMX6 leu2::pATG8-link-yeGFP-SPO20(51-91)::LEU2/leu2::pATG8-link-yeGFP-SPO20(51-91)::LEU2 flo8::KanMX6/flo8::KanMX6 spr3::HygB/ spr3::HygB spr28::HygB/ spr28::HygB*

UB19762	*MAT**a** /MATalpha Hsp104-mCherry::NatMX6/Hsp104-mCherry::NatMX6 leu2::pATG8-link-yeGFP-SPO20(51-91)::LEU2/leu2::pATG8-link-yeGFP-SPO20(51-91)::LEU2 flo8::KanMX6/flo8::KanMX6 irc10::HygB/ irc10::HygB*
UB 20504	*MAT**a** /MATalpha Htb1-mCherry::HISMX6/Htb1-mCherry::HISMX6 PMA2-eGFP::KanMX6/ PMA2-eGFP::KanMX6*
UB 20506	*MAT**a** /MATalpha Htb1-mCherry::HISMX6/Htb1-mCherry::HISMX6 his3::VPH1-eGFP::HIS3/ his3::VPH1-eGFP::HIS3 pma2::HYGB/pma2::HYGB*
UB 25986	*MAT**a** /MATalpha Htb1-mCherry::HISMX6/Htb1-mCherry::HISMX6 his3::VPH1-eGFP::HIS3/ his3::VPH1-eGFP::HIS3 tgl3::HYGB/tgl3::HYGB*
UB 26367	*MAT**a** /MATalpha Htb1-mCherry::HISMX6/Htb1-mCherry::HISMX6 his3::VPH1-eGFP::HIS3/ his3::VPH1-eGFP::HIS3 tgl4::HYGB/tgl4::HYGB*
UB 26711	*MAT**a** /MATalpha Htb1-mCherry::HISMX6/Htb1-mCherry::HISMX6 his3::VPH1-eGFP::HIS3/ his3::VPH1-eGFP::HIS3 tgl3::HYGB/tgl3::HYGB tgl4::HYGB/tgl4::HYGB*
UB 26366	*MAT**a** /MATalpha Htb1-mCherry::HISMX6/Htb1-mCherry::HISMX6 his3::VPH1-eGFP::HIS3/ his3::VPH1-eGFP::HIS3 yca1::HYGB/yca1::HYGB*
UB 26870	*MAT**a** /MATalpha Htb1-mCherry::HISMX6/Htb1-mCherry::HISMX6 his3::VPH1-eGFP::HIS3/ his3::VPH1-eGFP::HIS3 pma2::HYGB/pma2::HYGB yca1::HYGB/yca1::HYGB*
UB 27264	*MAT**a** /MATalpha Htb1-mCherry::HISMX6/Htb1-mCherry::HISMX6 his3::VPH1-eGFP::HIS3/ his3::VPH1-eGFP::HIS3 pma2::HYGB/pma2::HYGB trp1::pPMA2-PMA1::TRP1/ trp1::pPMA2-PMA1::TRP1/*
UB 27266	*MAT**a** /MATalpha Htb1-mCherry::HISMX6/Htb1-mCherry::HISMX6 his3::VPH1-eGFP::HIS3/ his3::VPH1-eGFP::HIS3 pma2::HYGB/pma2::HYGB trp1::TRP1/trp1::TRP1*
UB 28193	*MAT**a** /MATalpha Htb1-mCherry::HISMX6/Htb1-mCherry::HISMX6 his3::VPH1-eGFP::HIS3/ his3::VPH1-eGFP::HIS3 pma2::HYGB/pma2::HYGB trp1::pPMA2-PMA2::TRP1/ trp1::pPMA2-PMA2::TRP1*

Table B1.2. Primers used for strain construction.

Construct name	Forward primer	Reverse primer
HEH1-3xeGFP	GGAACTCAATGAACCTAAGGATTCCGCTGAAAACAAAATACGGATCCCCGGGTTAATTAA	TTTGAGAAGAGAAAACTACGTTTGAGTTTCATTTTGTGGGGAATTCGAGCTCGTTTAAAC
NUP53-eGFP	AAATAGATTGAATAATTGGTTATTTGGATGGAATGATTTGGGTGACGGTCTGGTTTA	AATCGCACCAAAGCACTACATTTGGGGGTAAGGTTTTTCATCGATGAATTCGAGC
NUP84-GFP	GTATCTGGATCTCGTTGCTCGCACAGCAACCCTTTCGAATCGGATCCCCGGGTTAATTAA	TTACTTAAAATATAAACTTATTCTGCAATACATTAATTGAGAATTCGAGCTCGTTTAAAC
NUP120-GFP	GGTTACTTTAACTGATTTAAGAGATGAGTTACGAGGTCTACGGATCCCCGGGTTAATTAA	ATTTTTTAAATGAAGTATTAATTTACAGTTTATATATTCAGAATTCGAGCTCGTTTAAAC
NUP170-GFP	GAACAGCGGCAATAATTTGGGGATTTGTTTCTACAAAGAACGGATCCCCGGGTTAATTAA	ACGTACATTACCCTGCTATCTATATGTCGAACATGAATTTGAATTCGAGCTCGTTTAAAC
POM34-GFP	TGCATATATGATGAACTCACAGTCCCCAAGGGGTAAAATACGGATCCCCGGGTTAATTAA	TATATAGCTATGGAAAGTATTAAATGTTTTTTTGCTGTTTGAATTCGAGCTCGTTTAAAC
NUP188-GFP	AGACATTAAAGCATTACAAGATTCACTATTCAAGGACGTTCGGATCCCCGGGTTAATTAA	ATTATTATATTATGTAGCTTTACATAACTTACAAAATAAGGAATTCGAGCTCGTTTAAAC
NDC1-GFP	GTTTCTAGAAGTGTACGCCTCAGGCAACCCTAATGCTACGCGGATCCCCGGGTTAATTAA	ACATGAAATGGGAGGAGGGGTGCTCCTCGGTTGAATTGTAGAATTCGAGCTCGTTTAAAC
HSP104-mCherry	CGATAATGAGGACAGTATGGAAATTGATGATGACCTAGATCGGATCCCCGGGTTAATTAA	ATTCTTGTTCGAAAGTTTTTAAAAATCACACTATATTAAAGAATTCGAGCTCGTTTAAAC
ssp1Δ	GGCGACACAAAATCATGAAG	TGATGTTTATGTATAGATCTCTCGA
NSR1-GFP	AAATACCGCTTCTTTCGCTGGTTCAAAGAAAACATTTGATCGGATCCCCGGGTTAATTAA	AAGAGAAAAAATTGAAATTGAAATTCATTTCATTTTCTCAGAATTCGAGCTCGTTTAAAC

don1Δ	TTTGGCTGGTATTTAAACACAAGTA AGAGAAGCATCAAACCGGATCCCC GGGTTAATTAA	GCACTTTGCCGAAAGAGTT AATAAACATTACCGCTATA CAGAATTCGAGCTCGTTTA AAC
DON1-GFP	AAAGCAGGTTCATCCATCTAGACAA GAATTAAGTTTTACGCGGATCCCCG GGTTAATTAA	GCACTTTGCCGAAAGAGTT AATAAACATTACCGCTATA CAGAATTCGAGCTCGTTTA AAC
ady3Δ	TTTTGAATGGGATAGTTGAATACAA CAAACTTCTCCGAATCGGATCCCCG GGTTAATTAA	ACACCATTGAATATATTAGT TCTAAATAAAAAAAAAAAAG GAATTCGAGCTCGTTTAAA C
irc10Δ	AGTCTGCGGTATAATCACCTGGCCT AGTGCTTTTTCAATCCGGATCCCCG GGTTAATTAA	CTATATGTCAAGGGTGTCC CAAAATAAAAACTAACAGT ACGAATTCGAGCTCGTTTA AAC
NUP60-GFP	TGAAAATAAAGTTGAGGCTTTCAAG TCCCTATATACCTTTCGGATCCCCG GGTTAATTAA	GGGCTATACGGTAATTATG TCACGGCTAAAATTTTCATT AGAATTCGAGCTCGTTTAA AC
NUP159-GFP	GCAAATTGGTGATTTCTTCAAAAATT TGAACATGGCAAAACGGATCCCCG GGTTAATTAA	TTATTAACGGCACTAACAA CGTACATATAGCTAAATAT CAGAATTCGAGCTCGTTTA AAC
NUP82-GFP	ATTGTTACAAGTTTCTCAGGAATTTA CTACTAAAACTCAACGGATCCCCGG GTTAATTAA	TAGCGTACATATATGATAG CAGACTATGCAAGTCGCTT ACGAATTCGAGCTCGTTTA AAC
NUP57-GFP	GAAAGATGCTGCAATTGTAAAAAAA TATAAAAATAAAACGCGGATCCCCG GGTTAATTAA	CGATCTTTATACAATTCAGT CATTGATTTAAGTAACCTG AGAATTCGAGCTCGTTTAA AC
NUP1-GFP	GGCGAACAGAAAGATTGCAAGAAT GAGGCACTCTAAAAGGCGGATCCC CGGGTTAATTAA	TTCAGAAAAGCAACACAAT ACCTAATTACATAACCGAT ATGAATTCGAGCTCGTTTA AAC
NUP2-GFP	ATTTACGAAAGCTATTGAAGATGCT AAAAAAGAAATGAAACGGATCCCCG GGTTAATTAA	AGGGTTCTATTCTATTTAAA ATTGTTAACTGTATTTACTC GAATTCGAGCTCGTTTAAA C
spr3Δ	TAAAAACCTAAAATTCCTTTTGCGTC ATTGAATTTTTATTCGGATCCCCGG GTTAATTAA	TTGCGCGAAATTATTGGCT TTTTTTTTTTTTTAATTAATA GAATTCGAGCTCGTTTAAA C
spr28Δ	AAAGAGCTACTATACGTACATAAAG TCAGTAAATAATCAACGGATCCCCG	ATTTCATATGTATCTAACGC TAACAAGGCCGTATATTTA

	GGTTAATTAA	TGAATTCGAGCTCGTTTAAAC
VPH1-mCherry	GGAAGTCGCTGTTGCTAGTGCAAGCTCTTCCGCTTCAAGCCGTACGCTGCAGGTCGAC	AGTACTTAAATGTTTCGCTTTTTTTAAAAGTCCTCAAAATATCGATGAATTCGAGCTCG
NUP49-GFP NUP49-mCherry	GAATCGCCGTGTTACATCAAAAAACGAAAACACTGGCATCATTGAGCATACGGATCCCCGGGTTAATTAA	AGACATTTGTACTTGTTATACGCACTATATAAACTTTCAGGGCGATTTACGAATTCGAGCTCGTTTAAAC
PMA2-GFP	TGCTATGCAAAGAGTTTCTACTCAACACGAAAAAAGCAGTCGGATCCCCGGGTTAATTAA	TCAATAAGAAAAAAAATCAGATGGATGATGTTTAAAATTAGAATTCGAGCTCGTTTAAAC
pma2Δ	GTGCTAGTACAATTTAAGCAAAAGGAAACTGTTTTGCGTTCGGATCCCCGGGTTAATTAA	TCAATAAGAAAAAAAATCAGATGGATGATGTTTAAAATTAGAATTCGAGCTCGTTTAAAC
tgl3 Δ	TCATCTATTCATATATCACATCTTTGAGTTGCCGTTAAGCCGGATCCCCGGGTTAATTAA	ATCAATAAAAAAAATAAGACAGAAAAAAGTGGAAACGATAGAATTCGAGCTCGTTTAAAC
tgl4Δ	ATTATTGAAGGGAGTACAGGTATATGTAATAAAAGTCTGACGGATCCCCGGGTTAATTAA	AAAGAATATCTAGAGGATATATAAGCAAGCCCGTGTTTTCGAATTCGAGCTCGTTTAAAC
yca1Δ	TCTAAACTACCACCAAAGAAGACCGACTAGATTTACAATCCGGATCCCCGGGTTAATTAA	CAGTCTGAATACATCTACCAACGTACACATTCATATATTTGAATTCGAGCTCGTTTAAAC

Table B1.3. Plasmids used for strain construction.

Plasmid Name	Description
pUB4	pFA6a-GFP(S65T)-KanMX6
pUB72	pFA6a-mCherry-KanMX6
pUB73	pFA6a-mCherry-NatMX6
pUB76	pFA6a-link-yeGFP-Kan
pUB217	pFA6a-HphNT1
pUB691	pNH603-HIS3-VPH1-eGFP
pUB985	pFA6a-3xeGFP-KanMX6
pUB1104	pLC605-pATG8-link-mKate-SPO20(51-91)
pUB1196	pLC605-pARO10-eGFP-h2NLS-L-TM
pUB1197	pYM28-mCherry-His3MX6
pUB1992	pNH604-pPMA2-PMA1
pUB2000	pNH604-pPMA2-PMA2

B.2 Sporulation conditions

Sporulation was induced using the traditional starvation method unless otherwise indicated. Diploid cells were first grown in YPD (1% yeast extract, 2% peptone, 2% glucose, 22.4 mg/L uracil, and 80 mg/L tryptophan) at room temperature for around 24 hr until the cultures reached a cell density of OD_{600} ≥10. The cultures were then diluted in BYTA (1% yeast extract, 2% bacto tryptone, 1% potassium acetate, and 50 mM potassium phthalate) to OD_{600} = 0.25 and grown for 12–16 hr at 30°C. After reaching an OD_{600} ≥5, the cells were pelleted, washed in sterile MilliQ water, and resuspended in the sporulation media SPO to OD_{600} = 1.85. SPO was 0.5% potassium acetate alone, 1% potassium acetate alone, or 2% potassium acetate supplemented with amino acids (40 mg/L adenine, 40 mg/L uracil, 10 mg/L histidine, 10 mg/L leucine and 10 mg/L tryptophan); the media's pH was adjusted to seven with acetic acid and 0.02% raffinose was added to improve sporulation. For buffered media experiments in Chapter 3, diploid cells were treated with 2% potassium acetate supplemented with amino acids, raffinose and 200 mM MOPS (pHed to either 7.0, 7.5 or 8.0) prior to live imaging. Meiotic cultures were shaken at 30°C for the duration of the experiment. At all stages, the flask size was 10 times the culture volume to ensure proper aeration.

To selectively enrich for the formation of dyads and triads, diploid cells were induced to sporulate in reduced carbon media (Eastwood et al., 2012). Cells were grown in YPD and BYTA as described above and then resuspended in SPO with reduced potassium acetate (0.1% potassium acetate) to an OD_{600} = 1.85. After 5 hr at 30°C, the cells were then pelleted, washed in sterile MilliQ, and resuspended in 0.15% KCl.

B.3 Aged cell isolation and sporulation

Aged cells were enriched using a biotin-labeling and magnetic-sorting assay (Smeal et al., 1996). Cells were grown in YPD at room temperature or 30°C overnight until saturation (OD_{600} ≥10) and then diluted to a cell density of OD_{600} = 0.2 in a new YPD culture. Cells were harvested before the cultures reached OD_{600} = 1 and were labeled with 8 mg/ml EZ-Link Sulfo-NHS-LC-biotin (ThermoFisher Scientific) for 30 min at 4°C. Biotinylated cells were grown for 12-16 hours in YPD with 100 µg/ml ampicillin at 30°C. Cells were subsequently harvested and mixed with 100 µl of anti-biotin magnetic beads (Miltenyi Biotechnology) for 15 min at 4°C. Cells were washed with PBS pH 7.4, 0.5% BSA buffer and sorted magnetically using LS depletion columns with a QuadroMacs sorter following the manufacturer's protocol. A fraction of the flow-through (biotin-negative) was kept as young cells and was budscar labeled with eluted aged cells (biotin-positive) for 20 min at room temperature using 1 µg/ml Wheat Germ Agglutinin, Alexa Fluor 350 Conjugate (ThermoFisher Scientific). A mixture of aged and young cells was subsequently washed twice in H_2O and once with SPO (0.5% or 1% potassium acetate, 0.02% raffinose, pH 7). The cell mixture was resuspended with SPO at a cell density of OD_{600} = 1.85 with 100 µg/ml ampicillin and incubated at 30°C. The number of doublings in subsequent experiments was measured by counting the number of budscars.

B.4 Fluorescence microscopy

Images were acquired using a DeltaVision Elite wide-field fluorescence microscope (GE Healthcare). Live cell images were generated using a 60x/1.42 NA oil-immersion objective; fixed cell images were generated using a 100x/1.40 NA oil-immersion objective. Specific imaging conditions for each experiment are indicated in Table B.4.1. Images were deconvolved using softWoRx imaging software (GE Healthcare). Unless otherwise noted, images were maximum intensity z-projected over the range of acquisition in FIJI (RRID:SCR_002285, Schindelin et al., 2012).

B.4.1 Live-cell imaging

Live cells were imaged in an environmental chamber heated to 30°C, using either the CellASIC ONIX Microfluidic Platform (EMD Millipore) or concanavalin A-coated, glass-bottom 96-well plates (Corning). Unless otherwise stated, imaging experiments used conditioned sporulation media (SPO filter-sterilized after five hours of sporulation at 30°C), as this was found to enhance meiotic progression. With the CellASIC system, cultures in SPO (OD_{600} = 1.85) were transferred to a microfluidic Y04D plate and were loaded with a pressure of 8 psi for 5 s. Conditioned SPO was subsequently applied with a constant flow rate pressure of 2 psi for 15–20 hr. For the germination experiment described in chapter 3, gametes (diluted to OD_{600} = 0.37) were transferred to a microfluidic

Y04D plate and were loaded with a pressure of 8 psi for 5 s. SC media (containing 6.7 g/L YNB, 2X amino acid supplement powder [US biological sciences, D9515] and 2% glucose) was subsequently applied with a constant flow rate pressure of 2 psi for 10 hr. With the 96-well plates, cells were adhered to the bottom of the wells and 100 µl of conditioned SPO was added to each well. Images were acquired every 15 min for 16–24 hr.

B.4.2 Fixed-cell imaging

Fixed cells were prepared by treating 500–1000 µl of meiotic culture with 3.7% formaldehyde for 15 min at room temperature. Cells were permeabilized with either 1% Triton X-100 or 70% ethanol. (1) For Figures A1.3.1-2, cells were washed with 0.1 M potassium phosphate pH 6.4 and subsequently treated with 0.05 µg DAPI and 1% Triton in KPi sorbitol (0.1 M potassium phosphate, 1.2 M sorbitol, pH 7.5). Cells were then immediately washed with KPi sorbitol before imaging. (2) For Figure 2.6A-B, cells were treated for five minutes with 1% Triton in KPi sorbitol and then resuspended in KPi sorbitol. Cells were then adhered on a poly-lysine treated multi-well slide and mounted with Vectashield Mounting Medium with DAPI (Vector Labs). (3) For Figures 2.5A-B, 2.8C-D and 2.8F, cells were washed with 0.1 M potassium phosphate pH 6.4 and then resuspended in KPi sorbitol buffer. Cells were then adhered to a poly-lysine treated multi-well slide, quickly permeabilized with 70% ethanol, and mounted with Vectashield Mounting Medium with DAPI (Vector Labs).

Table B4.1. Imaging conditions. Transmission, exposure time, and excitation/emission wavelengths are specified for each channel. Distance between z-sections and number of z-sections acquired are indicated.

Figure	RFP	GFP	BFP/DAPI	POL	Z Sectioning
2.3B-G, A1.2.1A-B, A1.2.2, A1.2.3, A1.2.4, A1.2.5, A1.2.6A-B, A1.5.1A, 2.8A, A1.6.1A-B, A1.6.2A-B	10%T, 0.025s EX: 575/25 EM: 632/60	10%T, 0.025s EX: 475/28 EM: 523/36	N/A	32%T, 0.1s	1 µm, 8 sections
2.1B-C, A1.1A, A1.1.2, 2.2A-2.2B, 2.2E, 2.3H, 2.4A-C, A1.4.1A-B, 2.6C-2.6D*, A1.5.1B, A1.5.2A-B, A1.5.3, 2.7A, 2.7C, A1.6.1C, A1.6.2C, 2.9A-2.9-B, 2.9D-E, A1.7.1, A1.7.2, 3.2A, 3.2C, 3.3A-B, 3.4A-C. A2.2A-F, A2.5A-D, A2.6A-D	32%T, 0.025s EX: 575/25 EM: 632/60	10%T, 0.025s EX: 475/28 EM: 523/36	N/A	32%T, 0.1s	1 µm, 8 sections
2.5A-B, 2.6A**, 2.6B, 2.8C-D	100%T, 0.1s EX: 575/25 EM: 632/60	100%T, 0.1s EX: 475/28 EM: 523/36	100%T, 0.01s EX: 390/18 EM: 435/48	32%T, 0.1s	0.2 µm, 40 sections
2.8F	100%T, 0.1s EX: 575/25 EM: 632/60	100%T, 0.1s EX: 475/28 EM: 523/36	100%T, 0.01s EX: 390/18 EM: 435/48	32%T, 0.1s	1 µm, 8 sections
A1.3.1-2**	100%T, 0.1s EX: 575/25 EM: 632/60	100%T, 0.1s EX: 475/28 EM: 523/36	100%T, 0.1s EX: 390/18 EM: 435/48	32%T, 0.1s	0.2 µm, 50 sections

*In 2.6C-D, POL images were not acquired.
**In 2.6A, the early and late meiosis II cells were acquired with 0.2 µm over 30 sections.
***In A1.3.1-2, pre-meiosis cells were acquired with 0.3 µm over 33 sections.

B.4.3 Image quantification

To quantify the percentage of Nsr1 sequestration in chapter 2, measurements of Nsr1-GFP signal intensity were taken with Fiji (RRID:SCR_002285, Schindelin et al., 2012) from maximum intensity z-projection movies of young and aged cells that eventually formed tetrads. Nsr1 signal was measured after nucleolus segregation to the four dividing nuclei, determined by the appearance of four Nsr1 foci in the four nuclei. Percent

sequestration was measured by calculating the raw integrated intensity in the fifth compartment and dividing it by the sum of the signal present in the four nuclei and the fifth compartment. The mean intensity measured from non-cellular background was subtracted in each field of view before quantifying Nsr1 levels.

For the vacuolar lysis experiments in chapter 2, the timing of vacuolar membrane disruption was scored in cells that eventually became tetrads. Vacuolar membrane disruption was defined as the time point at which Vph1 signal becomes diffuse, instead of localizing to the membrane. Protein aggregate and NPC disappearance was defined as the time point at which the excluded fluorescence signal was no longer visible. Only cells in which both vacuolar membrane disruption and nucleoporin or protein aggregate disappearance could be confidently called were included in our analysis. In less than 25% of cells, the vacuole appeared to crumple and collapse over more than an hour prior to vacuolar membrane disappearance. Since we were unable to interpret these changes in vacuolar morphology, these cells were not included in our quantification. The vacuolar lysis experiments in chapter 3 were similarly quantified in chapter 2. The of timing of anaphase II was defined as the first time point when four distinct nuclei were observed.

For protein aggregate and nucleolar sequestration experiments in chapter 2, sequestration was scored in WT cells that formed tetrads and *spo21Δ* cells that progressed through anaphase II, as tetrad formation cannot be assessed in *spo21Δ* cells. Protein aggregate sequestration was scored in aged cells and was defined as the aggregate no longer associating with chromatin after the four anaphase II nuclei became distinct. Nucleolar sequestration was scored in young cells and was defined as the presence of a fifth focus that did not associate with a gamete nucleus after the four anaphase II nuclei became distinct.

For the Pma2-GFP experiments in chapter 3, timing of Pma2-GFP expression was defined as the first time point GFP signal appeared in the gametes. Onset of anaphase II was defined as the first time point displaying four nuclei.

B.5 Electron microscopy

Yeast cells were concentrated by vacuum filtration onto a nitrocellulose membrane and then scrape-loaded into 50- or 100- µm-deep high pressure freezing planchettes (McDonald and Müller-Reichert, 2002). Freezing was done in a Bal-Tec HPM-010 high-pressure freezer (Bal-Tec AG).

High pressure frozen cells stored in liquid nitrogen were transferred to cryovials containing 1.5 ml of fixative consisting of 1% osmium tetroxide, 0.1% uranyl acetate, and 5% water in acetone at liquid nitrogen temperature (−195°C) and

processed for freeze substitution according to the method of McDonald and Webb (McDonald, 2014; McDonald and Webb, 2011). Briefly, the cryovials containing fixative and cells were transferred to a cooled metal block at −195°C; the cold block was put into an insulated container such that the vials were horizontally oriented and shaken on an orbital shaker operating at 125 rpm. After 3 hr, the block and cryovials had warmed to 20°C and were transitioned to resin infiltration.

Resin infiltration was accomplished by a modification of the method of McDonald (2014). Briefly, cells were rinsed 4–5 times in pure acetone and infiltrated with Epon-Araldite resin in increasing increments of 25% over 3 hr plus 3 changes of pure resin at 30 min each. Cells were removed from the planchettes at the beginning of the infiltration series and spun down at 6000 x g for 1 min between solution changes. The cells in pure resin were placed in between 2 PTFE-coated microscope slides and polymerized over 2 hr in an oven set to 100°C.

Cells were cut out from the thin layer of polymerized resin and remounted on blank resin blocks for sectioning. Serial sections of 70 nm were cut on a Reichert-Jung Ultracut E microtome and picked up on 1 × 2 mm slot grids covered with a 0.6% Formvar film. Sections were post-stained with 1% aqueous uranyl acetate for 10 min and lead citrate for 10 min (Reynolds, 1963). Images of cells on serial sections were taken on an FEI Tecnai 12 electron microscope operating at 120 kV equipped with a Gatan Ultrascan 1000 CCD camera.

Models were constructed from serial sections with the IMOD package (Kremer et al., 1996), using 3DMOD version 4.9.8. Initial alignment was performed using the Midas tool in the ETomo interface of the IMOD package; afterwards, sections were rotated and minorly warped in Midas to improve alignment. The plasma membrane, nuclear envelope, and nucleoli were segmented in IMOD by manual tracing using the Drawing Tools plugin created by Andrew Noske. If a serial section was missing or unusable, the Interpolator plugin created by Andrew Noske was used to approximate any contours in the missing slice. Movies were made in 3DMOD and assembled in QuickTime Pro Version 7.6.6; EM movie sizes were compressed to below 10 MB by exporting as HD 720p movies in QuickTime.

B.6 Immunoblotting

For each meiotic time point, 3.7 OD_{600} equivalents of cells were pelleted and resuspended in 2 mL of 5% trichloroacetic acid and incubated at 4°C for ≥10 min. The cells were subsequently washed with 1 mL 10 mM Tris pH 8.0 and then 1 mL of acetone, before being left to dry overnight. Then, ~100 µl glass beads and 100 µl of lysis buffer (50 mM Tris-HCl pH 8.0, 1 mM EDTA, 15 mM Tris pH 9.5, 3 mM DTT, 1X cOmplete EDTA-free inhibitor cocktail [Roche])

were added to each dried pellet. Protein extracts were generated by pulverization using a Mini-Beadbeater-96 (BioSpec). The samples were then treated with 50 µl of 3X SDS sample buffer (187.5 mM Tris pH 6.8, 6% β-mercaptoethanol, 30% glycerol, 9% SDS, 0.05% bromophenol blue) and heated at 37°C for 5 min.

Proteins were separated by polyacrylamide gel electrophoresis using 4–12% Bis-Tris Bolt gels (Thermo Fisher) and transferred onto nitrocellulose membranes (0.45 µm, Bio-rad). The Nup84-GFP blot was generated using a semi-dry transfer apparatus (Trans-Blot Turbo Transfer System, Bio-Rad). The Nup170-GFP blot was generated using a Mini-PROTEAN Tetra tank (Bio-Rad) filled with 25 mM Tris, 195 mM glycine, and 15% methanol, run at 180 mA (max 80 V) for 3 hr at 4°C. The membranes were blocked for at least 30 min with Odyssey PBS Blocking Buffer (LI-COR Biosciences) at room temperature. The blots were incubated overnight at 4°C with a mouse anti-GFP antibody (RRID:AB_2313808, 632381, Clontech) at a 1:2000 dilution in blocking buffer. As a loading control, we monitored Hxk2 levels using a rabbit anti-hexokinase antibody (RRID:AB_219918, 100–4159, Rockland) at a 1:10,000 dilution in blocking buffer. Membranes were washed in PBST (PBS with 0.1% Tween-20) and incubated with an anti-mouse secondary antibody conjugated to IRDye 800CW at a 1:15,000 dilution (RRID:AB_621847, 926–32212, LI-COR Biosciences) and an anti-rabbit antibody conjugated to IRDye 680RD at a 1:15,000 dilution (RRID:AB_10956166, 926–68071, LI-COR Biosciences) to detect the GFP epitope and Hxk2, respectively. Immunoblot images were generated using the Odyssey CLx system (LI-COR Biosciences).